The Dissertation Committee for Christopher Robin Fietz
certifies that this is the approved version of the following dissertation:

Homogenization of Metamaterials with Spatial Dispersion

Committee:

Gennady Shvets, Supervisor

Manfred Fink

Chih-Kang Shih

James Chelikowsky

Hao Ling

Homogenization of Metamaterials with Spatial Dispersion

by

Christopher Robin Fietz, B.S.

DISSERTATION

Presented to the Faculty of the Graduate School of

The University of Texas at Austin

in Partial Fulfillment

of the Requirements

for the Degree of

DOCTOR OF PHILOSOPHY

THE UNIVERSITY OF TEXAS AT AUSTIN

August 2011

In a sense, every material is a composite ...

–John B. Pendry

Acknowledgments

I am grateful to all the members of my research group for their help and advice on papers and presentations. In particular, I would like to thank Burton Neuner and Dmitriy Korobkin for their experimental work which made all of our collaborative papers possible. I am grateful to Yoav Avitzour, Simeon Trendafilov, Yaroslav Urzhumov and Hossein Mousavi for many useful and interesting conversations on electromagnetism and computer simulations. Finally, I am forever indebted to the American taxpayer for funding my graduate education.

Homogenization of Metamaterials with Spatial Dispersion

Publication No. _____

Christopher Robin Fietz, Ph.D.
The University of Texas at Austin, 2011

Supervisor: Gennady Shvets

A study is made of the problem of metamaterial homogenization, which is the attempt to represent an artificially fabricated inhomogeneous periodic structure as a homogeneous medium with an electromagnetic response described by a number of constitutive parameters (permittivity, permability, etc.) In particular, the importance of spatial dispersion in metamaterials and the need to characterize metamaterials with wavevector dependent constitutive parameters is explained an examined. A brief survey of important previous attempts at metamaterial homogenization is presented. This is followed by a discussion of spatial dispersion in metamaterial crystals. The importance of spatial dispersion in metamaterials is justified and some manifestations of spatial dispersion described. In particular the little known phenomenon of bianisotropy in centrosymmetric crystals due to spatial dispersion is explained. Also, the effects of spatial dispersion on physical quantities such as energy flux and dissipation are identified. We then describe a new method

for solving for the free eigenmodes of a metamaterial crystal with a complex wavevector eigenvalue simulation. Next, two different theoretical attempts by the author at metamaterial homogenization are described, both accompanied by tests of the calculated constitutive parameters and critical examination of the strengths and weaknesses of each approach. Finally, strong evidence of the presence and importance of spatial dispersion in metamaterials is presented.

Table of Contents

List of Figures

Conventions and Notation

Through out this dissertation we use the convention that a plane wave with a complex valued amplitude changes in time and space with the exponential factor

$$e^{\mathrm{i}(\omega t - \mathbf{k}\cdot\mathbf{x})}, \tag{1}$$

where ω is the frequency and $\mathbf{k}$ is the wavevector of the plane wave. Among other things, this implies that in a passive medium the imaginary parts of the permittivity and permeability are less than or equal to zero or $\mathrm{Im}(\epsilon) \leq 0$ and $\mathrm{Im}(\mu) \leq 0$.

We also use Heaviside-Lorentz units. These are similar to Gaussian units except that the charge/current is redefined to absorb the 4π factor. The Maxwell equations in Heaviside-Lorentz assuming the dependence on time stated above are

$$\begin{aligned} \nabla \cdot \mathbf{D} &= \rho & \nabla \times \mathbf{H} - \mathrm{i}\frac{\omega}{c} D &= \frac{\mathbf{J}}{c}, \\ \nabla \cdot \mathbf{B} &= \phi & -\nabla \times \mathbf{E} - \mathrm{i}\frac{\omega}{c} B &= \frac{\mathbf{I}}{c}. \end{aligned} \tag{2}$$

Here ρ and $\mathbf{J}$ are electric charge and current and ϕ and $\mathbf{I}$ are magnetic charge and current.

The main topic of this dissertation is the averaging of inhomogeneous microscopic fields into homogeneous macroscopic fields. We differentiate between the two by modifying the case of the microscopic fields

$$\begin{array}{ll} \mathbf{e} & \text{Microscopic electric field} \\ \mathbf{h} & \text{Microscopic magnetic field} \\ \mathbf{d} & \text{Microscopic electric displacement} \\ \mathbf{b} & \text{Microscopic magnetic flux density} \end{array} \tag{3}$$

vs. the macroscopic fields

$$\begin{array}{ll} \mathbf{E} & \text{Macroscopic electric field} \\ \mathbf{H} & \text{Macroscopic magnetic field} \\ \mathbf{D} & \text{Macroscopic electric displacement} \\ \mathbf{B} & \text{Macroscopic magnetic flux density.} \end{array} \tag{4}$$

The microscopic fields have the constitutive relations

$$\mathbf{d} = \epsilon \mathbf{e}, \qquad \mathbf{b} = \mu \mathbf{h}, \tag{5}$$

where ϵ and μ are the microscopic and inhomogeneous permittivity and permeability.

The macroscopic fields have the constitutive relation

$$\begin{pmatrix} \mathbf{D} \\ \mathbf{B} \end{pmatrix} = \begin{pmatrix} \hat{\epsilon} & \hat{\xi} \\ \hat{\zeta} & \hat{\mu} \end{pmatrix} \cdot \begin{pmatrix} \mathbf{E} \\ \mathbf{H} \end{pmatrix}, \tag{6}$$

where $\hat{\epsilon}$ and $\hat{\mu}$ are 3×3 spatial tensors and $\hat{\xi}$ and $\hat{\zeta}$ are 3×3 spatial pseudotensors.

Chapter 1

A Survey of Metamaterial Homogenization Methods

1.1 Introduction

The primary assumption made in the field of metamaterial research is that when analyzing a inhomogeneous material, if the length scale of the inhomogeneity is small compared to the free space wavelength of light, then it is possible to describe the inhomogeneous material with effective constitutive parameters (ϵ, μ, etc.). It is assumed these effective parameters accurately describe the electromagnetic response of the metamaterial as if it were in fact a homogeneous medium. Given the intense interest in metamaterials that has developed over the past decade, it is surprising that relatively little research has been directed towards defining or measuring these effective constitutive parameters. Indeed, today metamaterial homogenization/characterization represents a small niche in the larger and ever growing field of metamaterial research.

To appreciate the challenge of metamaterial homogenization, let us begin by understanding how complicated a metamaterial can in principle be. Most conventional materials have an electromagnetic response that can be described with a single number known as the permittivity or ϵ. This includes

dielectrics, metals, most liquids and gases and to a good approximation plasmas. The permittivity describes the electric response of the material according to the constitutive relations

$$\mathbf{D} = \epsilon \mathbf{E}, \qquad \mathbf{B} = \mathbf{H}, \tag{1.1}$$

where $\mathbf{E}$ and $\mathbf{H}$ are the electric and magnetic fields and $\mathbf{D}$ and $\mathbf{B}$ are the electric displacement and the magnetic flux density. However there are some materials that have a magnetic response as well. In fact, much of the interest in metamaterials is due to their potential to exhibit a magnetic response at high (optical) frequencies. Most natural magnetic materials have a simple magnetic response characterized by the permeability or μ according to the constitutive relations

$$\mathbf{D} = \epsilon \mathbf{E}, \qquad \mathbf{B} = \mu \mathbf{H}, \tag{1.2}$$

These two constitutive parameters are in general not constant, but actually functions of the frequency ω or $\epsilon = \epsilon(\omega)$ and $\mu = \mu(\omega)$. This dependence of the parameters on ω is known as temporal dispersion.

So far, we have only considered materials with an isotropic response which can be described with two parameters. However, in practice most metamaterials are anisotropic, which means they have an electromagnetic response that depends on the polarization direction of the electric and magnetic fields. These anisotropic materials have the constitutive relation

$$\mathbf{D} = \hat{\epsilon}\cdot\mathbf{E} = \begin{pmatrix} \epsilon_{xx} & \epsilon_{xy} & \epsilon_{xz} \\ \epsilon_{yx} & \epsilon_{yy} & \epsilon_{yz} \\ \epsilon_{zx} & \epsilon_{zy} & \epsilon_{zz} \end{pmatrix} \cdot \mathbf{E}, \qquad \mathbf{B} = \hat{\mu}\cdot\mathbf{H} = \begin{pmatrix} \mu_{xx} & \mu_{xy} & \mu_{xz} \\ \mu_{yx} & \mu_{yy} & \mu_{yz} \\ \mu_{zx} & \mu_{zy} & \mu_{zz} \end{pmatrix} \cdot \mathbf{H}. \quad (1.3)$$

Here $\hat{\epsilon}$ and $\hat{\mu}$ are the permittivity and permeability *tensors*. Each as nine components for a total of 18 parameters to describe an anisotropic material. Each of these 18 parameters is in general a function of ω.

In addition to anisotropy, as we will describe in later chapters, in many metamaterials there is a coupling between the electric and magnetic fields. This phenomenon is known as bianisotropy. Bianisotropic materials obey the constitutive relation

$$\begin{pmatrix} \mathbf{D} \\ \mathbf{B} \end{pmatrix} = \begin{pmatrix} \hat{\epsilon} & \hat{\xi} \\ \hat{\zeta} & \hat{\mu} \end{pmatrix} \cdot \begin{pmatrix} \mathbf{E} \\ \mathbf{H} \end{pmatrix}. \quad (1.4)$$

Now in addition to the tensors $\hat{\epsilon}$ and $\hat{\mu}$ we also see the *pseudotensors* $\hat{\xi}$ and $\hat{\zeta}$ [32]. These pseudotensors characterize the coupling between the electric and magnetic fields. Each of these pseudotensors contain nine components, for a total of 36 constitutive parameters to characterize a general metamaterial.

Finally, perhaps the main theme of this dissertation is that in addition to temporal dispersion (the dependence of the constitutive parameters on ω) many metamaterials also exhibit strong spatial dispersion. This manifests itself as a dependence of the constitutive parameters on the wavevector $\mathbf{k}$ of the electromagnetic field or

$$\begin{aligned} \hat{\epsilon} &= \hat{\epsilon}(\omega, \mathbf{k}) \qquad & \hat{\xi} &= \hat{\xi}(\omega, \mathbf{k}) \\ \hat{\zeta} &= \hat{\zeta}(\omega, \mathbf{k}) \qquad & \hat{\mu} &= \hat{\mu}(\omega, \mathbf{k}) \end{aligned} \tag{1.5}$$

So in general, we need as many as 36 constitutive parameters, all of which are functions of ω and $\mathbf{k}$, to describe the electromagnetic response of a metamaterial. Successfully calculating all of these parameters under general conditions is a difficult task and one that will only be partially fullfilled in this dissertation. But along the way important insights into the nature of metamaterials, particularly with respect to spatial dispersion, will be discovered.

Before describing the author's attempts at metamaterial homogenization, it is useful to review a few other methods of characterizing metamaterials. This is important to relate to the reader the current state of the art of metamaterial theory in the published literature and to weigh the relative strengths and weaknesses of different methods. It is also important for comparing and contrasting our attempts at metamaterial homogenization to these other methods. Therefore the remainder of this chapter is a survey of published methods for numerically calculating the effective constitutive parameters. The list of methods described is not exhaustive, but it represents the best of metamaterial homogenization theory that is currently available. It also helps put into perspective the two homogenization methods described in Chapters 4 and 5. The notations used in the original papers have been modified to be consistent with the conventions used in this dissertation.

1.2 Pendry's averaging method

In 1999, a paper titled *Magnetism from Conductors and Enhanced Nonlinear Phenomena* by John Pendry et al. [50] began the field of research on materials with exotic electromagnetic properties that would later be known as metamaterials. This paper described how coiled rolls of metal could exhibit a resonant magnetic response. In this initial metamaterial paper there was proposed a simple method for averaging the microscopic fields inside an inhomogeneous material into macroscopic fields. The averaging method consists of averaging the E and H fields over the edges of the crystal unit cell and averaging the B and D fields over the faces of the unit cell. Consider two of the Maxwell equations for microscopic fields in the absence of sources

$$-\nabla \times \mathbf{e} = \frac{\partial \mathbf{b}}{\partial t}, \qquad \nabla \times \mathbf{h} = \frac{\partial \mathbf{d}}{\partial t}. \tag{1.6}$$

A surface integral of these equations over an edge of the unit cell results in

$$-\oint_{\partial S} \mathbf{e} \cdot d\mathbf{l} = \frac{\partial}{\partial t} \int_S \mathbf{b} \cdot d\mathbf{a} \qquad \oint_{\partial S} \mathbf{h} \cdot d\mathbf{l} = \frac{\partial}{\partial t} \int_S \mathbf{d} \cdot d\mathbf{a} \tag{1.7}$$

where S is a face of the unit cell and ∂S is the boundary of that face. The form of these equations suggest a possible prescription for averaging the microscopic fields, namely that the $\mathbf{e}$ and $\mathbf{h}$ fields should be averaged along the edges of the unit cell

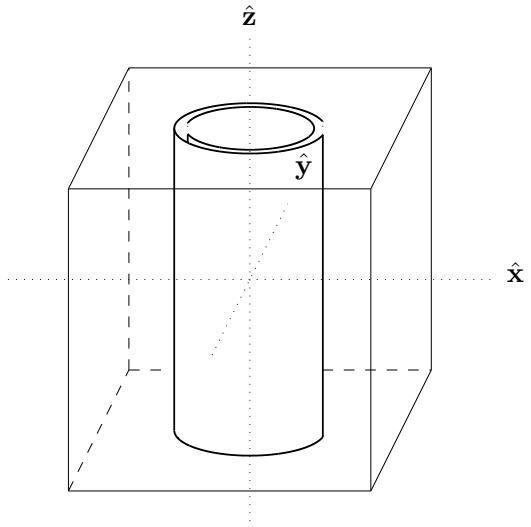

Figure 1.1: An example from Ref. [50] of an inclusion with a magnetic response. This split ring structure is made of two concentric cylinders, each with a gap preventing current from traveling all the way around the cylinder.

$$\begin{aligned}
\mathrm{E}_x &= \frac{1}{a_x}\int_{-\frac{a_x}{2}}^{\frac{a_x}{2}} dx\ \mathrm{e}_x(x, y=-\tfrac{a_y}{2}, z=-\tfrac{a_z}{2}),\\
\mathrm{E}_y &= \frac{1}{a_y}\int_{-\frac{a_y}{2}}^{\frac{a_y}{2}} dy\ \mathrm{e}_y(x=-\tfrac{a_x}{2}, y, z=-\tfrac{a_z}{2}),\\
\mathrm{E}_z &= \frac{1}{a_z}\int_{-\frac{a_z}{2}}^{\frac{a_z}{2}} dz\ \mathrm{e}_z(x=-\tfrac{a_x}{2}, y=-\tfrac{a_y}{2}, z),
\end{aligned} \tag{1.8}$$

with similar formulas for averaging the $\mathbf{h}$ field. Here a_x, a_y and a_z are the lattice constants of the crystal unit cell. Similarly the $\mathbf{b}$ is averaged over faces of the unit cell

$$\mathrm{B}_x = \frac{1}{a_y a_z} \int_{-\frac{a_y}{2}}^{\frac{a_y}{2}} dy \int_{-\frac{a_z}{2}}^{\frac{a_z}{2}} dz \; \mathrm{b}_x(x = -a_x/2, y, z)$$

$$\mathrm{B}_y = \frac{1}{a_x a_z} \int_{-\frac{a_x}{2}}^{\frac{a_x}{2}} dx \int_{-\frac{a_z}{2}}^{\frac{a_z}{2}} dz \; \mathrm{b}_y(x, y = -a_y/2, z) \tag{1.9}$$

$$\mathrm{B}_z = \frac{1}{a_x a_y} \int_{-\frac{a_x}{2}}^{\frac{a_x}{2}} dx \int_{-\frac{a_y}{2}}^{\frac{a_y}{2}} dy \; \mathrm{b}_y(x, y, z = -a_z/2)$$

with similar formulas for averaging the **d** field.

This averaging procedure produced some of the first theoretical evidence of unusual magnetic responses in composite materials including approximate analytic expressions for the magnetic permeability [50]. Still, there was room for improvement in these equations. If this averaging procedure is applied to a plane wave propagating through a homogeneous medium, say a simple dielectric with an arbitrary unit cell, Eqs. (1.8,1.9) will not produce the correct averaged field amplitude (which should be equal to the amplitude of the microscopic plane wave). In Ref [62] this method was modified to correct this. Two factors are multiplied to Eqs. (1.8,1.9). The first is a simple phase factor adjusting for the fact that different field components are averaged in different locations on the unit cell. The second factor is an effective volume term. The new expressions for the **E** and **B** fields are

$$\mathrm{E}_x = \frac{e^{-\mathrm{i}(k_y a_y/2 + k_z a_z/2)}}{s_x} \int_{-\frac{a_x}{2}}^{\frac{a_x}{2}} dx \ \mathrm{e}_x(x, y = -\tfrac{a_y}{2}, z = -\tfrac{a_z}{2})$$

$$\mathrm{E}_y = \frac{e^{-\mathrm{i}(k_x a_x/2 + k_z a_z/2)}}{s_y} \int_{-\frac{a_y}{2}}^{\frac{a_y}{2}} dy \ \mathrm{e}_y(x = -\tfrac{a_x}{2}, y, z = -\tfrac{a_z}{2}) \tag{1.10}$$

$$\mathrm{E}_z = \frac{e^{-\mathrm{i}(k_x a_x/2 + k_y a_y/2)}}{s_z} \int_{-\frac{a_z}{2}}^{\frac{a_z}{2}} dz \ \mathrm{e}_z(x = -\tfrac{a_x}{2}, y = -\tfrac{a_y}{2}, x)$$

and

$$\mathrm{B}_x = \frac{e^{-\mathrm{i}k_x a_x/2}}{s_y s_z} \int_{-\frac{a_y}{2}}^{\frac{a_y}{2}} dy \int_{-\frac{a_z}{2}}^{\frac{a_z}{2}} dz \ \mathrm{b}_x(x = -a_x/2, y, z)$$

$$\mathrm{B}_y = \frac{e^{-\mathrm{i}k_x a_x/2}}{s_x s_z} \int_{-\frac{a_x}{2}}^{\frac{a_x}{2}} dx \int_{-\frac{a_z}{2}}^{\frac{a_z}{2}} dz \ \mathrm{b}_y(x, y = -a_y/2, z) \tag{1.11}$$

$$\mathrm{B}_z = \frac{e^{-\mathrm{i}k_x a_x/2}}{s_x s_y} \int_{-\frac{a_x}{2}}^{\frac{a_x}{2}} dx \int_{-\frac{a_y}{2}}^{\frac{a_y}{2}} dy \ \mathrm{b}_y(x, y, z = -a_z/2)$$

The effective volumes s_x, s_y and s_z are given by the formulas

$$s_x = \frac{\sin k_x a_x/2}{a_x/2} \qquad s_y = \frac{\sin k_y a_y/2}{a_y/2} \qquad s_z = \frac{\sin k_z a_z/2}{a_z/2} \tag{1.12}$$

This modified averaging procedure has been used to characterize simple metamaterials by averaging the microscopic fields of Bloch eigenmodes of the metamaterial crystals [60]. The homogenization procedure is partially successful but it is limited in its applicability. Primarily, it can only be used on

crystals with enough symmetry that the permittivity and permeability tensors are diagonalizable and the bianisotropic tensors are zero. This method is unable to characterize crystals with little or no symmetry. Finally, as we will see later in this chapter, bianisotropy can occur in highly symmetric crystals due to spatial dispersion. Because this homogenization procedure assumes no bianisotropy it mistakenly excludes this possibility.

1.3 S parameter retrieval

Most of the averaging procedures described in this chapter are not widely used by the metamaterial community. We are describing each of them either because they represent important contributions to homogenization theory or because they represent important advances in metamaterial knowledge in general. The method described in this section is an exception. This is the most widely used homogenization procedure in the metamaterial literature.

In 2002, Smith et al. published the paper *Determination of effective permittivity and permeability of metamaterials from reflection and transmission coefficients* [61]. The concept of this procedure is simple. The scattering matrix for a slab of a metamaterial crystal is calculated numerically. This slab has a finite width, generally three to five lattice constants, and an infinite length in the two remaining directions. The question is then asked: for a homogeneous slab, what constitutive parameters would be necessary for the slab to produce the same scattering matrix as that measured from the metamaterial slab.

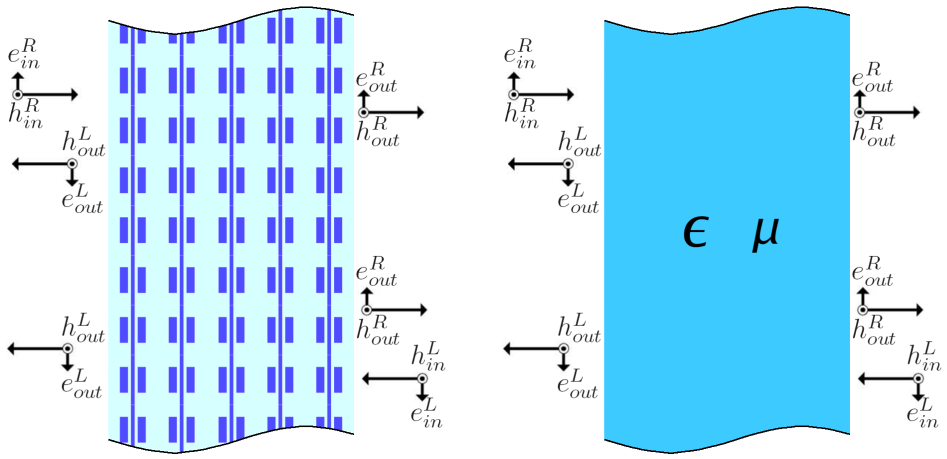

Figure 1.2: A schematic of the S-parameter retrieval method. The scattering matrix is measured from a thin slab of the metamaterial of interest (left) and the constitutive parameters ϵ and μ are inferred for a thin slab of a homogeneous medium (right) which is assumed to have the same scattering matrix.

To solve this inverse scattering problem several assumptions are made. First, it is assumed that the metamaterial crystal of interest has reflection symmetry in three orthogonal directions. This implies that the $\hat{\epsilon}$ and $\hat{\mu}$ tensors are both diagonal in the same basis which is known as the principle axes. This symmetry also implies that the bianisotropic tensors $\hat{\xi}$ and $\hat{\zeta}$ are zero. This assumption about the lack of bianisotropy is common for crystals with inversions symmetry though we will see later that it is incorrect. The second assumption is that light propagating though the crystal is propagating along a principle axis and is polarized along another principle axis. This allows us to consider only one component of $\hat{\epsilon}$ and one component of $\hat{\mu}$, which we will simply refer to as ϵ and μ respectively. The assumption of propagation

along a principle axis also implies that the interface between vacuum and the metamaterial crystal is perpendicular to a principle axis and that the incident beam is normal to this interface. The third assumption is that boundary conditions at the interface are Maxwellian, meaning that the components of the **e** and **h** fields tangential to the interface are continuous across the interface. This seems like an obvious assumption, but it may not be true for materials with string spatial dispersion. Finally, it is assumed that the metamaterial is passive (only losses, no gain) and that it obeys Lorentz reciprocity [36, 2].

After stating all assumptions, the next step is to analytically calculate the scattering matrix from a slab of a homogeneous medium. Since most of the examples in this dissertation involve p polarized waves (waves with the magnetic field perpendicular to the plane containing the wavevector) we define our scattering matrix with the magnetic field amplitudes. The scattering matrix is defined according to

$$\begin{pmatrix} \mathrm{h}_{out}^{L} \\ \mathrm{h}_{out}^{R} \end{pmatrix} = \underbrace{\begin{pmatrix} S_{11}^{\mathrm{H}} & S_{12}^{\mathrm{H}} \\ S_{21}^{\mathrm{H}} & S_{22}^{\mathrm{H}} \end{pmatrix}}_{S^{\mathrm{H}}} \begin{pmatrix} \mathrm{h}_{in}^{R} \\ \mathrm{h}_{in}^{L} \end{pmatrix}. \tag{1.13}$$

The two relevent constitutive parameters ϵ and μ define an index of refraction $n = \sqrt{\epsilon\mu}$ which describes propagation through the slab according to the dispersion relation $k = n\omega/c$. The constitutive parameters also define an impedance $z = \sqrt{\mu/\epsilon}$. With our assumption of Maxwellian boundary conditions at the interface between the vacuum and the homogeneous slab, the impedance determines reflection of an incident wave at the interface $r = (1 - z)/(1 + z)$ as

well as the transmission from the slab into vacuum $t = 1 + r = 2/(1 + z)$.

The scattering matrix of the slab can be calculated from these parameters.

$$S_{11} = r + \frac{rt^2 e^{-2\mathrm{i}n\omega d/c}}{1 - r^2 e^{-2\mathrm{i}n\omega d/c}} = \frac{(1 - z^2)\mathrm{i}\sin(n\omega d/c)}{(1 + z^2)\mathrm{i}\sin(n\omega d) + 2z\cos(n\omega d/c)} \tag{1.14}$$

$$S_{21} = \frac{t^2 e^{-\mathrm{i}n\omega d/c}}{1 - r^2 e^{-2\mathrm{i}n\omega d/c}} = \frac{2z}{(1 + z^2)\mathrm{i}\sin(n\omega d/c) + 2z\cos(n\omega d/c)} \tag{1.15}$$

Here ω is the angular frequency of the incident beam, d is the thickness of the slab and c is the speed of light. Because we are only considering metamaterials that are symmetric and that obey Lorentz reciprocity the reflection and transmission amplitudes are equal regardless of the direction of incident radiation implying $S_{11} = S_{22}$ and $S_{12} = S_{21}$. Eqs. (1.14,1.15) can be inverted to solve for the index of refraction

$$\cos(n\omega d/c) = \frac{1 - S_{11}^2 + S_{21}^2}{2S_{21}}, \tag{1.16}$$

There is some ambiguity in this expression. There are an infinite number of solutions to Eq. (1.16) for the index of refraction. For any solution n, there also exists the solution $n + 2\pi m/d$ where m is an integer. The solution for n should always be chosen so that the resulting wavenumber lies in the primary Brillouin zone or $-\pi/a \leq \mathrm{Re}(n\omega/c) \leq \pi/a$. Also, because of the assumption

of the passivity of the metamaterial the sign of n should be chosen so that $\mathrm{Im}(n) \leq 0$ indicating a wave that is decaying in the positive $\hat{\mathbf{x}}$ direction. Still, since $d \geq a$ there could be several possible solutions to Eq. (1.16) that satisfy these conditions. The authors of Ref. [61] suggest that to pick the correct index one should perform the S parameter retrieval procedure on different slabs of the metamaterial each with different thicknesses and pick the index that is consistant with the different slabs thicknesses.

Eqs. (1.14,1.15) can also be inverted to solve for the impedance

$$z^2 = \frac{(1 - S_{11})^2 - S_{21}^2}{(1 + S_{11})^2 - S_{21}^2}. \tag{1.17}$$

The sign of the impedance should be chosen so that $\mathrm{Re}(z) > 0$.

Once the index of refraction and the impedance are known it is straightforward to calculate the permittivity and permeability

$$\epsilon = \sqrt{\frac{n}{z}}, \qquad \mu = \sqrt{nz}. \tag{1.18}$$

One limitation of this procedure is that it assumes reflection symmetry in the direction of propagation, that is it assumes the crystal is symmetric under a reflection transformation in the direction of the wavevector $\mathbf{k}$. A more general method was presented in Ref. [41] that allows for the extraction of three constitutive parameters ϵ, μ and κ from a metamaterial with no reflection symmetry in the propagation direction. Here κ is a bianisotropic parameter. This method takes into account the fact the the intrinsic bianisotropy of an

asymmetric metamaterial crystal causes the crystal to have two impedances, one each for two waves moving in opposite directions. This causes the reflection amplitudes of the scattering matrix to be unequal allowing for the extraction of three constitutive parameters.

There are several limitations of both the symmetric and asymmetric versions of the S parameter retrieval method. First, both the symmetric and asymmetric methods assume that the metamaterial has reflection symmetry in two orthogonal directions, allowing for the permittivity and permeability tensors to be diagonalizable (for the asymmetric retrieval the bianisotropic pseudotensors each have two off-diagonal elements). The retrieval methods further assume that both the propagation wavevector and the polarization are along principle axes of the crystal. As a result, the wave traveling through the metamaterial slab is only affected by a small number of constitutive parameters, one component of ϵ one component of μ and one bianisotropic parameter κ. This simplification is essential for calculating the constitutive parameters through an inverse scattering problem. By rotating the polarization of the incident wave onto another principle axis three more parameters can also be calculated in this way. Still this allows only 6 constitutive parameters to be calculated out of a possible 36. The S parameter retrieval method only works on highly symmetric metamaterial crystals and can only retrieve a small number of parameters.

The second limitation of this method is that it assumes that the constitutive parameters are all functions solely of ω. As we shall see as we look

at some other proposed homogenization methods, this is not true in general. The presence of spatial dispersion can cause the constitutive parameters to depend on $\mathbf{k}$ as well as ω [3]. As we shall see in Chapter 2 spatial dispersion is a common and important phenomenon in metamaterials. Among its other effects, spatial dispersion can cause the boundary conditions between the interface of a metamaterial and some other medium to be non-Maxwellian. This brings us to the third drawback of the S parameter retrieval method, it assume Maxwellian boundary conditions at the interfaces.

Despite the limitations of S parameter retrieval, it is the most commonly used method for characterizing metamaterial crystals and has played an important role in the development of the field of metamaterial research.

1.4 Calculation of non-local permittivity

The two remaining homogenization procedures we discuss are not widely used in metamaterial research. Nonetheless, they represent some of the best recent attempts at a more general method of metamaterial homogenization. Both have an important factor in common, they excite microscopic fields inside a metamaterial crystal with external currents.

The first example of this comes from a paper by Mário G. Silveirinha [54]. As we with the first two homogenization procedures earlier in this chapter, any metamaterial homogenization procedure that is based on averaging the microscopic electromagnetic fields of eigenmodes of a metamaterial crystal can only solve for a small number of constitutive parameters. The

most novel aspect of Silveirinha's approach is that instead of averaging the electromagnetic fields of free eigenmodes of a metamaterial crystal, he drives the metamaterial crystal with the external electric current

$$\mathbf{J} = \mathbf{J}_0 e^{\mathrm{i}(\omega t - \mathbf{x}\cdot\mathbf{k})}. \tag{1.19}$$

This current is harmonic both in time and in space. This external current generates microscopic electromagnetic fields inside the metamaterial crystal according to the Maxwell equations. These driven fields are also harmonic in time with frequency ω but the field distribution in space is Bloch periodic [29, 52] with the Bloch wavevector being equal to the wavevector of the driving current $\mathbf{k}$.

The idea of driving electromagnetic fields inside a metamaterial crystal is an important departure from previous homogenization procedures that analyze eigenmode field distributions. In particular, driving the electromagnetic fields with external currents helps solve the problem of calculating all of the constitutive parameters.

Once a the driven electromagnetic fields are solved for numerically, they can be averaged into macroscopic fields to solve for the constitutive parameters. The averaging procedure described by Silveirinha is as follows. The macroscopic electric field is $\mathbf{E} = \mathbf{E}_0 e^{\mathrm{i}(\omega t - \mathbf{k}\cdot\mathbf{x})}$ where the amplitude $\mathbf{E}_0$ is calculated from the integral

$$\mathbf{E}_0 = \int_\Omega d^3x \ \mathbf{e}e^{\mathbf{i}\mathbf{k}\cdot\mathbf{x}} \tag{1.20}$$

where Ω is the crystal unit cell. Similarly, the macroscopic electric polarization is $\mathbf{P} = \mathbf{P}_0 e^{\mathrm{i}(\omega t - \mathbf{k}\cdot\mathbf{x})}$ where the amplitude $\mathbf{P}_0$ is calculated as

$$\mathbf{P}_0 = \int_\Omega d^3x \ (\epsilon - 1)\mathbf{e} \tag{1.21}$$

The macroscopic electric displacement field is simply the sum of the macroscopic electric and polarization fields or $\mathbf{D} = \mathbf{E} + \mathbf{P}$.

The macroscopic magnetic and magnetic flux fields are averaged in a similar way. However, since Silveirinha only considers either metallic or dielectric inclusions he assumes $\mu = 1$ resulting in the fact that the macroscopic magnetic and magnetic flux fields are identical

$$\mathbf{H}_0 = \int_\Omega d^3x \ \mathbf{h}, \qquad \mathbf{B}_0 = \int_\Omega d^3x \ \mathbf{b} = \int_\Omega d^3x \ \mathbf{h} = \mathbf{H}_0. \tag{1.22}$$

The result is that there is no macroscopic magnetization. The macroscopic electromagnetic response is completely contained within the macroscopic electric polarization $\mathbf{P}$.

Because the response of the metamaterial is determined by $\mathbf{P}$ the metamaterial can be described solely with an effective permittivity. This permittivity is determined by performing three simulations, each driving the metamaterial crystal with a different electric current vector $\mathbf{J}_0$. The only condition

on these three current vectors is that they must be linearly independent. The three simulations return three sets of microscopic electromagnetic fields which can then be averaged into three sets of linearly independent macroscopic electric and electric displacement fields

$$\mathcal{E} = \begin{pmatrix} \mathrm{E}_x^1 & \mathrm{E}_x^2 & \mathrm{E}_x^3 \\ \mathrm{E}_y^1 & \mathrm{E}_y^2 & \mathrm{E}_y^3 \\ \mathrm{E}_z^1 & \mathrm{E}_z^2 & \mathrm{E}_z^3 \end{pmatrix}, \qquad \mathcal{D} = \begin{pmatrix} \mathrm{D}_x^1 & \mathrm{D}_x^2 & \mathrm{D}_x^3 \\ \mathrm{D}_y^1 & \mathrm{D}_y^2 & \mathrm{D}_y^3 \\ \mathrm{D}_z^1 & \mathrm{D}_z^2 & \mathrm{D}_z^3 \end{pmatrix}. \tag{1.23}$$

Here the superscript indicates that the macroscopic fields come from averaged microscopic fields driven with the external currents $\mathbf{J}_0^1$, $\mathbf{J}_0^2$ and $\mathbf{J}_0^3$.

Once we have three sets of macroscopic $\mathbf{E}$ and $\mathbf{D}$ fields we can calculate the permittivity tensor

$$\hat{\epsilon}_{nl}(\omega, \mathbf{k}) \equiv \mathcal{D}\mathcal{E}^{-}1 \tag{1.24}$$

The subscript of $\hat{\epsilon}_{nl}$ indicates that this is a non-local permittivity. This means that $\hat{\epsilon}_{nl}$ is a function of $\mathbf{k}$ as well as ω. This is the most interesting feature of the calculated permittivity. Both of these parameters are determined by the applied driving current. The dependence of $\hat{\epsilon}$ on $\mathbf{k}$ is due to spatial dispersion in the metamaterial crystal. As we shall see in Chapter 2, spatial dispersion is a defining characteristic of metamaterials. Any general method of describing metamaterials with effective constitutive parameters must take spatial dispersion into account.

At the same time, it is strange that the entire response of the metamaterial is described by $\hat{\epsilon}$. This is a striking departure from most metamaterial theory where a separate $\hat{\epsilon}(\omega)$ and $\hat{\mu}(\omega)$ are assigned to a metamaterial. Silveirinha connects his nonlocal $\hat{\epsilon}_{nl}$ to the local constitutive parameters metamaterial researchers are familiar with by expanding $\hat{\epsilon}_{nl}$ in powers of $\mathbf{k}$.

$$\begin{aligned}\hat{\epsilon}_{nl}(\omega,\mathbf{k}) &= \hat{\epsilon}_l - \hat{\xi}_l \cdot \hat{\mu}_l^{-1} \cdot \hat{\zeta}_l + \left(\hat{\xi}_l \cdot \mu_l^{-1} \times \frac{\mathbf{k}}{\omega/c} - \frac{\mathbf{k}}{\omega/c} \times \hat{\mu}_l^{-1} \cdot \hat{\zeta}_l\right) \\ &\quad + \frac{\mathbf{k}}{\omega/c} \times \left(\hat{\mu}_l^{-1} - 1\right) \times \frac{\mathbf{k}}{\omega/c}.\end{aligned} \tag{1.25}$$

Here $\hat{\epsilon}_l(\omega)$, $\hat{\mu}_l(\omega)$, $\hat{\xi}_l(\omega)$ and $\hat{\zeta}_l(\omega)$ are the local constitutive parameters normally used to describe the electromagnetic response of a metamaterial crystal. Each of the local constitutive parameters are functions solely of ω. They can be calculated by taking partial derivative of the nonlocal permittivity $\hat{\epsilon}_{nl}(\omega,\mathbf{k})$ with respect to $\mathbf{k}$ evaluated at $\mathbf{k}=0$.

There remain questions as to why only the permittivity is allowed to be nonlocal. There are metamaterial models that in general allow all of the 36 constitutive parameters to be nonlocal and there are good reasons to insist that $\hat{\xi}$, $\hat{\zeta}$ and $\hat{\mu}$ should exhibit spatial dispersion. As we will see in Chapter 3 (Ref. [23]), in some crystals there exist magnetically polarized longitudinal modes or magnetic bulk plasmons. If these modes are ever to be successfully characterized with constitutive parameters, it will be by demonstrating that they obey the dispersion relation $\mathbf{k}\cdot\hat{\mu}=0$, which for a real valued ω implies a

dependence of $\hat{\mu}$ on $\mathbf{k}$. Though Silveirinha's procedure successfully reproduces the dispersion relation for transverse modes, it clearly would be unable to do so for a magnetic bulk plasmon. It is clear however, that if the microscopic electromagnetic fields excited in the metamaterial crystal are driven with electric current, then one is limited to three linearly independent sets of electromagnetic fields. This allows for the calculation of at most nine components of a 3×3 constitutive matrix. Still, Silveirinha's homogenization procedure is an important contribution to metamaterial theory. Its most notable feature is that it relies on microscopic fields driven by external currents. Because the external currents have an arbitrary ω and $\mathbf{k}$ the resulting constitutive parameters that depend not only on ω but also on $\mathbf{k}$. The dependence of the constitutive parameters on $\mathbf{k}$ provides information about spatial dispersion in the metamaterial crystal. This information is essential to any successful characterization of metamaterials.

1.5 Calculation of 36 non-local constitutive parameters

Around the same time that Silveirinha suggested that metamaterials could be characterized by driving them with external electric currents, a second paper came to a similar but slightly different conclusion. In the paper *Non-local effective medium of metamaterial* [40] Jensen Li and John Pendry proposed a metamaterial homogenization procedure involving the driving of a metamaterial crystal by external electric and magnetic fields $\mathbf{E}_{ext}$ and $\mathbf{H}_{ext}$. These external fields were said to be induced by external electric and magnetic

polarization densities. Unlike the induced external fields in Silveirinha's homogenization scheme these fields are not generated by electric current alone. In addition to an external electric polarization density (essentially electric current) these fields are also induced by an external magnetic polarization density (which can be thought of as magnetic current). The result is that unlike Silveirinha whose method calculates the nine components of the nonlocal permittivity tensor, Li's method produces six linearly independent electromagnetic fields allowing him to calculate all 36 nonlocal constitutive parameters.

Li models a metamaterial crystal by representing the inclusions of a unit cell as a collection of N electric and magnetic point dipoles. The moment of each dipole is product of the local electromagnetic field and a polarizability matrix

$$\begin{pmatrix} \mathbf{p}(\mathbf{R}+\mathbf{r}_i) \\ \mathbf{m}(\mathbf{R}+\mathbf{r}_i) \end{pmatrix} = \hat{\alpha}_i \cdot \begin{pmatrix} \mathbf{e}_{loc}(\mathbf{R}+\mathbf{r}_i) \\ \mathbf{h}_{loc}(\mathbf{R}+\mathbf{r}_i) \end{pmatrix}. \tag{1.26}$$

Here $\mathbf{p}_i(\mathbf{R}+\mathbf{r}_i)$ and $\mathbf{m}_i(\mathbf{R}+\mathbf{r}_i)$ are the magnetic moments of the i'th particle in the unit cell represented by the lattice vector $\mathbf{R}$, α_i is the polarizability of the i'th particle and $\mathbf{e}_{loc}(\mathbf{R}+\mathbf{r}_i)$ and $\mathbf{h}_{loc}(\mathbf{R}+\mathbf{r}_i)$ are the local microscopic fields at the location of the i'th particle in the $\mathbf{R}$ unit cell. As mentioned earlier, the metamaterial crystal is driven with external currents that are harmonic in time and space

$$\begin{aligned} \mathbf{E}_{ext}(\mathbf{r}) &= \mathbf{E}^0_{ext} e^{\mathrm{i}(\omega t - \mathbf{k}\cdot\mathbf{x})}, \\ \mathbf{H}_{ext}(\mathbf{r}) &= \mathbf{H}^0_{ext} e^{\mathrm{i}(\omega t - \mathbf{k}\cdot\mathbf{x})}. \end{aligned} \tag{1.27}$$

These externally imposed fields are in principle generated by external electric and magnetic polarizations/currents. The dipole moments are related to the external fields and are solved for using a Green's function. The solution is available in the original paper (Ref. [40]) but for the sake of brevity we will not reprint it. The average polarization density is assumed to be

$$\begin{pmatrix}\mathbf{P}(\mathbf{r})\\ \mathbf{M}(\mathbf{r})\end{pmatrix} \equiv \frac{e^{-i\mathbf{k}\cdot\mathbf{r}}}{V}\sum_{j}^{n}\begin{pmatrix}\mathbf{p}(\mathbf{r}_j)\\ \mathbf{m}(\mathbf{r}_j)\end{pmatrix} e^{i\mathbf{k}\cdot\mathbf{r}_j} \tag{1.28}$$

This is the same field averaging method used by Silveirinha [54] for the electrical polarization density though Li allows for the possibility of magnetic inclusions being present in the unit cell and therefore a nonzero macroscopic magnetic polarization density. The ratio between the macroscopic polarization density and the external driving fields is then related to the macroscopic susceptibility $\hat{\chi}$ (we will do the same in Chapter 5), and the constitutive parameters are calculated as $\hat{C} = 1 + \hat{\chi}$. Li's method is the first that the author is aware of that claims to calculate all 36 constitutive parameters of a metamaterial. Andrea Alu has a similar method for calculating the constitutive parameters of arrays of interacting dipoles with similar results [6].

The limitation of these approaches is similar to the limitation of Silveirinha's method (Sec 1.4). Primarily, if one considers only electric inclusions in the unit cell then the entire response of the metamaterial is described by the permittivity and the permeability is equal to 1. However, there is a very important discovery in Li's paper. In the field of metamaterials it is conventional

wisdom that crystals with inversion symmetry do not exhibit bianisotropy (the coupling of electric and magnetic fields). Li's paper is the first to claim that bianisotropy can in fact exist in a metamaterial crystal with inversion symmetry if spatial dispersion is present. This was later predicted by the author [20, 21] as well as by Alu [6]. We will explain this unexpected result in Sec 2.2. This is still a relatively unknown phenomenon that has significant implications for the field of metamaterial research.

Chapter 2

Spatial Dispersion in Metamaterials

2.1 Nonlocal media

The electromagnetic interaction between light and matter is for most conventional materials described only with an electric permeability ϵ. This permeability is often a function of the frequency of light interacting with the material or $\epsilon = \epsilon(\omega)$. We say that this dependence of the permeability on the frequency indicates that the material is temporally dispersive. Metamaterials often are very temporally dispersive but they often have a second dependence that ordinary materials do not. Many metamaterials are also spatially dispersive (nonlocal). This means that the permittivity, and other constitutive parameters, depend not just on the frequency ω but also the wavevector $\mathbf{k}$.

Why do conventional materials not display spatial dispersion? Let's consider a typical crystalline material, say a crystal of SiO_2, and imagine a ray of red light propagating through the crystal. The lattice constant of SiO_2 is about $0.734nm$ while the wavelength of the red light beam could be about $750nm$ Because the wavelength of light is so much longer than the lattice constant of the crystal the dependence of the constitutive parameters on the wavevector is small and we can say that spatial dispersion is negligible and can

be ignored. In many metamaterials however, both the free space wavelength and the effective wavelength ($2\pi/|\mathbf{k}|$) of electromagnetic radiation propagating through the metamaterial are comparable in size to the crystal lattice constant. At best the free space wavelength might be ten times longer than the crystal lattice constant, often it is only three or four times longer. In this regime, the constitutive parameters become strongly dependent on the wavevector of the electromagnetic radiation or

$$\begin{aligned} \hat{\epsilon} &= \hat{\epsilon}(\omega, \mathbf{k}) \qquad & \hat{\xi} &= \hat{\xi}(\omega, \mathbf{k}) \\ \hat{\zeta} &= \hat{\zeta}(\omega, \mathbf{k}) \qquad & \hat{\mu} &= \hat{\mu}(\omega, \mathbf{k}) \end{aligned} \tag{2.1}$$

This dependence of the constitutive parameters on the wavevector is a phenomenon often neglected by most methods of characterizing metamaterials. For example, in S parameter retrieval (Sec. 1.3), the metamaterial is characterized by analyzing the scattering of an wave incident upon the metamaterial slab. Both the reflected and transmitted waves are coupled to a wave propagating through the metamaterial slab and reflecting off of the interior boundaries. The constitutive parameters retrieved from the measurement are the constitutive parameters at the frequency ω as well as the wavevector $\mathbf{k}$ of the internally propagating wave. However, since the wave inside the metamaterial slab is a freely propagating wave it is restricted by a dispersion relation that relates the wavevector to the frequency or $\mathbf{k} = \mathbf{k}(\omega)$. Thus the constitutive parameters returned by S parameter retrieval are actually functions of ω or $\epsilon = \epsilon(\omega, \mathbf{k}(\omega))$ and $\mu = \mu(\omega, \mathbf{k}(\omega))$.

Ignoring the spatial dependence of the constitutive parameters has a number of consequences. Much of the strange and apparently unphysical behavior of metamaterials can be traced to the fact that researchers often overlook that metamaterials are spatially dispersive. The focus of this chapter is to illuminate the effects of spatial dispersion in metamaterial crystals and look at some of the ways that spatial dispersion manifests in metamaterials.

2.2 Symmetry of Crystals and their Constitutive Parameters

The symmetry of a crystal affects the symmetry of its constitutive tensors and pseudotensors. For example, take a dielectric crystal whose permittivity depends only on ω (we are ignoring spatial dispersion for the moment). In general the permittivity of this temporally dispersive crystal is represented by a 3×3 permittivity tensor

$$\hat{\epsilon}(\omega) = \begin{pmatrix} \epsilon_{xx} & \epsilon_{xy} & \epsilon_{xz} \\ \epsilon_{yx} & \epsilon_{yy} & \epsilon_{yz} \\ \epsilon_{zx} & \epsilon_{zy} & \epsilon_{zz} \end{pmatrix} \tag{2.2}$$

If the crystal has a geometric symmetry, this will constrict the possible values of the permittivity tensor. We refer to $\hat{\epsilon}$ as a tensor because if we perform a simple coordinate transformation $\hat{\epsilon}$ will transform according to the rule $\hat{\epsilon}(\omega)' = \mathrm{T}\hat{\epsilon}(\omega)\mathrm{T}^{\mathsf{T}}$ where T is a spatial transformation matrix that defines a rotation or spatial reflection (here we limit ourselves to the simple transformations that make up the *orthogonal group* of transformations in three spatial

dimensions or $O(3)$). Any geometric symmetry of the crystal will manifest itself in the structure of the tensor. If the crystal remains invariant under a certain transformation, then any tensor (pseudotensor) describing the crystal should also remain invariant under that transformation. So if the crystal is symmetric under a spatial reflection, say a reflection in the $\hat{\mathbf{x}}$ direction, this implies that the permittivity must be invariant under that spatial reflection or $\hat{\epsilon}(\omega) = \mathrm{T}_{-\hat{\mathbf{x}}}\hat{\epsilon}(\omega)\mathrm{T}^{\mathsf{T}}_{-\hat{\mathbf{x}}}$. Here the spatial reflection transformation operator is $\mathrm{T}_{-\hat{\mathbf{x}}} = diag(-1, 1, 1)$. For the individual components of the permittivity tensor, this implies

$$\hat{\epsilon} = \begin{pmatrix} \epsilon_{xx} & \epsilon_{xy} & \epsilon_{xz} \\ \epsilon_{yx} & \epsilon_{yy} & \epsilon_{yz} \\ \epsilon_{zx} & \epsilon_{zy} & \epsilon_{zz} \end{pmatrix} = \begin{pmatrix} \epsilon_{xx} & -\epsilon_{xy} & -\epsilon_{xz} \\ -\epsilon_{yx} & \epsilon_{yy} & \epsilon_{yz} \\ -\epsilon_{zx} & \epsilon_{zy} & \epsilon_{zz} \end{pmatrix} = \begin{pmatrix} \epsilon_{xx} & 0 & 0 \\ 0 & \epsilon_{yy} & \epsilon_{yz} \\ 0 & \epsilon_{zy} & \epsilon_{zz} \end{pmatrix} \tag{2.3}$$

Additional reflection symmetries will also constrain the structure of the permittivity tensor. A symmetry under reflection in the $\hat{\mathbf{y}}$ direction implies

$$\hat{\epsilon} = \begin{pmatrix} \epsilon_{xx} & 0 & 0 \\ 0 & \epsilon_{yy} & \epsilon_{yz} \\ 0 & \epsilon_{zy} & \epsilon_{zz} \end{pmatrix} = \begin{pmatrix} \epsilon_{xx} & 0 & 0 \\ 0 & \epsilon_{yy} & -\epsilon_{yz} \\ 0 & -\epsilon_{zy} & \epsilon_{zz} \end{pmatrix} = \begin{pmatrix} \epsilon_{x} & 0 & 0 \\ 0 & \epsilon_{y} & 0 \\ 0 & 0 & \epsilon_{z} \end{pmatrix} \tag{2.4}$$

If the crystal has more symmetries, then the permittivity tensor will be constrained in other ways. If, for example, the crystal is symmetric under a 90° rotation around the $\hat{\mathbf{z}}$ axis then the permittivity tensor must be invariant under the 90° rotation described by the transformation matrix

$$\mathrm{T}_{90^\circ} = \begin{pmatrix} 0 & 1 & 0 \\ 1 & 0 & 0 \\ 0 & 0 & 1 \end{pmatrix}. \tag{2.5}$$

This implies that the permittivity tensor has the symmetry $\hat{\epsilon}(\omega) = \mathrm{T}_{90^\circ}\hat{\epsilon}(\omega)\mathrm{T}_{90^\circ}^{\mathsf{T}}$ or

$$\hat{\epsilon} = \begin{pmatrix} \epsilon_x & 0 & 0 \\ 0 & \epsilon_y & 0 \\ 0 & 0 & \epsilon_z \end{pmatrix} = \begin{pmatrix} \epsilon_y & 0 & 0 \\ 0 & \epsilon_x & 0 \\ 0 & 0 & \epsilon_z \end{pmatrix} = \begin{pmatrix} \epsilon_\perp & 0 & 0 \\ 0 & \epsilon_\perp & 0 \\ 0 & 0 & \epsilon_z \end{pmatrix}, \tag{2.6}$$

giving us a so-called uniaxial permittivity tensor [32].

While $\hat{\epsilon}$ and $\hat{\mu}$ are tensors, the bianisotropic constitutive matrices $\hat{\xi}$ and $\hat{\zeta}$ are pseudotensors. This means that when transforming under a simple $O(3)$ transformation (spatial rotations and reflections) the pseudotensors transform like $\hat{\xi}(\omega)' = det(\mathrm{T})\mathrm{T}\hat{\xi}(\omega)\mathrm{T}^{\mathsf{T}}$ where $det(\mathrm{T})$ is the determinant of the transformation matrix T. For a crystal that has inversion symmetry the transformation matrix is $\mathrm{T}_{inv} = diag(-1,-1,-1)$ implying (ignoring spatial dispersion) $\hat{\xi}(\omega) = det(\mathrm{T})\mathrm{T}\hat{\xi}(\omega)\mathrm{T}^{\mathsf{T}} = -\hat{\xi}(\omega) = 0$ as well as $\zeta(\omega) = 0$. Thus we see that for a crystal with inversion symmetry and negligible spatial dispersion there should be no bianisotropy.

The belief that metamaterial crystals with inversion symmetry cannot manifest bianisotropy is widely held but is not correct. The argument we just reviewed assumed that the constitutive parameters were only functions of ω, but for metamaterial crystals where the free space wavelength is often of comparable size to the crystal lattice constant, spatial dispersion becomes a

strong and important effect. As a result, the constitutive parameters become functions of both ω and $\mathbf{k}$.

Let us review the above argument about the transformation of the bianisotropic pseudotensors while taking into consideration spatial dispersion. If the metamaterial crystal is geometrically symmetric under a spatial inversion then then this implies $\hat{\xi}(\omega, \mathbf{k}) = det(\mathrm{T}_{inv})\mathrm{T}_{inv}\hat{\xi}(\omega, \mathrm{T}_{inv}\mathbf{k})\mathrm{T}_{inv}^{\mathsf{T}} = -\hat{\xi}(\omega, -\mathbf{k})$ and similarly $\hat{\zeta}(\omega, \mathbf{k}) = -\hat{\zeta}(\omega, -\mathbf{k})$. So for a crystal with spatial dispersion, inversion symmetry does not imply absence of bianisotropy but instead implies a symmetry of the bianisotropic pseudotensor under the reversal of the wavevector $\mathbf{k}$. Thus, when spatial dispersion is present a crystal with inversion symmetry can exhibit bianisotropy. We refer to this bianisotropy as *extrinsic* bianisotropy as opposed to the *intrinsic* bianisotropy caused by a crystal's asymmetry. This was first suggested by Jensen Li [40] and later confirmed by the author [20, 21] and Andrea Alu [6]. Another implication of this result is that the bianisotropy has an odd dependence on $\mathbf{k}$ which also implies that $\hat{\xi}(\omega, 0) = 0$ and $\hat{\zeta}(\omega, 0) = 0$.

We now examine the argument earlier in this section about the symmetry of the permittivity tensor $\hat{\epsilon}$ only now let us apply it to the pseudotensor $\hat{\xi}$ while accounting for spatial dispersion. For a crystal with reflection symmetry in the $\hat{\mathbf{x}}$ direction we must distinguish between wavevectors that are parallel and perpendicular to the $\hat{\mathbf{x}}$ direction. If we assume that the wavevector is parallel to the $\hat{\mathbf{x}}$ direction or $\mathbf{k} = k_x\hat{\mathbf{x}}$, the result of reflection symmetry in the $\hat{\mathbf{x}}$ direction is $\hat{\xi}(\omega, k_x\hat{\mathbf{x}}) = det(\mathrm{T}_{-\hat{\mathbf{x}}})\mathrm{T}_{-\hat{\mathbf{x}}}\hat{\xi}(\omega, \mathrm{T}_{-\hat{\mathbf{x}}}k_x\hat{\mathbf{x}})\mathrm{T}_{-\hat{\mathbf{x}}}^{\mathsf{T}} = -\mathrm{T}_{-\hat{\mathbf{x}}}\hat{\xi}(\omega, -k_x\hat{\mathbf{x}})\mathrm{T}_{-\hat{\mathbf{x}}}^{\mathsf{T}}$

or

$$\begin{aligned}\hat{\xi}(\omega,\mathbf{k}) &= \begin{pmatrix}\xi_{xx}(\omega,k_x\hat{\mathbf{x}}) & \xi_{xy}(\omega,k_x\hat{\mathbf{x}}) & \xi_{xz}(\omega,k_x\hat{\mathbf{x}})\\ \xi_{yx}(\omega,k_x\hat{\mathbf{x}}) & \xi_{yy}(\omega,k_x\hat{\mathbf{x}}) & \xi_{yz}(\omega,k_x\hat{\mathbf{x}})\\ \xi_{zx}(\omega,k_x\hat{\mathbf{x}}) & \xi_{zy}(\omega,k_x\hat{\mathbf{x}}) & \xi_{zz}(\omega,k_x\hat{\mathbf{x}})\end{pmatrix}\\ &= \begin{pmatrix}-\xi_{xx}(\omega,-k_x\hat{\mathbf{x}}) & \xi_{xy}(\omega,-k_x\hat{\mathbf{x}}) & \xi_{xz}(\omega,-k_x\hat{\mathbf{x}})\\ \xi_{yx}(\omega,-k_x\hat{\mathbf{x}}) & -\xi_{yy}(\omega,-k_x\hat{\mathbf{x}}) & -\xi_{yz}(\omega,-k_x\hat{\mathbf{x}})\\ \xi_{zx}(\omega,-k_x\hat{\mathbf{x}}) & -\xi_{zy}(\omega,-k_x\hat{\mathbf{x}}) & -\xi_{zz}(\omega,-k_x\hat{\mathbf{x}})\end{pmatrix},\end{aligned} \tag{2.7}$$

If, as before, we assume additional reflection symmetries, symmetry of the crystal under reflection in the $\hat{\mathbf{y}}$ direction implies $\hat{\xi}(\omega,k_x\hat{\mathbf{x}}) = det(\mathrm{T}_{-\hat{\mathbf{y}}})\mathrm{T}_{-\hat{\mathbf{y}}}\hat{\xi}(\omega,\mathrm{T}_{-\hat{\mathbf{y}}}k_x\hat{\mathbf{x}})\mathrm{T}^{\mathsf{T}}_{-\hat{\mathbf{y}}} = -\mathrm{T}_{-\hat{\mathbf{y}}}\hat{\xi}(\omega,k_x\hat{\mathbf{x}})\mathrm{T}^{\mathsf{T}}_{-\hat{\mathbf{y}}}$ or

$$\begin{aligned}\hat{\xi}(\omega,\mathbf{k}) &= \begin{pmatrix}\xi_{xx}(\omega,k_x\hat{\mathbf{x}}) & \xi_{xy}(\omega,k_x\hat{\mathbf{x}}) & \xi_{xz}(\omega,k_x\hat{\mathbf{x}})\\ \xi_{yx}(\omega,k_x\hat{\mathbf{x}}) & \xi_{yy}(\omega,k_x\hat{\mathbf{x}}) & \xi_{yz}(\omega,k_x\hat{\mathbf{x}})\\ \xi_{zx}(\omega,k_x\hat{\mathbf{x}}) & \xi_{zy}(\omega,k_x\hat{\mathbf{x}}) & \xi_{zz}(\omega,k_x\hat{\mathbf{x}})\end{pmatrix}\\ &= \begin{pmatrix}-\xi_{xx}(\omega,k_x\hat{\mathbf{x}}) & \xi_{xy}(\omega,k_x\hat{\mathbf{x}}) & -\xi_{xz}(\omega,k_x\hat{\mathbf{x}})\\ \xi_{yx}(\omega,k_x\hat{\mathbf{x}}) & -\xi_{yy}(\omega,k_x\hat{\mathbf{x}}) & \xi_{yz}(\omega,k_x\hat{\mathbf{x}})\\ -\xi_{zx}(\omega,k_x\hat{\mathbf{x}}) & \xi_{zy}(\omega,k_x\hat{\mathbf{x}}) & -\xi_{zz}(\omega,k_x\hat{\mathbf{x}})\end{pmatrix}\\ &= \begin{pmatrix}0 & \xi_{xy}(\omega,k_x\hat{\mathbf{x}}) & 0\\ \xi_{yx}(\omega,k_x\hat{\mathbf{x}}) & 0 & \xi_{yz}(\omega,k_x\hat{\mathbf{x}})\\ 0 & \xi_{zy}(\omega,k_x\hat{\mathbf{x}}) & 0\end{pmatrix},\end{aligned} \tag{2.8}$$

And similarly, an additional symmetry of the crystal under reflection in the $\hat{\mathbf{z}}$ direction implies $\hat{\xi}(\omega,k_x\hat{\mathbf{x}}) = det(\mathrm{T}_{-\hat{\mathbf{z}}})\mathrm{T}_{-\hat{\mathbf{z}}}\hat{\xi}(\omega,\mathrm{T}_{-\hat{\mathbf{z}}}k_x\hat{\mathbf{x}})\mathrm{T}^{\mathsf{T}}_{-\hat{\mathbf{z}}} =$
$-\mathrm{T}_{-\hat{\mathbf{z}}}\hat{\xi}(\omega,k_x\hat{\mathbf{x}})\mathrm{T}^{\mathsf{T}}_{-\hat{\mathbf{z}}}$ or

$$
\begin{aligned}
\hat{\xi}(\omega, \mathbf{k}) &= \begin{pmatrix} 0 & \xi_{xy}(\omega, k_x\hat{\mathbf{x}}) & 0 \\ \xi_{yx}(\omega, k_x\hat{\mathbf{x}}) & 0 & \xi_{yz}(\omega, k_x\hat{\mathbf{x}}) \\ 0 & \xi_{zy}(\omega, k_x\hat{\mathbf{x}}) & 0 \end{pmatrix} \\
&= \begin{pmatrix} 0 & -\xi_{xy}(\omega, k_x\hat{\mathbf{x}}) & 0 \\ -\xi_{yx}(\omega, k_x\hat{\mathbf{x}}) & 0 & \xi_{yz}(\omega, k_x\hat{\mathbf{x}}) \\ 0 & \xi_{zy}(\omega, k_x\hat{\mathbf{x}}) & 0 \end{pmatrix} \qquad (2.9) \\
&= \begin{pmatrix} 0 & 0 & 0 \\ 0 & 0 & \xi_{yz}(\omega, k_x\hat{\mathbf{x}}) \\ 0 & \xi_{zy}(\omega, k_x\hat{\mathbf{x}}) & 0 \end{pmatrix},
\end{aligned}
$$

Thus we see the reflection symmetry in the $\hat{\mathbf{y}}$ and $\hat{\mathbf{z}}$ directions force a number of components of $\hat{\xi}$ to zero, but because $\mathbf{k} = k_x\hat{\mathbf{x}}$, the wavevector breaks the symmetry of the crystal in the $\hat{\mathbf{x}}$ direction and implies that the remaining components ξ_{yz} and ξ_{zy} are odd in k_x. The pseudotensor $\hat{\zeta}$ has the same symmetry.

Though the main result of this section is that spatial dispersion can cause bianisotropy to be present in crystals with inversion symmetry, spatial dispersion does not just affect the bianisotropic constitutive parameters. Let us take another look at the symmetry of the permittivity tensor $\hat{\epsilon}$ while accounting for spatial dispersion. Once again we assume that the wavevector is parallel to the $\hat{\mathbf{x}}$ direction. For a crystal with reflection symmetry in the $\hat{\mathbf{x}}$ direction this implies

$$\begin{aligned}
\hat{\epsilon}(\omega,\mathbf{k}) &= \begin{pmatrix} \epsilon_{xx}(\omega,k_x\hat{\mathbf{x}}) & \epsilon_{xy}(\omega,k_x\hat{\mathbf{x}}) & \epsilon_{xz}(\omega,k_x\hat{\mathbf{x}}) \\ \epsilon_{yx}(\omega,k_x\hat{\mathbf{x}}) & \epsilon_{yy}(\omega,k_x\hat{\mathbf{x}}) & \epsilon_{yz}(\omega,k_x\hat{\mathbf{x}}) \\ \epsilon_{zx}(\omega,k_x\hat{\mathbf{x}}) & \epsilon_{zy}(\omega,k_x\hat{\mathbf{x}}) & \epsilon_{zz}(\omega,k_x\hat{\mathbf{x}}) \end{pmatrix} \\
&= \begin{pmatrix} \epsilon_{xx}(\omega,-k_x\hat{\mathbf{x}}) & -\epsilon_{xy}(\omega,-k_x\hat{\mathbf{x}}) & -\epsilon_{xz}(\omega,-k_x\hat{\mathbf{x}}) \\ -\epsilon_{yx}(\omega,-k_x\hat{\mathbf{x}}) & \epsilon_{yy}(\omega,-k_x\hat{\mathbf{x}}) & \epsilon_{yz}(\omega,-k_x\hat{\mathbf{x}}) \\ -\epsilon_{zx}(\omega,-k_x\hat{\mathbf{x}}) & \epsilon_{zy}(\omega,-k_x\hat{\mathbf{x}}) & \epsilon_{zz}(\omega,-k_x\hat{\mathbf{x}}) \end{pmatrix},
\end{aligned} \tag{2.10}$$

An additional symmetry of the crystal under reflection in the $\hat{\mathbf{y}}$ direction implies

$$\begin{aligned}
\hat{\epsilon}(\omega,\mathbf{k}) &= \begin{pmatrix} \epsilon_{xx}(\omega,k_x\hat{\mathbf{x}}) & \epsilon_{xy}(\omega,k_x\hat{\mathbf{x}}) & \epsilon_{xz}(\omega,k_x\hat{\mathbf{x}}) \\ \epsilon_{yx}(\omega,k_x\hat{\mathbf{x}}) & \epsilon_{yy}(\omega,k_x\hat{\mathbf{x}}) & \epsilon_{yz}(\omega,k_x\hat{\mathbf{x}}) \\ \epsilon_{zx}(\omega,k_x\hat{\mathbf{x}}) & \epsilon_{zy}(\omega,k_x\hat{\mathbf{x}}) & \epsilon_{zz}(\omega,k_x\hat{\mathbf{x}}) \end{pmatrix} \\
&= \begin{pmatrix} \epsilon_{xx}(\omega,k_x\hat{\mathbf{x}}) & -\epsilon_{xy}(\omega,k_x\hat{\mathbf{x}}) & \epsilon_{xz}(\omega,k_x\hat{\mathbf{x}}) \\ -\epsilon_{yx}(\omega,k_x\hat{\mathbf{x}}) & \epsilon_{yy}(\omega,k_x\hat{\mathbf{x}}) & -\epsilon_{yz}(\omega,k_x\hat{\mathbf{x}}) \\ \epsilon_{zx}(\omega,k_x\hat{\mathbf{x}}) & -\epsilon_{zy}(\omega,k_x\hat{\mathbf{x}}) & \epsilon_{zz}(\omega,k_x\hat{\mathbf{x}}) \end{pmatrix} \\
&= \begin{pmatrix} \epsilon_{xx}(\omega,k_x\hat{\mathbf{x}}) & 0 & \epsilon_{xz}(\omega,k_x\hat{\mathbf{x}}) \\ 0 & \epsilon_{yy}(\omega,k_x\hat{\mathbf{x}}) & 0 \\ \epsilon_{zx}(\omega,k_x\hat{\mathbf{x}}) & 0 & \epsilon_{zz}(\omega,k_x\hat{\mathbf{x}}) \end{pmatrix},
\end{aligned} \tag{2.11}$$

Again we seen that reflection symmetry in the $\hat{\mathbf{y}}$ direction restricts a number of components of $\hat{\epsilon}$ to zero, but the wavevector $\mathbf{k} = k_x\hat{\mathbf{x}}$ breaks the symmetry of the crystal in the $\hat{\mathbf{x}}$ direction forcing the components ϵ_{xx}, ϵ_{yy} and ϵ_{zz} to be even with respect to k_x and ϵ_{xz} and ϵ_{zx} to be odd with respect to k_x. The tensor μ has the same symmetry.

All of the symmetry properties we have derived depend on the particular symmetry of the crystal of interest. Different crystals will have different

geometric symmetries and therefore different symmetries of their constitutive parameters. However, one general conclusion can be drawn: for crystals with spatial dispersion the wavevector $\mathbf{k}$ can break the preexisting symmetry of a crystal, causing components of the constitutive parameters that would normally be zero to have a nonzero value. This is true for both the tensor parameters ϵ and μ as well as the pseudotensor parameters ξ and ζ.

2.3 Energy Density and Poynting Flux

It is well known that materials with strong temporal dispersion physically manifest this dispersion in a way that makes them different from nondispersive materials. A well known example is the energy density of an electromagnetic wave inside a medium. For a nondispersive material the energy density is

$$U = \frac{\epsilon}{2}\mathbf{E}^2 + \frac{\mu}{2}\mathbf{H}^2. \tag{2.12}$$

where ϵ and μ are the isotropic permittivity and permeability of the material. However, in a material with strong temporal dispersion the energy density is [26]

$$U = \frac{1}{2}\frac{\partial(\omega\epsilon)}{\partial\omega}\mathbf{E}^2 + \frac{1}{2}\frac{\partial(\omega\mu)}{\partial\omega}\mathbf{H}^2. \tag{2.13}$$

Here we have allowed for temporal dispersion in μ as well as ϵ. We see that the dependence of ϵ and μ on the frequency ω has altered the expression for

energy density. If ϵ and μ are approximately constant with respect to ω then Eq.(2.13) reduces to Eq.(2.12).

It is less well known that spatial dispersion can also modify the standard expressions for energy. Specifically, spatial dispersion affects the expression for energy flux [4, 37, 30]. The standard treatment of the Poynting flux in a material with spatial dispersion only considers spatial dispersion in ϵ. A more general treatment for metamaterials that potentially have spatial dispersion in the other constitutive parameters μ, ξ and ζ is required. Here we present a general derivation of the energy density, Poynting flux and energy loss inside a linear material characterized by 36 constitutive parameters with both temporal and spatial dispersion. In doing so we will shed some light on an important aspect of calculating loss inside a metamaterial.

The time averaged work done by electric current onto an electromagnetic field in volume V of an effective medium is given by

$$\begin{aligned} W &= \left\langle -\int_V d^3x \mathbf{E}\cdot\mathbf{J} \right\rangle \\ &= \int_V d^3x \left\langle \nabla\cdot(c\mathbf{E}\times\mathbf{H}) + \mathbf{E}\cdot\frac{\partial\mathbf{D}}{\partial t} + \mathbf{H}\cdot\frac{\mathbf{B}}{\partial t} \right\rangle . \end{aligned} \tag{2.14}$$

Here the angled brackets indicate time averaging. In order to evaluate the last two terms in Eq. (2.14) it is convenient to express the electromagnetic fields as the 6 component vectors

$$\mathbf{F} = \begin{pmatrix} \mathbf{E} \\ \mathbf{H} \end{pmatrix}, \qquad \mathbf{G} = \begin{pmatrix} \mathbf{D} \\ \mathbf{B} \end{pmatrix}. \tag{2.15}$$

We are mostly interested in plane waves, or at least long wave packets that can be approximated as plane waves. Thus, we can represent the $\mathbf{F}$ and $\mathbf{G}$ fields as

$$\begin{aligned}\mathbf{F}(t,\mathbf{x}) &= \frac{\mathbf{F}_0(t,\mathbf{x})e^{\mathrm{i}(\omega_0 t-\mathbf{k}_0\cdot\mathbf{x})}+c.c.}{2}\\ \mathbf{G}(t,\mathbf{x}) &= \frac{\mathbf{G}_0(t,\mathbf{x})e^{\mathrm{i}(\omega_0 t-\mathbf{k}_0\cdot\mathbf{x})}+c.c.}{2}\end{aligned} \tag{2.16}$$

where *c.c.* denotes the complex conjugate of the preceding term, ω_0 and $\mathbf{k}_0$ are the real valued carrier frequency and wavevector of the approximately monochromatic fields. Any change in the field amplitude including exponential decay is included in the slowly varying field envelopes given by

$$\begin{aligned}\mathbf{F}_0(t,\mathbf{x}) &= \int \frac{d\alpha d^3q}{(2\pi)^4}\ \ \mathbf{F}_0(\alpha,\mathbf{q})e^{\mathrm{i}(\alpha t-\mathbf{q}\cdot\mathbf{x})},\\ \mathbf{G}_0(t,\mathbf{x}) &= \int \frac{d\alpha d^3q}{(2\pi)^4}\ \ C(\omega_0+\alpha,\mathbf{k}_0+\mathbf{q})\cdot\mathbf{F}_0(\alpha,\mathbf{q})e^{\mathrm{i}(\alpha t-\mathbf{q}\cdot\mathbf{x})}.\end{aligned} \tag{2.17}$$

We evaluate the partial derivative of $\mathbf{G}_0e^{\mathrm{i}(\omega_0 t-\mathbf{k}_0\cdot\mathbf{x})}$ with respect to time and by expanding ωC as a Taylor series to first order in $\omega-\omega_0$ and $\mathbf{k}-\mathbf{k}_0$ we get

$$
\begin{aligned}
&\frac{\partial}{\partial t}\left(\mathbf{G}_0(t,\mathbf{x})e^{\mathrm{i}(\omega_0 t-\mathbf{k}_0\cdot\mathbf{x})}\right)\\
\simeq\ &\left|\mathrm{i}\omega C(\omega,\mathbf{k})\cdot\mathbf{F}_0+\alpha\frac{\partial(\omega C(\omega,\mathbf{k}))}{\partial\omega}\cdot\mathbf{F}_0+q_i\frac{\partial(\omega C(\omega,\mathbf{k}))}{\partial k_i}\cdot\mathbf{F}_0\right|_{\substack{\omega=\omega_0\\ \mathbf{k}=\mathbf{k}_0}} e^{\mathrm{i}(\omega_0 t-\mathbf{k}_0\cdot\mathbf{x})}\\
=\ &\left|\mathrm{i}\omega C(\omega,\mathbf{k})\cdot\mathbf{F}_0+\frac{\partial(\omega C(\omega,\mathbf{k}))}{\partial\omega}\cdot\frac{\partial\mathbf{F}_0}{\partial t}-\frac{\partial(\omega C(\omega,\mathbf{k}))}{\partial k_i}\cdot\frac{\partial\mathbf{F}_0}{\partial x_i}\right|_{\substack{\omega=\omega_0\\ \mathbf{k}=\mathbf{k}_0}} e^{\mathrm{i}(\omega_0 t-\mathbf{k}_0\cdot\mathbf{x})}.
\end{aligned}
\tag{2.18}
$$

We emphasize that ωC and its partial derivatives are evaluated at $\omega=\omega_0$ and $\mathbf{k}=\mathbf{k}_0$ which are real valued. After time averaging the last two terms in Eq. (2.14) we get the result

$$
\begin{aligned}
&\left\langle\mathbf{E}\cdot\frac{\partial\mathbf{D}}{\partial t}+\mathbf{H}\cdot\frac{\partial\mathbf{G}}{\partial t}\right\rangle=\left\langle\mathbf{F}\cdot\frac{\partial\mathbf{G}}{\partial t}\right\rangle\\
=\ &\frac{1}{2}\left[-\mathbf{F}_0^{\dagger}\cdot\left|\frac{\omega C(\omega,\mathbf{k})}{2\mathrm{i}}+h.c.\right|_{\substack{\omega=\omega_0\\ \mathbf{k}=\mathbf{k}_0}}\cdot\mathbf{F}_0\right.\\
&+\frac{1}{2}\frac{\partial}{\partial t}\left(\mathbf{F}_0^{\dagger}\cdot\frac{1}{2}\left|\frac{\partial(\omega C(\omega,\mathbf{k}))}{\partial\omega}+h.c.\right|_{\substack{\omega=\omega_0\\ \mathbf{k}=\mathbf{k}_0}}\cdot\mathbf{F}_0\right)\\
&-\frac{1}{2}\left(\frac{\partial\mathbf{F}_0{}^{\dagger}}{\partial t}\cdot\frac{1}{2}\left|\frac{\partial(\omega C(\omega,\mathbf{k}))}{\partial\omega}-h.c.\right|_{\substack{\omega=\omega_0\\ \mathbf{k}=\mathbf{k}_0}}\cdot\mathbf{F}_0\right)+
\end{aligned}
$$

$$
\begin{aligned}
&+\frac{1}{2}\left(\mathbf{F}_0^\dagger\cdot\frac{1}{2}\left|\frac{\partial(\omega C(\omega,\mathbf{k}))}{\partial\omega}-h.c.\right|_{\substack{\omega=\omega_0\\ \mathbf{k}=\mathbf{k}_0}}\cdot\frac{\partial\mathbf{F}_0}{\partial t}\right)\\
&-\frac{1}{2}\frac{\partial}{\partial x_k}\left(\mathbf{F}_0^\dagger\cdot\frac{1}{2}\left|\frac{\partial(\omega C(\omega,\mathbf{k}))}{\partial k_k}+h.c.\right|_{\substack{\omega=\omega_0\\ \mathbf{k}=\mathbf{k}_0}}\cdot\mathbf{F}_0\right)\\
&+\frac{1}{2}\left(\frac{\partial\mathbf{F}_0}{\partial x_k}^\dagger\cdot\frac{1}{2}\left|\frac{\partial(\omega C(\omega,\mathbf{k}))}{\partial k_k}-h.c.\right|_{\substack{\omega=\omega_0\\ \mathbf{k}=\mathbf{k}_0}}\cdot\mathbf{F}_0\right)\\
&-\frac{1}{2}\left(\mathbf{F}_0^\dagger\cdot\frac{1}{2}\left|\frac{\partial(\omega C(\omega,\mathbf{k}))}{\partial k_k}-h.c.\right|_{\substack{\omega=\omega_0\\ \mathbf{k}=\mathbf{k}_0}}\cdot\frac{\partial\mathbf{F}_0}{\partial x_k}\right)\Bigg]\\
=\;&-\frac{1}{2}\mathbf{F}_0^*\cdot M^L\cdot\mathbf{F}_0+\frac{1}{4}\frac{\partial}{\partial t}\left(\mathbf{F}_0^*\cdot M^E\cdot\mathbf{F}_0\right)-\frac{1}{4}\frac{\partial}{\partial x_k}\left(\mathbf{F}_0^*\cdot M_i^S\cdot\mathbf{F}_0\right)\\
&+\frac{\mathrm{i}}{2}\Bigg[-\frac{\partial\mathbf{F}_0}{\partial t}^\dagger\cdot M_\omega^A\cdot\mathbf{F}_0+\mathbf{F}_0^\dagger\cdot M_\omega^A\cdot\frac{\partial\mathbf{F}_0}{\partial t}\\
&+\frac{\partial\mathbf{F}_0}{\partial x_i}^\dagger\cdot M_{k_i}^A\cdot\mathbf{F}_0-\mathbf{F}_0^\dagger\cdot M_{k_i}^A\cdot\frac{\partial\mathbf{F}_0}{\partial x_i}\Bigg],
\end{aligned}
\tag{2.19}
$$

where h.c. denotes the hermitian conjugate of the preceding term and the 6×6 matrices M^L, M^E, M_k^S, M_ω^A and $M_{k_i}^A$ are given by

$$
\begin{aligned}
M^L &= \frac{1}{2\mathrm{i}}\left|\omega C(\omega,\mathbf{k}) - h.c.\right|_{\substack{\omega=\omega_0\\ \mathbf{k}=\mathbf{k}_0}}, \\
M^E &= \frac{1}{2}\left|\frac{\partial(\omega C(\omega,\mathbf{k}))}{\partial\omega} + h.c.\right|_{\substack{\omega=\omega_0\\ \mathbf{k}=\mathbf{k}_0}}, \\
M_i^S &= \frac{1}{2}\left|\frac{\omega\partial(C(\omega,\mathbf{k}))}{\partial k_i} + h.c.\right|_{\substack{\omega=\omega_0\\ \mathbf{k}=\mathbf{k}_0}}, \\
M_\omega^A &= \frac{1}{2\mathrm{i}}\left|\frac{\partial(\omega C(\omega,\mathbf{k}))}{\partial\omega} - h.c.\right|_{\substack{\omega=\omega_0\\ \mathbf{k}=\mathbf{k}_0}}, \\
M_{k_i}^A &= \frac{1}{2\mathrm{i}}\left|\frac{\omega\partial(C(\omega,\mathbf{k}))}{\partial k_i} - h.c.\right|_{\substack{\omega=\omega_0\\ \mathbf{k}=\mathbf{k}_0}}.
\end{aligned}
\tag{2.20}
$$

When we combine Eq. (2.3) with Eq. (2.14) and group different terms depending on the partial derivatives operating on them, we see that terms entirely differentiated with respect to time are identified as the change in energy density, terms entirely differentiated with respect to space are identified with Poynting (energy) flux and terms with no derivatives represent energy loss. There are also several anomalous terms that have no total partial derivatives. When these terms are non-negligible, there is no simple way to divide the various terms into energy loss, Poynting flux or change in total energy [4]. When the anomalous terms are negligible, we get an equation relating time averaged work W, Poynting flux P and loss L to the change in the time averaged energy density U

$$W + P - L = \frac{\partial U}{\partial t}, \tag{2.21}$$

where

$$\begin{aligned} P &= -\textstyle\int_\Omega d\mathbf{n} \cdot \mathbf{S} \\ S_k &= \frac{1}{2}\left[\epsilon_{ijk} c \frac{E_j H_k^* + H_k E_j^*}{2} - \frac{1}{2}\mathbf{F}_0^\dagger \cdot M_i^S \cdot \mathbf{F}_0\right] \\ L &= -\frac{1}{2}\int_\Omega d^3x \mathbf{F}_0^\dagger \cdot M^L \cdot \mathbf{F}_0 \\ U &= \frac{1}{4}\int_\Omega d^3x \mathbf{F}_0^\dagger \cdot M^E \cdot \mathbf{F}_0 \end{aligned} \tag{2.22}$$

A few points should be made about these expressions. First, due to the presence of the bianisotropic constitutive parameters, there are now terms in Eq. (2.22) that are proportional to both $\mathbf{E}$ and $\mathbf{H}$. For example, the expression for energy is now

$$\begin{aligned} U = \frac{1}{4}\Bigg[&\mathbf{E}^\dagger \cdot \frac{1}{2}\left(\frac{\partial(\omega\hat{\epsilon})}{\partial\omega} + \frac{\partial(\omega\hat{\epsilon})}{\partial\omega}^\dagger\right) \cdot \mathbf{E} + \mathbf{E}^\dagger \cdot \frac{1}{2}\left(\frac{\partial(\omega\hat{\xi})}{\partial\omega} + \frac{\partial(\omega\hat{\xi})}{\partial\omega}^\dagger\right) \cdot \mathbf{H} \\ &+ \mathbf{H}^\dagger \cdot \frac{1}{2}\left(\frac{\partial(\omega\hat{\zeta})}{\partial\omega} + \frac{\partial(\omega\hat{\zeta})}{\partial\omega}^\dagger\right) \cdot \mathbf{E} + \mathbf{H}^\dagger \cdot \frac{1}{2}\left(\frac{\partial(\omega\hat{\mu})}{\partial\omega} + \frac{\partial(\omega\hat{\mu})}{\partial\omega}^\dagger\right) \cdot \mathbf{H}\Bigg] \end{aligned} \tag{2.23}$$

Now both the fields and the constitutive parameters are complex valued and the extra factor of 2 with respect to Eq. (2.12) is due to time averaging. Second, the presence of spatial dispersion creates an additional term contributing

to Poynting flux. This term is proportional to the hermitian part of first derivative of the constitutive matrix with respect to the wavevector. Though this additional term is not new for permittivity tensors with spatial dispersion [4, 37], we see that spatial dispersion in all of the constitutive parameters contribute, not just the permittivity. Third, though this is a subtle point, the matrices M^L, M^E and M_i^S are all evaluated for real valued frequencies and wavevectors. This is important in the field of metamaterials because often times constitutive parameters are calculated for waves freely propagating through a metamaterial crystal. These waves often decay in space, either due to losses or evanescence, and as a result the calculated constitutive parameters are evaluated for a complex valued wavevector. The misinterpretation of these constitutive parameters evaluated at complex valued wavevectors has resulted in the controversial phenomenon known as antiresonances. These will be discussed in Chapter 6. Next, as already mentioned, the presence of the anomalous terms in Eq. (2.3) prevents a simple division of energy changes into dissipative loss, Poynting flux and change in energy density. For practical purposes, these anomalous terms are usually negligible, but this is not always true.

Finally, this derivation relied on expanding the matrix ωC as a Taylor series to first order in $\omega - \omega_0$ and $\mathbf{k} - \mathbf{k}_0$. Implicitly, an assumption was made that higher order terms were negligible. This assumption fails in situations of anomalous dispersion, often times near a material resonance. This is important for metamaterials because metamaterial inclusions often rely on

such resonances. When this assumption fails, higher order terms become non-negligible, and the expressions in Eq. (2.22) fail.

Chapter 3

Complex Bloch Band Diagrams

3.1 Introduction

Of all the possible field configurations inside a metamaterial crystal, the ones most often of interest to researchers are eigenmodes: freely propagating modes that are uncoupled to an external current. The conventional method [29, 52] of numerically solving for crystal eigenmodes is to define the geometry of the unit cell of the crystal of interest and the differential equation that the fields must obey in this geometry and then impose Bloch periodic boundary conditions. The partial differential equation problem is then discretized using one of the many standard methods (finite element, finite integral, finite difference, etc.) thereby turning it into an algebraic eigenvalue problem with a finite number of degrees of freedom and the frequency ω as the eigenvalue. This finite size eigenvalue problem is then solved numerically. An important detail of this method is that the Bloch wavevector $\mathbf{k}$ is chosen beforehand, and the frequency is then computed as a function of the wavevector, yielding the dispersion curves $\omega = \omega(\mathbf{k})$. This is the most commonly used method for calculating dispersion curves of the electromagnetic waves propagating in photonic crystals or in closely related metamaterial crystals.

There are however, many instances where it is more convenient to specify the frequency ω and solve for the wavevector as a function of frequency: $\mathbf{k} = \mathbf{k}(\omega)$. At least four such instances can be identified. First, metamaterials often contain dispersive materials such as metals, where the dielectric function strongly depends on the frequency on the wave. In this case, the eigenfrequency problem is a nonlinear eigenvalue problem and must be solved iteratively [53]. In contrast, when solving for the wavevector as a function of frequency, the resulting eigenvalue problem only needs to be solved once. Second, it is often useful to solve for the wavevector as the eigenvalue because of the information contained in the complex wavevector including the decay lengths of the electromagnetic modes (either due to dissipative loss or because of the evanescent nature of the mode) and the figure of merit [70] of negative index modes. Third, in the majority of experiments the electromagnetic fields inside metamaterial/photonic crystals are excited by external sources producing time harmonic fields with real valued frequencies. A complex wavevector eigenvalue simulation provides the correct field distribution in the photonic crystal relevant to such an experiment as opposed to the conventional $\omega = \omega(\mathbf{k})$ eigenvalue problem which returns a complex valued ω. Fourth, this approach provides an alternative way of calculating the so-called isofrequency surfaces corresponding to $\omega(\mathbf{k}) = Constant$, where ω is real. Isofrequency diagrams are fundamentally important for predicting wave refraction at photonic crystal interfaces [47].

There are several previously published methods on calculating $\mathbf{k}(\omega)$

dispersion curves including variations of the plane wave expansion method [63, 25] and diagonalizing the crystal transfer matrix [68, 42]. A method of solving for complex wavevector dispersion curves using the Finite Element Method (FEM) has been proposed [14, 17] but only for 2D crystals. The benefits of the complex wavevector 2D FEM are becoming better appreciated and use of this method is becoming more common [72, 71, 21, 12, 22, 11]. Due to the interest in the 2D complex wavevector FEM it is appropriate to generalize it to 3D, which is in this chapter.

The FEM theory of solving for complex wavevector eigenvalue problems is explained in Sec. 3.2. The underlying field equation and the boundary conditions are discussed. In Sec. 3.3 we present a simple example of this method applied to a 3D photonic crystal. We demonstrate solving this model when the propagation direction is both parallel and oblique to the principal axes. This work was previously published in Ref. [23].

3.2 The finite element eigenvalue problem

3.2.1 The field equation

In this section we present the FEM formulation for solving for the magnetic field. Electromagnetic wave propagation is described by the Maxwell equations which can be rearranged into a wave equation for either the electric field $\mathbf{E}$ or the magnetic field $\mathbf{H}$. The wave equation for the magnetic field is

$$\nabla \times \left(\frac{1}{\epsilon} \nabla \times \mathbf{H} \right) - \mu \frac{\omega^2}{c^2} \mathbf{H} = 0. \tag{3.1}$$

Here $\epsilon(\mathbf{x})$ and $\mu(\mathbf{x})$ are the microscopic permittivity and permeability of the metamaterial/photonic crystal of interest. Due to the periodic nature of the crystal both are are assumed to be scalar functions, periodic in the crystal lattice. According to Bloch's theorem [29, 52] the magnetic field can be represented as the product of a periodic function and an exponential factor,

$$\mathbf{H}(\mathbf{x}) = \mathbf{u}(\mathbf{x}) e^{i(\omega t - \mathbf{k} \cdot \mathbf{x})}, \tag{3.2}$$

where ω is the frequency of the wave and $\mathbf{k}$ is the wavevector of the Bloch-Floquet wave. $\mathbf{u}(\mathbf{x})$ is a vector function which is periodic in the crystal lattice. By inserting Eq. (3.2) into Eq. (3.1) we obtain an equivalent field equation for $\mathbf{u}$:

$$\frac{k^2}{\epsilon}\mathbf{u} - \frac{\mathbf{k}}{\epsilon}(\mathbf{k} \cdot \mathbf{u}) - i\mathbf{k} \times \left(\frac{1}{\epsilon} \nabla \times \mathbf{u} \right) - i\nabla \times \left(\frac{1}{\epsilon} \mathbf{k} \times \mathbf{u} \right) + \nabla \times \left(\frac{1}{\epsilon} \nabla \times \mathbf{u} \right) - \mu \frac{\omega^2}{c^2} \mathbf{u} = 0, \tag{3.3}$$

which can be solved as an eigenvalue problem with the Bloch wavevector $\mathbf{k}$ as the eigenvalue. The spatial profile of the eigenmode $\mathbf{u}(\mathbf{x})$ is also recovered providing the magnetic field profile according to Eq. (3.2) and the electric field profile according to

$$\mathbf{E}(\mathbf{x}) = \frac{1}{\mathrm{i}\epsilon\omega/c}\nabla \times \mathbf{H} = \frac{1}{\mathrm{i}\epsilon\omega/c}\left(-\mathrm{i}\mathbf{k} \times \mathbf{u} + \nabla \times \mathbf{u}\right) e^{i(\omega t - \mathbf{k}\cdot\mathbf{x})} \tag{3.4}$$

3.2.2 The finite element model

There are several commercial FEM software programs (COMSOL Multiphysics by COMSOL, HFSS by Ansys, Vector Fields Opera by Cobham Technical Services, etc.) that are available for modeling metamaterial crystals. These commercial software packages provide a convenient graphical user interface for defining a crystal's geometry, meshing the computational domain, and visualizing the electromagnetic fields. This allows for models to be quickly developed and tested. Of the many commercial FEM codes available, the authors is only aware of one (COMSOL Multiphysics) that allows the user to specify the field equation to be solved. The simulation examples and results presented here were obtained using COMSOL. Several excellent references [74, 28, 56] describing the FEM are available.

The FEM is based on setting the integral of a so-called weak expression over the domain of interest to zero. Doing so ensures the field equation is satisfied and also creates boundary conditions. The weak expression corresponding to Eq. (3.3) is

$$\begin{aligned}
\mathrm{F_H}(\mathbf{v},\mathbf{u}) &= \frac{k^2}{\epsilon}\mathbf{v}\cdot\mathbf{u} - \frac{1}{\epsilon}\left(\mathbf{k}\cdot\mathbf{v}\right)\left(\mathbf{k}\cdot\mathbf{u}\right) - \mathrm{i}\frac{1}{\epsilon}\mathbf{v}\cdot\left[\mathbf{k}\times\left(\nabla\times\mathbf{u}\right)\right] \\
&\quad -\mathrm{i}\left(\nabla\times\mathbf{v}\right)\cdot\frac{1}{\epsilon}\left(\mathbf{k}\times\mathbf{u}\right) + \left(\nabla\times\mathbf{v}\right)\cdot\frac{1}{\epsilon}\left(\nabla\times\mathbf{u}\right) - \mu\frac{\omega^2}{c^2}\mathbf{v}\cdot\mathbf{u},
\end{aligned} \tag{3.5}$$

where $\mathbf{v}(\mathbf{x})$ is a test function. When the integral of the weak expression over the unit cell Ω of the crystal is set to zero, integrating by parts gives us two separate integrals (Eq. (3.6)). The first integral enforces the field equation. The second integral is over the boundary of the domain and represents a natural boundary condition [74, 28],

$$\begin{aligned}
0 &= \int_\Omega d^3x \;\; \mathrm{F_H}(\mathbf{v},\mathbf{u}) \\
&= \int_\Omega d^3x \;\; \mathbf{v}\cdot\left[-\frac{1}{\epsilon}\mathbf{k}\times\left(\mathbf{k}\times\mathbf{u}\right) - \mathrm{i}\frac{1}{\epsilon}\mathbf{k}\times\left(\nabla\times\mathbf{u}\right) - \mathrm{i}\nabla\times\left(\frac{1}{\epsilon}\mathbf{k}\times\mathbf{u}\right)\right. \\
&\quad \left. +\nabla\times\left(\frac{1}{\epsilon}\nabla\times\mathbf{u}\right) - \mu\frac{\omega^2}{c^2}\mathbf{u}\right] \\
&\quad + \oint_{\partial\Omega} dA \;\; \mathbf{v}\cdot\left[\hat{\mathbf{n}}\times\frac{1}{\epsilon}\left(-\mathrm{i}\mathbf{k}\times\mathbf{u} + \nabla\times\mathbf{u}\right)\right],
\end{aligned} \tag{3.6}$$

where $\hat{\mathbf{n}}$ is the vector normal to the boundary. On an external boundary, the natural boundary condition enforced by the integral in Eq. (3.6) over the boundary $\partial\Omega$ forces the expression $\hat{\mathbf{n}}\times\left(-\mathrm{i}\mathbf{k}\times\mathbf{u} + \nabla\times\mathbf{u}\right)/\epsilon$ to be equal to zero. Recalling the definition of $\mathbf{u}$ from Eq. (3.2) we note that this simply

enforces the boundary condition $\hat{\mathbf{n}} \times \mathbf{E} = 0$. This is known as the perfect electric conductor or PEC boundary condition. This natural boundary condition is the default if no other boundary condition is enforced. On an internal boundary within the unit cell the surface integrals over each side of the boundary must be equal to each other. The effect is that the tangential components of the electric field must be continuous across the internal boundary or $\hat{\mathbf{n}} \times \mathbf{E}^+ = \hat{\mathbf{n}} \times \mathbf{E}^-$ where $\mathbf{E}^+$ and $\mathbf{E}^-$ are the electric fields on opposite sides of the internal boundary.

The periodicity of $\mathbf{u}$ is enforced by imposing periodic boundary conditions on the exterior boundaries of the unit cell. In COMSOL, these periodic boundary conditions override the natural boundary condition. However, if a PEC boundary condition is desired inside the unit cell (e.g., on the surface of a metal inclusion) this can be accomplished by removing the subdomain representing the metal inclusion. Now only the exterior side of the metal boundary remains and the tangential electric fields are forced to zero at this boundary.

If a perfect magnetic conductor or PMC boundary condition ($\hat{\mathbf{n}} \times \mathbf{H}$) is desired while solving for the magnetic field this can be enforced with constraints [74] on the tangential magnetic field on the boundary.

To turn Eq. (3.6) into an eigenvalue problem, the three degrees of freedom that comprise the Bloch wavevector $\mathbf{k}$ must be reduced to one by restricting two degrees of freedom. This is accomplished by setting $\mathbf{k} = \mathbf{k}_0 + \lambda \hat{\mathbf{k}}_n$ where λ will be the eigenvalue solved for, $\mathbf{k}_0$ is an offset vector and $\hat{\mathbf{k}}_n$ is a normal vector ($\hat{\mathbf{k}}_n \cdot \hat{\mathbf{k}}_n = 1$) that defines the direction of the wavenumber eigenvalue λ.

The FEM turns the weak form and accompanying boundary conditions into an algebra problem, in this case a quadratic eigenvalue problem [64]

$$\mathrm{A}\vec{u} + \lambda \mathrm{B}\vec{u} + \lambda^2 \mathrm{C}\vec{u} = 0, \tag{3.7}$$

where A, B and C are N × N matrices and $\vec{u}$ is an N × 1 solution vector. N is the number of degrees of freedom of the discretized system. Terms in the weak form (Eq. (3.5)) that are zero, first and second order in λ contribute to the A, B and C matrices respectively. This quadratic eigenvalue problem can be linearized exactly

$$\begin{pmatrix} \mathrm{A} & \mathrm{B} \\ 0 & 1 \end{pmatrix} \begin{pmatrix} \vec{u} \\ \lambda\vec{u} \end{pmatrix} = \lambda \begin{pmatrix} 0 & -\mathrm{C} \\ 1 & 0 \end{pmatrix} \begin{pmatrix} \vec{u} \\ \lambda\vec{u} \end{pmatrix}, \tag{3.8}$$

and solved as a generalized linear eigenvalue problem [1, 39, 45, 8, 51]. When using COMSOL to solve the FEM problem, this linearization is performed automatically during the solution phase.

3.2.3 Solving for the Electric field

The previous discussion focused on solving for the magnetic field **H** or rather the periodic function **u** equal to the magnetic field with the exponential Bloch factor removed. This is especially convenient when an inclusion requires a PEC boundary condition since that is the natural boundary condition when solving for **H**. However, solving for the electric field is very similar to solving

for the magnetic field. The field equation for the electric field for a free wave is

$$\nabla \times \left(\frac{1}{\mu}\nabla \times \mathbf{E}\right) - \epsilon\frac{\omega^2}{c^2}\mathbf{E} = 0. \tag{3.9}$$

As before, we replace the electric field with a periodic vector field times an exponential factor

$$\mathbf{E}(\mathbf{x}) = \mathbf{u}(\mathbf{x})e^{i(\omega t - \mathbf{k}\cdot\mathbf{x})}, \tag{3.10}$$

producing the new field equation

$$\frac{k^2}{\mu}\mathbf{u} - \frac{\mathbf{k}}{\mu}(\mathbf{k}\cdot\mathbf{u}) - i\mathbf{k}\times\left(\frac{1}{\mu}\nabla\times\mathbf{u}\right) - i\nabla\times\left(\frac{1}{\mu}\mathbf{k}\times\mathbf{u}\right) + \nabla\times\left(\frac{1}{\mu}\nabla\times\mathbf{u}\right) - \epsilon\frac{\omega^2}{c^2}\mathbf{u} = 0. \tag{3.11}$$

The corresponding weak form for this field equation is

$$\begin{aligned} \mathrm{F_E}(\mathbf{v},\mathbf{u}) \;=\; & \frac{k^2}{\mu}\mathbf{v}\cdot\mathbf{u} - \frac{1}{\mu}(\mathbf{k}\cdot\mathbf{v})(\mathbf{k}\cdot\mathbf{u}) - \mathrm{i}\frac{1}{\mu}\mathbf{v}\cdot[\mathbf{k}\times(\nabla\times\mathbf{u})] \\ & -\mathrm{i}(\nabla\times\mathbf{v})\cdot\frac{1}{\mu}(\mathbf{k}\times\mathbf{u}) + (\nabla\times\mathbf{v})\cdot\frac{1}{\mu}(\nabla\times\mathbf{u}) - \epsilon\frac{\omega^2}{c^2}\mathbf{v}\cdot\mathbf{u}, \end{aligned} \tag{3.12}$$

which is equivalent to Eq. (3.5) if ϵ and μ are interchanged. Integrating this weak form over the crystal unit cell by parts and setting its value to zero again produces two integrals, a volume integral enforcing the field equation and a

surface integral enforcing the boundary condition $\hat{\mathbf{n}} \times \mathbf{H} = 0$. Thus the PMC boundary condition is the natural boundary condition when solving for the electric field.

3.3 Photonic Crystal

For a demonstration of this method of calculating complex $\mathbf{k}$ dispersion curves we use a simple photonic crystal as an example. The unit cell, pictured in Fig. 3.1, is a cube with a dielectric sphere at the center surrounded by vacuum. The sphere has a radius of $0.3a$, where a is the lattice constant of the cubic array, and a permittivity of $\epsilon = 5 - \mathrm{i}0.01$.

As mentioned in Sec. 3.2.2, it is necessary to restrict two of the three degrees of freedom of the Bloch wavevector $\mathbf{k}$. There are many possible ways to do this. The simplest dispersion curve we can solve is for eigenmodes that are propagating along a principle axis of the crystal. To simulate this we set $\mathbf{k}_0 = 0$ and $\hat{\mathbf{k}}_n = \hat{\mathbf{x}}$. The results of this eigenvalue simulation for the frequency range $1c/a \leq \omega \leq 5.5c/a$ are plotted in Fig. 3.1 as ω vs. $k_x \equiv \hat{\mathbf{x}} \cdot \mathbf{k} = \lambda$.

There are an infinite number of eigenmodes of the photonic crystal so for clarity we have only plotted a three eigenmodes that have the smallest values of $\mathrm{Im}(k_z)$. The three eigenmodes in Fig. 3.1 are described as either transverse or longitudinal according to their polarization. The symmetry of the dispersion curves is such that for every solution $\mathbf{k}(\omega)$ there is also the solution $-\mathbf{k}(\omega)$ indicating that this is a reciprocal crystal. The transverse mode dispersion curve plotted in Fig. 3.1 actually represents two polarization

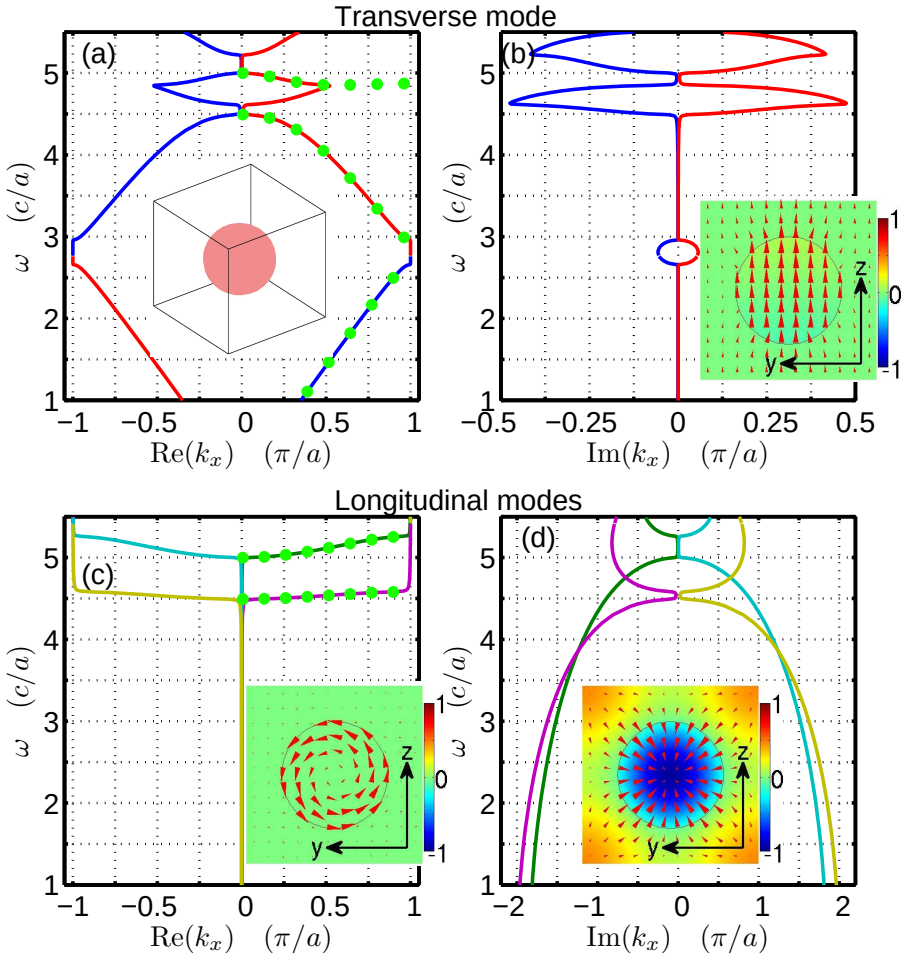

Figure 3.1: Complex $\mathbf{k}$ dispersion curves assuming $\mathbf{k}_0 = 0$ and $\hat{\mathbf{k}}_n = \hat{\mathbf{x}}$. (a) $\mathrm{Re}(k_x(\omega))$ for a transversely polarized mode and a diagram of the crystal unit cell. (b) $\mathrm{Im}(k_x(\omega))$ for a transversely polarized mode and a field profile for the $\hat{\mathbf{z}}$ polarized transverse mode. (c) $\mathrm{Re}(k_x(\omega))$ for two longitudinally polarized modes and a field profile for the magnetic longitudinal mode. (d) $\mathrm{Im}(k_x(\omega))$ for two longitudinally polarized modes and a field profile for the electric longitudinal mode. Dotted lines are the result of a $\omega(\mathbf{k})$ eigenvalue simulation. For all field profiles $\omega = 2c/a$, arrows represent D_y and D_z and color represents D_x.

degenerate transverse modes. The longitudinal mode with the passband near $\omega = 4.5c/a$ is magnetically polarized in the $\hat{\mathbf{x}}$ direction making it a magnetic bulk plasmon. The longitudinal mode with the passband near $\omega = 5c/a$ is electrically polarized in the $\hat{\mathbf{x}}$ direction and is an electric bulk plasmon. The field profiles of both longitudinal modes indicate that the passbands correspond to Mie's resonances of the dielectric sphere [10].

The transverse mode dispersion curve has a band in the approximate frequency range $4.6c/a < \omega < 4.8c/a$ with a large value of $\mathrm{Im}(k_x)$, indicating it is an evanescent band, but a $\mathrm{Re}(k_x)$ that is equal to neither 0 nor π/a as is typical of $\omega(\mathbf{k})$ dispersion curves. As described in Refs. [64, 14] for a quadratic eigenvalue problem with hermitian matrices (corresponding to a lossless crystal eigenvalue problem) the eigenvalues must always be real or come in complex conjugate pairs. The spherical photonic crystal is has very low loss so this approximately holds true for the dispersion curve in Fig. 3.1. The transverse band in the $4.6c/a < \omega < 4.8c/a$ frequency band is also one half of a complex conjugate pair, the other half is a transverse doubly degenerate mode not shown here. At the frequency of $\omega \approx 4.8c/a$ the two modes that make up this complex conjugate pair both enter a passband and split, the plotted mode going to the Γ point and the unplotted mode going to the band edge (this unplotted mode corresponds to the dotted lines from the $\omega(\mathbf{k})$ simulation). Note that in this passband there are two pairs of propagating doubly polarization degenerate modes or four propagating modes in total.

The transverse eigenmodes plotted in Fig. 3.1 can be excited at the

interface between a bulk sample of the photonic crystal and vacuum if the interface lies along the $\hat{\mathbf{y}}$-$\hat{\mathbf{z}}$ plane and the incident radiation is normal to this interface. The longitudinally polarized modes could not be excited by an wave with normal incidence without the aid of a coupling device at the interface. If the incident beam of light is not normal to the interface, if for example the incident beam has a wavevector laying in the $\hat{\mathbf{x}}$-$\hat{\mathbf{y}}$ plane but at a 30° angle from normal then a different set of eigenmodes will be excited at the interface. To solve for these eigenmodes we set $\mathbf{k}_0 = \omega/c \sin(\pi/6)\hat{\mathbf{y}}$ and $\hat{\mathbf{k}}_n = \hat{\mathbf{x}}$ and then solve the resulting eigenvalue problem. The results are plotted in Fig. 3.2.

The eigenmodes in Fig. 3.2 are roughly split into transverse and longitudinal modes. The propagating modes are predominantly transverse, but the finite k_y has broken the degeneracy between the two polarizations as well as caused the transverse modes to acquire a slight longitudinal polarization. Both the transverse hybrid modes and longitudinal hybrid modes in Fig. 3.2 can been characterized by the polarization of the incident light necessary to excite them. For a p polarized incident beam (electric field in the $\hat{\mathbf{x}}$-$\hat{\mathbf{y}}$ plane) the p polarized eigenmode is excited (plotted in Fig. 3.2 as a solid line) and for an s polarized incident beam (electric field in the $\hat{\mathbf{z}}$ direction) the s polarized eigenmode is excited (plotted in Fig. 3.2 with dashed lines).

At the frequency $\omega \approx 4c/a$ the transverse hybrid modes and the longitudinal hybrids modes appear to cross in a propagating band. An expanded view of this region in Fig. 3.2 plotting both transverse and longitudinal hybrid modes shows that the apparent crossing actually occurs in a band gap. Viewed

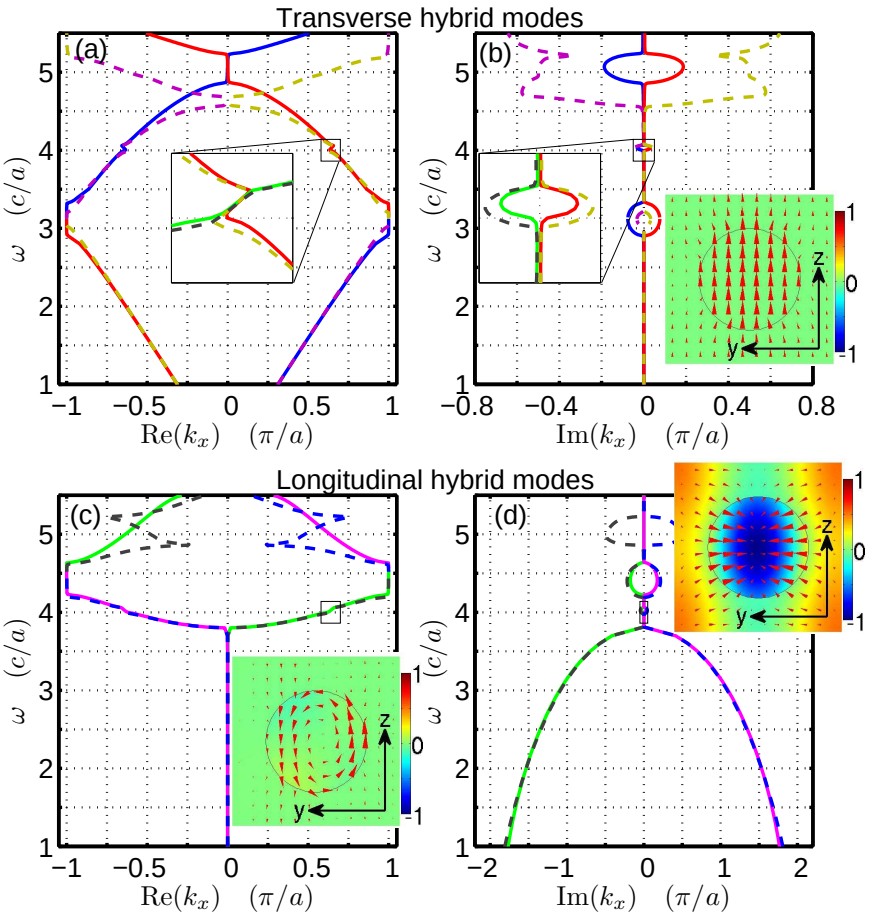

Figure 3.2: Complex $\mathbf{k}$ dispersion curves assuming $\mathbf{k}_0 = \omega/c \sin(\pi/6)\hat{\mathbf{y}}$ and $\hat{\mathbf{k}}_n = \hat{\mathbf{x}}$. Modes excited by p or s polarized incident light are plotted with solid or dashed lines respectively. (a) $\mathrm{Re}(k_x(\omega))$ for two transverse hybrid modes and a expanded view of the avoided crossing in $\mathrm{Re}(k_x)$ space. (b) $\mathrm{Im}(k_x(\omega))$ for two transverse hybrid modes, an expanded view of the avoided crossing in $\mathrm{Im}(k_x)$ space, and a field profile for the E_z polarized transverse hybrid mode. (c) $\mathrm{Re}(k_x(\omega))$ for two longitudinal hybrid modes and a field profile for the magnetic longitudinal hybrid mode. (d) $\mathrm{Im}(k_x(\omega))$ for two longitudinal hybrid modes and a field profile for the electric longitudinal hybrid mode. For all field profiles $\omega = 2c/a$, arrows represent D_y and D_z and color represents D_x.

in complex k_x space it is clear that this is actually an avoided crossing and in the band gap the transverse and longitudinal hybrid modes form approximate complex conjugate pairs [64, 14].

We see that even for a simple photonic crystal the $\mathbf{k}(\omega)$ method of calculating the dispersion curve produces rich and complex results. In particular, it is not possible to solve for evanescent eigenmodes using the conventional $\omega(\mathbf{k})$ method for calculating dispersion curves. In addition, the ability to solve the eigenmodes that are excited by an external laser beam by both allowing the frequency to be real and matching $k_y = \omega/c \sin(\theta)$ to the incident beam while solving for k_x as the eigenvalue is a unique capability of this method which is essential for understanding refraction at the interface between vacuum and a metamaterial/photonic crystal.

We will see in later chapters that the ability to solve complex $\mathbf{k}$ eigenvalue problems is crucial to understanding spatial dispersion in metamaterials. In Chapters 4 and 5 this ability is essential for calculating constitutive parameters on the dispersion curve. Also, in Chapter 6, we find that a nonzero $\mathrm{Im}(\mathbf{k})$ creates difficulties when we try to calculate energy flux in a metamaterial/photonic crystal.

Chapter 4

A First Attempt at Metamaterial Homogenization

4.1 A new homogenization method

Now that we have identified the pros and cons of previously reported homogenization procedures we can try to develop a new procedure. This new method will borrow the best aspects of the methods mentioned in Chapter 1 but hopefully avoid the pitfalls that those methods encountered. The method outlined in this chapter is very ambitious and in the end we will discover several problems with it. However, it is an important step in the right direction as it develops some key ideas which will be essential to any future superior method of metamaterial homogenization. The homogenization method described in this chapter was previously published in Refs. [20, 21].

Before we begin let's briefly review some of the shortcomings of the methods described in the Chapter 1. The first two methods described were only able to calculate a small number of constitutive parameters, often only four, two for each polarization. Since their are at most 36 linear constitutive parameters and since metamaterials tend to be much more complicated than natural materials this is a significant limitation. A complete homogenization

procedure should be able to calculate all 36 linear constitutive parameters. Second, many of the methods described in Chapter 1 assumed a great deal of symmetry in the crystal to be analyzed. This is necessary in all of the methods that calculated small numbers of constitutive parameters. In general however, complex metamaterials can be very asymmetric and/or non-reciprocal. Third, several of the methods relied on freely propagating eigenmodes propagating through the crystal of interest to characterize that crystal. These free waves are not coupled to any source and have a relationship between their frequency ω and $\mathbf{k}$ commonly known as the dispersion relation. These methods either ignore or assume no direct relationship between the constitutive parameters and the wavevector. They assume the constitutive parameters are only functions of the frequency ω. However, as we saw with the homogenization methods of Mário G. Silveirinha and Jenson Li, the constitutive parameters can be functions of both ω and $\mathbf{k}$, the dependence on $\mathbf{k}$ relating to spatial dispersion. As we saw in Chapter 1, spatial dispersion is an extremely important effect in many metamaterials and must not be ignored. We can summarize these requirements for an ideal metamaterial homogenization procedure in two points.

1. The homogenization procedure must be solve for all 36 linear constitutive parameters for an potentially asymmetric and non-reciprocal metamaterial crystal.

2. To accurately describe both temporal and spatial dispersion all 36 con-

stitutive parameters must be functions of both ω and $\mathbf{k}$.

Keeping these requirements in mind let's consider a new metamaterial homogenization procedure.

4.2 Metamaterials driven with electric and magnetic charge/current

To solve for all 36 constitutive parameters of a metamaterial crystal we must solve the equation

$$\begin{pmatrix} \mathbf{D} \\ \mathbf{B} \end{pmatrix} = \begin{pmatrix} \epsilon & \xi \\ \zeta & \mu \end{pmatrix} \begin{pmatrix} \mathbf{E} \\ \mathbf{H} \end{pmatrix}, \tag{4.1}$$

where the macroscopic field vectors $\mathbf{D}$, $\mathbf{B}$, $\mathbf{E}$ and $\mathbf{H}$, are the known variables and the constitutive parameters are the unknown variables. The matrix on the right hand side of Eq. (4.1) is a 6x6 matrix known as the constitutive matrix. Since there are 36 constitutive parameters we need 36 equations of constraint. A single set of EM fields related through Eq. (4.1) provides six equations of constraint. Therefore we need six sets of linearly independent EM fields obeying Eq. (4.1) to solve for the constitutive parameters. Specifically, we need six linearly independent sets of field vectors providing us with 36 equations of constraint that can be solved for 36 unknowns.

If we rely on eigenmodes supported by the medium free of source terms then as we saw in Chapter. 1 for a general material only one set of linearly independent fields is available for a particular set of $\omega(\mathbf{k})$ and $\mathbf{k}$ where $\omega = \omega(\mathbf{k})$

is the dispersion relation. As we saw in Sec. 1.4 we can obtain three sets of linearly independent fields by driving our crystal with electric charge and current. However, this is still not enough. A solution to this problem comes from the Maxwell equations when the addition of magnetic charge and current is allowed.

$$\begin{aligned} \nabla \cdot \mathbf{D} &= \rho \qquad & \nabla \times \mathbf{H} - \frac{1}{c}\frac{\partial \mathbf{D}}{\partial t} &= \frac{\mathbf{J}}{c}, \\ \nabla \cdot \mathbf{B} &= \phi \qquad & -\nabla \times \mathbf{E} - \frac{1}{c}\frac{\partial \mathbf{B}}{\partial t} &= \frac{\mathbf{I}}{c}. \end{aligned} \tag{4.2}$$

These are the Maxwell equations with the addition of magnetic charge density ϕ and magnetic current density $\mathbf{I}$ [27, 46]. In a homogeneous medium an electric current $\mathbf{J} = \mathbf{J}_0 e^{i(\omega t - \mathbf{k}\cdot\mathbf{x})}$ and magnetic current $\mathbf{I} = \mathbf{I}_0 e^{i(\omega t - \mathbf{k}\cdot\mathbf{x})}$ that are harmonic in time and space will generate an electromagnetic wave $\mathbf{E}(t, \mathbf{x}) = \mathbf{E}_0 e^{i(\omega t - \mathbf{k}\cdot\mathbf{x})}$ and $\mathbf{H}(t, \mathbf{x}) = \mathbf{H}_0 e^{i(\omega t - \mathbf{k}\cdot\mathbf{x})}$ according to Eq. (4.2), which can be rearranged in ω and $\mathbf{k}$ space and combined with the constitutive matrices to give us

$$\begin{pmatrix} \omega/c & \epsilon^{-1}(\mathbf{k} \times +\omega\xi/c) \\ -\mu^{-1}(\mathbf{k} \times -\omega\zeta/c) & \omega/c \end{pmatrix} \begin{pmatrix} \mathbf{E}_0 \\ \mathbf{H}_0 \end{pmatrix} = \frac{\mathrm{i}}{c} \begin{pmatrix} \epsilon^{-1}\mathbf{J}_0 \\ \mu^{-1}\mathbf{I}_0 \end{pmatrix}. \tag{4.3}$$

Here the four terms in the matrix on the left hand side are all 3x3 matrices and $\mathbf{k}\times$ is a matrix cross product of the Bloch wavevector

$$\mathbf{k}\times = \begin{pmatrix} 0 & -k_z & k_y \\ k_z & 0 & -k_x \\ -k_y & k_x & 0 \end{pmatrix}. \tag{4.4}$$

.

If ω and $\mathbf{k}$ are not on the dispersion curve of the crystal then the matrix on the left hand side of Eq. (4.3) is always invertible and we can solve for $\mathbf{E}_0$ and $\mathbf{H}_0$. From this equation it is obvious that if we limit ourselves to electric current only, we can obtain at most three linearly independent field vectors. Thus, we would be unable to solve Eq. (4.1) for the constitutive parameters. However, if we allow ourselves to drive our crystal with both electric and magnetic current we can obtain six linearly independent field vectors and solve Eq. (4.1) for all 36 constitutive parameters. This is the same solution that was suggested by Jensen Li et al. in the homogenization procedure described in Sec. 1.5, except Li used electric and magnetic external polarization densities.

Once it is understood how to obtain six linearly independent field vectors, it is straightforward to solve six electromagnetic simulations, each one driving the metamaterial crystal with a different current polarization, then average the microscopic fields returned by the simulation into macroscopic fields and solve Eq. (4.1) for the constitutive parameters. Thus to calculate all 36 constitutive parameters we define the following 6x6 matrices

$$\begin{aligned}
\mathcal{D} &\equiv \begin{pmatrix} \mathbf{D}^{(1)}, \mathbf{D}^{(2)}, \ ... \ \mathbf{D}^{(6)} \\ \mathbf{B}^{(1)}, \mathbf{B}^{(2)}, \ ... \ \mathbf{B}^{(6)} \end{pmatrix}, \\
\mathcal{E} &\equiv \begin{pmatrix} \mathbf{E}^{(1)}, \mathbf{E}^{(2)}, \ ... \ \mathbf{E}^{(6)} \\ \mathbf{H}^{(1)}, \mathbf{H}^{(2)}, \ ... \ \mathbf{H}^{(6)} \end{pmatrix}, \\
\mathcal{J} &\equiv \begin{pmatrix} \mathbf{J}^{(1)}, \mathbf{J}^{(2)}, \ ... \mathbf{J}^{(6)} \\ \mathbf{I}^{(1)}, \mathbf{I}^{(2)}, \ ... \ \mathbf{I}^{(6)} \end{pmatrix}.
\end{aligned} \tag{4.5}$$

Each column of the matrices in Eq. (4.5) is associated with a single electromagnetic simulation. For example, in the first simulation our driving current is $\mathcal{J}_{i1} = (1, 0, 0, 0, 0, 0)$, or $\mathbf{J}_0 = \mathbf{e}_x$ and $\mathbf{I}_0 = 0$. That is, we drive our crystal with electric current in the $\hat{\mathbf{x}}$ direction according to Eq. (4.2). We numerically solve for the microscopic electromagnetic fields $\mathbf{e}$, $\mathbf{h}$, $\mathbf{d}$ and $\mathbf{b}$. We then take the microscopic fields solved for in our first simulation and average them into the macroscopic fields $\mathcal{D}_{i1} = (\mathbf{D}^{(1)}, \mathbf{B}^{(1)})$ and $\mathcal{E}_{i1} = (\mathbf{E}^{(1)}, \mathbf{H}^{(1)})$. In our second simulation the driving current is $\mathcal{J}_{i2} = (0, 1, 0, 0, 0, 0)$. We average the microscopic fields from the second simulation into the macroscopic fields $\mathcal{D}_{i2} = (\mathbf{D}^{(2)}, \mathbf{B}^{(2)})$ and $\mathcal{E}_{i2} = (\mathbf{E}^{(2)}, \mathbf{H}^{(2)})$. We follow the same steps for the next four simulations, each one driving the crystal with a different current polarization so that the matrix $\mathcal{J}$ has a nonzero determinant and as a result $\mathcal{D}$ and $\mathcal{E}$ also have nonzero determinants. Finally, with a full set of electromagnetic fields in the matrices $\mathcal{D}$ and $\mathcal{H}$ which by definition are related by C according to Eq. (4.1) we are able to solve for the constitutive parameters:

$$\mathrm{C} \equiv \begin{pmatrix} \epsilon & \xi \\ \zeta & \mu \end{pmatrix} = \mathcal{D}\mathcal{E}^{-1}. \tag{4.6}$$

Since the driving current in these simulations is harmonic in time with frequency ω and in space with wavevector $\mathbf{k}$, our calculated constitutive parameters are functions of ω and $\mathbf{k}$, that is $\mathrm{C} = \mathrm{C}(\omega, \mathbf{k})$.

This method of driving our metamaterial crystal with electric and magnetic current is independent of the averaging procedure used, provided that the

averaging procedure works on Bloch waves with arbitrary ω and $\mathbf{k}$ driven by external electric and magnetic currents. We now present a new averaging procedure that predicts dispersion relations correctly and provides approximately correct boundary conditions.

4.3 Field Averaging

Metamaterials by their nature are very inhomogeneous. The unit cell of a metamaterial may consist of various arbitrarily shaped material inclusions such as metals and/or dielectrics. The microscopic EM fields $\mathbf{e}$, $\mathbf{h}$, $\mathbf{d}$ and $\mathbf{b}$ inside the unit cell are related with the microscopic Maxwell equations,

$$\begin{aligned} \nabla \cdot \mathbf{d} &= \rho, \qquad & \nabla \times \mathbf{h} - \frac{1}{c}\frac{\partial \mathbf{d}}{\partial t} &= \frac{\mathbf{J}}{c}, \\ \nabla \cdot \mathbf{b} &= \phi, \qquad & -\nabla \times \mathbf{e} - \frac{1}{c}\frac{\partial \mathbf{b}}{\partial t} &= \frac{\mathbf{I}}{c}. \end{aligned} \tag{4.7}$$

Solving Maxwell's Eqs. (4.2) for the microscopic fields inside a single unit cell for a fixed frequency ω can be accomplished using a commercial finite element software package. Microscopic EM fields are subject to Bloch periodic boundary conditions determined by the potentially complex wavevector $\mathbf{k}$. Calculating the constitutive parameters of a metamaterial requires averaging strongly inhomogeneous microscopic fields inside the unit cell into the macroscopic plane waves $\mathbf{E} = \mathbf{E}_0 e^{i(\omega t - \mathbf{k}\cdot\mathbf{x})}$, $\mathbf{H} = \mathbf{H}_0 e^{i(\omega t - \mathbf{k}\cdot\mathbf{x})}$, $\mathbf{D} = \mathbf{D}_0 e^{i(\omega t - \mathbf{k}\cdot\mathbf{x})}$ and $\mathbf{B} = \mathbf{B}_0 e^{i(\omega t - \mathbf{k}\cdot\mathbf{x})}$ in order to obtain the matrix of macroscopic fields in Eq. (4.5). The constitutive parameters are then calculated according to Eqs. (4.5,4.6).

If we integrate the microscopic Maxwell equations (Eq. (4.7)) over the crystal unit cell volume Ω, the volume integrals of the left hand sides of Eq. (4.7) become area integrals over the boundary of the unit cell $\partial\Omega$. Our prescription for averaging the microscopic fields is to force the boundary integrals over the macroscopic field to equal the boundary integrals over the microscopic fields or

$$-i\mathbf{k}\cdot\begin{Bmatrix}\mathbf{D}_0\\ \mathbf{B}_0\end{Bmatrix} S_V \;= \int_\Omega d^3x \nabla\cdot\begin{Bmatrix}\mathbf{D}\\ \mathbf{B}\end{Bmatrix} = \int_\Omega d^3x \nabla\cdot\begin{Bmatrix}\mathbf{d}\\ \mathbf{b}\end{Bmatrix} \;= \oint_{\partial\Omega} d\mathbf{n}\cdot\begin{Bmatrix}\mathbf{d}\\ \mathbf{b}\end{Bmatrix}, \tag{4.8}$$

and

$$-i\mathbf{k}\times\begin{Bmatrix}\mathbf{E}_0\\ \mathbf{H}_0\end{Bmatrix} S_V = \int_\Omega d^3x \nabla\times\begin{Bmatrix}\mathbf{E}\\ \mathbf{H}\end{Bmatrix} = \int_\Omega d^3x \nabla\times\begin{Bmatrix}\mathbf{e}\\ \mathbf{h}\end{Bmatrix} = \oint_{\partial\Omega} d\mathbf{n}\times\begin{Bmatrix}\mathbf{e}\\ \mathbf{h}\end{Bmatrix} \tag{4.9}$$

Here $d\mathbf{n}$ is an infinitesimal integration area normal to the boundary $\partial\Omega$ pointing out of the unit cell, $\mathbf{k}$ is the Bloch wavevector. S_V is an effective volume [62] given by the equation

$$S_V = \frac{\sin(k_x a_x/2)}{k_x/2}\cdot\frac{\sin(k_y a_y/2)}{k_y/2}\cdot\frac{\sin(k_z a_z/2)}{k_z/2}, \tag{4.10}$$

where a_x, a_y and a_z are the lattice constants of the crystal unit cell. This effective volume ensures we get the correct macroscopic field if we average a plane wave in an already homogeneous medium. Eq. (4.8) only restricts the longitudinal component of $\mathbf{D}_0$ (the D field parallel to $\mathbf{k}^*$, where the $*$

indicates complex conjugation) and the transverse components of $\mathbf{H}_0$ (the H field perpendicular to $\mathbf{k}$). The remaining components of $\mathbf{D}_0$ and $\mathbf{H}_0$ are determined from simple averages:

$$\mathbf{k}^* \times \left\{ \begin{array}{c} \mathbf{D}_0 \\ \mathbf{B}_0 \end{array} \right\} S_V = \int_\Omega \frac{d^3x}{V} \mathbf{k}^* \times \left\{ \begin{array}{c} \mathbf{d} \\ \mathbf{b} \end{array} \right\} \tag{4.11}$$

and

$$\mathbf{k}^* \cdot \left\{ \begin{array}{c} \mathbf{E}_0 \\ \mathbf{H}_0 \end{array} \right\} S_V = \int_\Omega \frac{d^3x}{V} \mathbf{k}^* \cdot \left\{ \begin{array}{c} \mathbf{e} \\ \mathbf{h} \end{array} \right\}. \tag{4.12}$$

The macroscopic field components $\mathbf{E}_0$, $\mathbf{H}_0$, $\mathbf{D}_0$ and $\mathbf{B}_0$ are then defined as the method of least squares solution the the system of equations Eqs. (4.8,4.9) and Eqs. (4.11,4.12).

It is essential that different field components are averaged in different ways. For example, for a metamaterial with only metal or dielectric inclusions where $\mu = 1$ throughout the unit cell, without introducing different averaging prescriptions for $\mathbf{H}$ and $\mathbf{B}$, we could come to the conclusion that $\mathbf{H} = \mathbf{B}$. It would not be possible to predict effective magnetic activity ($\zeta \neq 0$ or $\mu \neq 1$) for metamaterials which do not contain any magnetic inclusions. Also, it should be noted that if $\mathbf{k}$ is parallel to the principle axis of a crystal and if the inclusions in the metamaterial are small then our averaging method for the transverse components of $\mathbf{E}_0$ and $\mathbf{H}_0$ are equivalent to the transversely averaged fields used in [58]. Also, this averaging procedure is similar to the method of averaging over faces and edges of a unit cell published in Refs [50, 60] and outlined in Sec. 1.2. That averaging procedure can be combined with the

method of driving a crystal with both electric and magnetic current described in Sec. 4.2 and when done so produces results very similar to this averaging procedure. Finally, because of the nature of the definitions in Eqs. (4.8,4.9) and Eqs. (4.11,4.12), we cannot rigorously compute the constitutive parameters at the Γ point ($\mathbf{k} = 0$). It is, however, possible to compute the constitutive parameters for any finite wavevector.

4.4 Ambiguity of Constitutive Parameters

Examining the left hand side Eq. (4.3) we see the 3x3 matrix $\mu^{-1}(\mathbf{k} \times -\omega\zeta)$. Any experiment designed to test the extracted constitutive parameters will be limited to using electric current only and no magnetic current. Without magnetic current, Eq. (4.3) develops an ambiguity. We can transform between the current driven constitutive parameters predicted by our theory to a second "effective" set of parameters that obey the following equation.

$$\mu^{-1}\left(\mathbf{k} \times -\frac{\omega}{c}\zeta\right) = (\mu^{eff})^{-1}\left(\mathbf{k} \times -\frac{\omega}{c}\zeta^{eff}\right) \tag{4.13}$$

Eq. (4.3) predicts the fields generated by a source, but it is clear that this ambiguity also exists for the dispersion relation of free waves. It is easy to see that a transformation in spatial coordinates changes both sides of Eq. (4.13) equally so that Eq. (4.13) is still true after the transformation. Andrea Alu has shown that the difference between the true constitutive parameters and the effective parameters in Eq. (4.13) help explain some of the apparently

unphysical lineshapes associated with the constitutive parameters of metamaterials [7]. We will see in Sec. 6 that using the true parameters instead of the effective parameters is essential for calculating quantities such as Poynting flux and dissipative loss.

This issue at once both illustrates the essential role that using magnetic charge and current in our simulations plays in restricting the possible values of the constitutive parameters and at the same time illuminates the problem of the experimental ambiguity of these parameters. In the next section (Sec. 4.5) we'll see that this ambiguity is important for comparing our predicted constitutive parameters to those predicted by simpler, more established theories. Specifically, we'll see that the parameters predicted by S-Parameter retrieval [61] do not agree with our theory unless we perform a transformation according to Eq. (4.13).

Finally, we note that if one is restricted is to experiments that do not use electric charge and current then there is a similar ambiguity effecting ϵ and ξ,

$$\epsilon^{-1}\left(\mathbf{k}\times+\frac{\omega}{c}\xi\right)=(\epsilon^{eff})^{-1}\left(\mathbf{k}\times+\frac{\omega}{c}\xi^{eff}\right), \tag{4.14}$$

as can be seen from the upper right part of the matrix in eq 4.3.

4.5 Example: Split Pair One Film (SPOF)

We now show results from a 2D metamaterial crystal known as a Strip Pair-One Film or a SPOF [43]. A diagram of the SPOF is given in Fig. 4.1. Our SPOF is a square crystal lattice with a thin Au film in the center of the unit cell and two Au strips on both sides of the film. The permittivity of the Au is $\epsilon = 1 - \omega_p^2/(\omega(\omega - \mathrm{i}\Gamma))$ with $\omega_p = 1.32 \cdot 10^{16}/s$ and $\Gamma = 1.2 \cdot 10^{14}/s$. The rest of the SPOF is dielectric with permittivity $\epsilon = 1.56^2$.

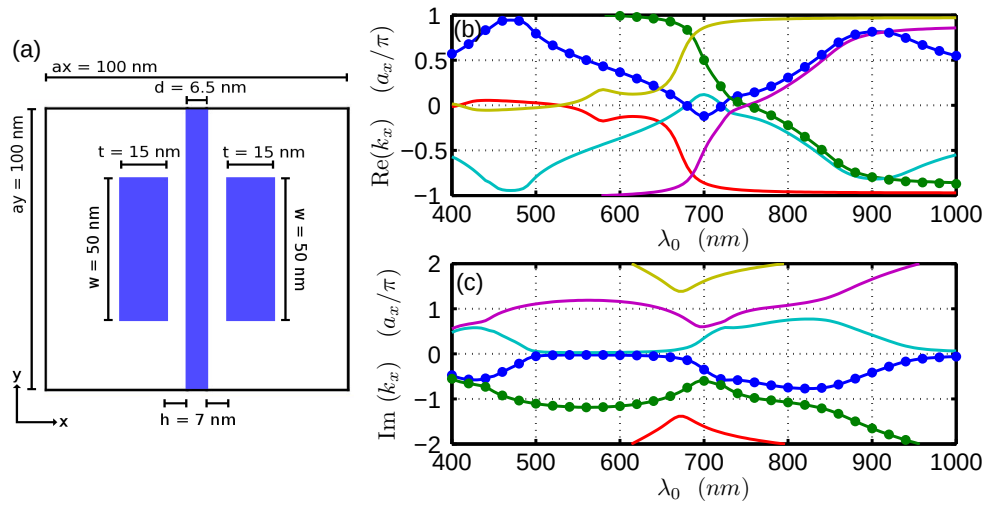

Figure 4.1: (a) The unit cell of the SPOF. The two strips and center film of the SPOF are Au with permittivity $\epsilon = 1 - \omega_p^2/(\omega(\omega - i\Gamma))$ where $\omega_p = 1.32 \cdot 10^{16}/s$ and $\Gamma = 1.2 \cdot 10^{14}/s$. The rest of the SPOF is made of dielectric with permittivity $\epsilon = 1.56^2$. (b) Real and (c) imaginary parts of k_x vs. λ_0 where $\mathbf{k} = k_x\hat{\mathbf{x}}$. Solid lines are dispersion curves for a p-polarized wave solved by a finite element eigenvalue simulation [14]. Dotted lines are dispersion curves calculated from Eq. (4.15) using current driven constitutive parameters calculated from Eq. (4.6) by driving the SPOF at ω and $\mathbf{k} = k_x(\omega)\hat{\mathbf{x}}$ for two of the p-polarized eigenmodes. Note there is only one propagating mode.

In Fig. 4.1 we plot two different dispersion curves. First we plot the real and imaginary parts of the complex wavenumber for p-polarized (electric field in the $\hat{\mathbf{x}}$-$\hat{\mathbf{y}}$ plane) eigenmodes propagating through the SPOF along the $\hat{\mathbf{x}}$ direction calculated from an eigenvalue simulation [14] (solid lines). We calculated the full set of constitutive parameters as functions of ω and $\mathbf{k} = \mathbf{k}(\omega)$ for two of the eigenmodes as described in sections 4.2 and 4.3. It should be noted that instead of driving the crystal on the dispersion curve, it is important to drive the crystal close to but slightly off of the dispersion curve so as to prevent the matrix in Eq. (4.3) from becoming singular. We used these current driven constitutive parameters to calculate the real and imaginary parts of the complex wavenumber for each eigenmode according to the dispersion relation of the SPOF (dotted lines), which for a p-polarized wave propagating in the $\hat{\mathbf{x}}$ direction is

$$\left(\frac{k_x - \omega\zeta_{zy}/c}{\mu_{zz}}\right)\left(\frac{k_x - \omega\xi_{yz}/c}{\epsilon_{yy}}\right) - \frac{\omega^2}{c^2} = 0. \tag{4.15}$$

Fig. 4.1 clearly shows that calculate constitutive constitutive parmeters predict the correct dispersion relation for two of the modes, one of which is radiative for some frequencies and evanescent for others and the other mode being always evanescent. Though not shown in Fig. 4.1, the current driven constitutive parameters fail to predict the dispersion of the third mode (red line) which is a longitudinally polarized electric bulk plasmon.

Testing the current driven constitutive parameters to see if they produce the correct dispersion relation is an important physical test but does

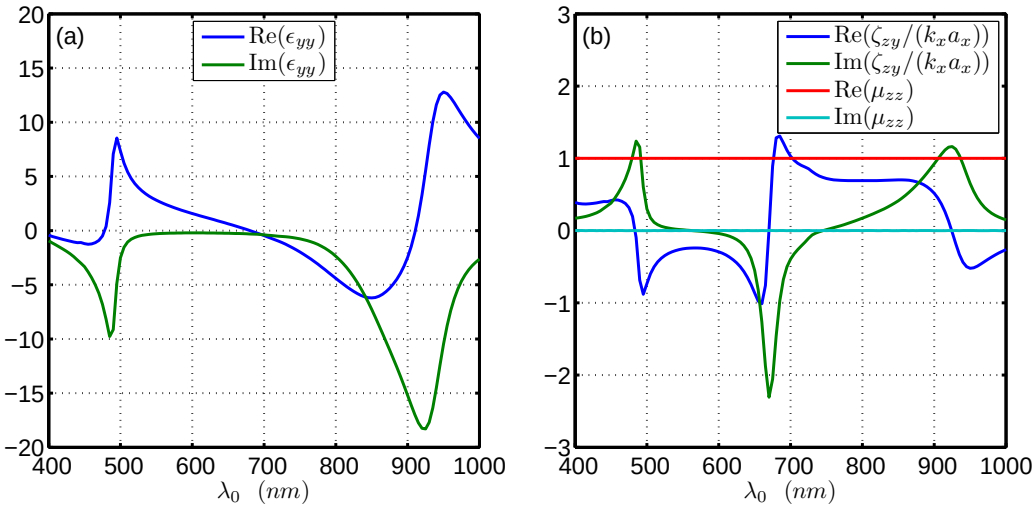

Figure 4.2: (a) Real and imaginary parts of ϵ_{yy}. (b) Real and imaginary parts of ζ_{zy} and μ_{zz}. All constitutive parameters are calculated on the dispersion curve $\mathbf{k} = k_x(\omega)\hat{\mathbf{x}}$ shown in Fig. 4.1 according to Eq. (4.6). Notice that μ_{zz} is unity for all wavelengths. Also, all components of ξ (not shown) are uniformly zero.

prove the accuracy of the parameters. Different averaging procedures can pass this test while predicting slightly different constitutive parameters. For example the averaging procedure in Smith [62] passes the dispersion relation test but fails a test of the boundary conditions. This brings us to our next test of our current driven constitutive parameters.

In Fig. 4.2 we plot the ϵ_{yy}, ζ_{zy} and μ_{zz} components of the SPOF extracted along the dispersion curve of the propagating (blue line) p-polarized eigenmode in Fig. 4.1. Note that since the dispersion curve in Fig. 4.1 is for a p-polarized wave propagating in the x direction and given the nonzero structure of the constitutive matrices for propagation in the $\hat{\mathbf{x}}$ direction in a

centrosymmetric crystal, only four of the total 36 constitutive parameters, ϵ_{yy}, ζ_{zy}, μ_{zz} and ξ_{yz} effect the p-polarized wave. Also, though we do not show ξ_{yz} in Fig. 4.2, the values of ξ calculated with the field averaging procedure described in Sec. 4.3 turn out to be uniformly zero. The values of μ_{zz} are uniformly 1. as can be seen in Fig. 4.2. This is the first indication of a serious problem with the averaging procedure and will be discuss at the end of this chapter.

The calculated constitutive parameters disagree with the parameters return by the S-parameter retrieval (Ref. [61] and Sec. 1.3) method for the SPOF structure. This discrepancy can be explained using with the experimental ambiguity expressed in Eq. (4.13). For a pseudotensor $\zeta(\omega, \mathbf{k} = k_x\mathbf{x})$ describing a centrosymmetric crystal, the p-polarized part of Eq. (4.13) can be rewritten as $(k_x - \omega\zeta_{zy}/c)/\mu_{zz} = (k_x - \omega\zeta_{zy}^{eff}/c)/\mu_{zz}^{eff}$. There is a second part of Eq. (4.13) that involves ζ_{yz} but this only affects s-polarized waves so we ignore it here. Since we have two unknown effective parameters μ_{zz}^{eff} and ζ_{zy}^{eff} and one equation of constraint, we have one degree of freedom in our effective parameters. Essential to symmetric version of S-parameter retrieval is the assumption that ζ and ξ are zero, so we use our one degree of freedom to set $\zeta_{zy}^{eff} = 0$ giving us

$$\mu_{zz}^{eff} = \frac{\mu_{zz}}{1 - \dfrac{\omega\zeta_{zy}}{ck_x}}. \tag{4.16}$$

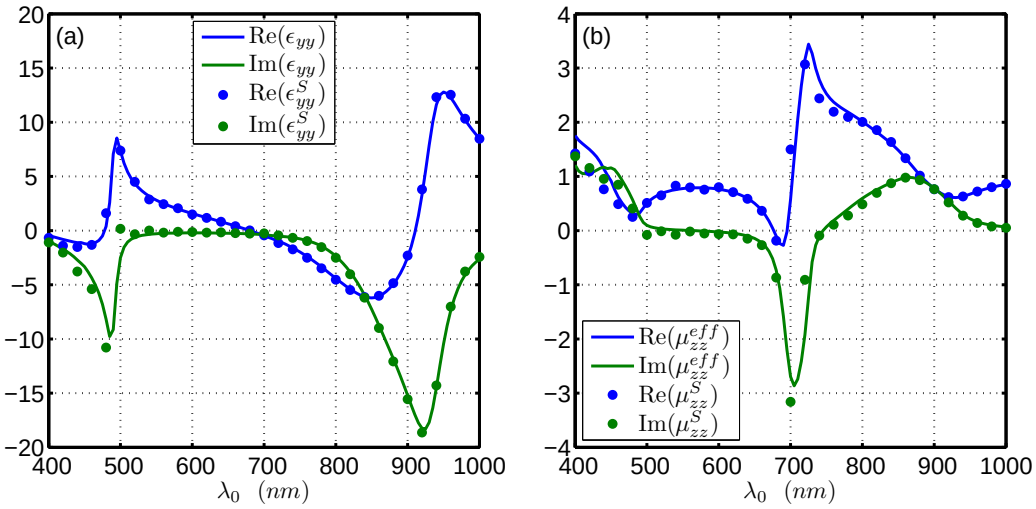

Figure 4.3: (a) Real and imaginary parts of constitutive parameters ϵ_{yy} (solid lines) calculated with Eq. (4.6) and ϵ^S_{yy} (dotted lines) calculated with S-parameter retrieval [61] for the SPOF. (b) Real and imaginary parts of μ^{eff}_{zz} (solid lines) calculated from Eq. (4.16) using ζ_{zy} and μ_{zz} calculated with Eq. (4.6) and μ^S_{zz} (dotted lines) calculated with S-parameter retrieval for the SPOF.

Fig. 4.3 shows a comparison of the current driven ϵ_{yy} calculated from Eq. (4.6) and effective μ^{eff}_{zz} calculated from Eq. (4.16) using current driven ζ_{zy} and μ_{zz} vs. ϵ^S_{yy} and μ^S_{zz} determined with S-parameter retrieval of a SPOF slab five unit cells thick. We see a good agreement between ϵ_{yy} and the S-parameter retrieved ϵ^S_{yy}. We also see a good agreement between effective μ^{eff}_{zz} and the S-parameter retrieved μ^S_{zz}. As mentioned in Sec. 1.3, S-parameter retrieval calculates ϵ and μ from the the index of refraction n and impedance z of the matematerial where n and z are inferred from reflection and transmission amplitudes through a metamaterial slab. The index is proportional to the

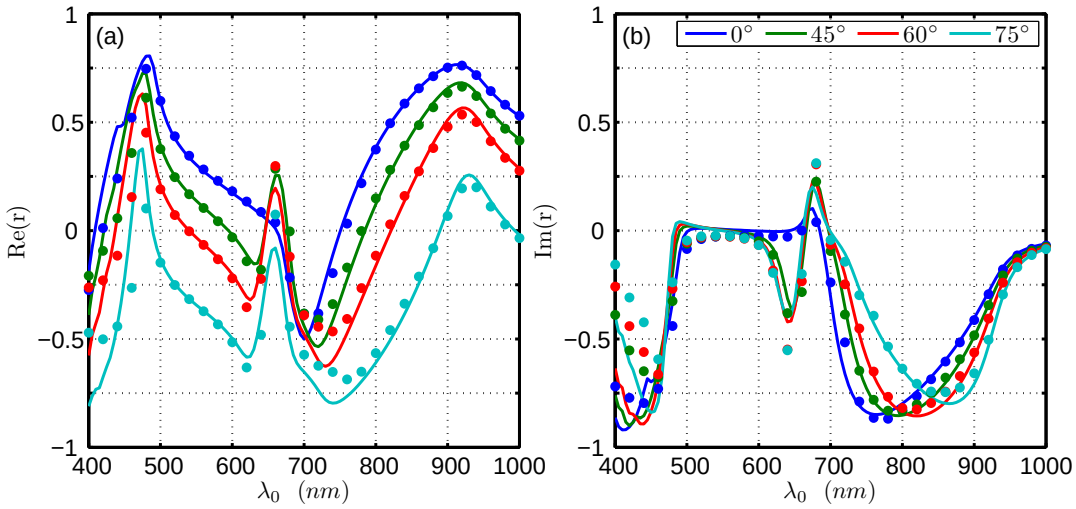

Figure 4.4: Real (left plot) and imaginary (right plot) parts of the reflection amplitude ($r = H_z^{ref}/H_z^{inc}$) of a plane wave with incident angles 0°, 45°, 60° and 75° off of a SPOF (solid lines) and off of a homogeneous medium with the current driven constitutive parameters of the SPOF (dotted line).

wavenumber, and as we've seen in Fig. 4.1 the calculated constitutive parameters predict the correct wavenumber very well. The impedance is related to the boundary conditions at the interface between the slab and vacuum. This is where the small error in Fig. 4.3 comes from. It is the Maxwell boundary conditions (continuity of the tangential components of $\mathbf{E}$ and $\mathbf{H}$ and the normal components of $\mathbf{D}_{\text{norm}}$ and $\mathbf{B}_{\text{norm}}$) where disagreement in Fig. 4.3 originates.

We can see this in our next test of the constitutive parameters shown in Fig. 4.4. The solid lines in Fig. 4.4 are reflection amplitudes ($r = H_z^{refl}/H_z^{inc}$) of p-polarized plane waves reflecting from the interface between semi-infinite vacuum and a semi-infinite SPOF crystal and the dotted lines are the reflection

amplitudes of p-polarized plane waves reflecting the interface of semi-infinite vacuum and a semi-infinite homogeneous medium with the constitutive parameters of a SPOF metamaterial. Each point in Fig. 4.4 has a particular free-space wavelength λ_0 and incidence angle θ. There is a corresponding k_x determined from an eigenvalue simulation [14] and $k_y = 2\pi/\lambda_0 \sin(\theta)$. We calculate the current driven constitutive parameters for $\omega = 2\pi/\lambda_0$ and $\mathbf{k} = k_x\hat{\mathbf{x}} + k_y\hat{\mathbf{y}}$ and use them to calculate the reflection off of a homogeneous medium.

$$r = \frac{\mathrm{H_z^{refl}}}{\mathrm{H_z^{inc}}} = \frac{\cos(\theta) - z_{yz}}{\cos(\theta) + z_{yz}}. \tag{4.17}$$

Here $z_{yz} = \mathrm{E_y^{trans}}/\mathrm{H_z^{trans}}$ and the transmitted fields $\mathrm{E_y^{trans}}$ and $\mathrm{H_z^{trans}}$ are given by the null vector of the matrix in Eq. (4.3).

In Fig. 4.4 there are two bands $500nm < \lambda_0 < 600nm$ and $\lambda_0 > 800nm$ where we see very good agreement between the actual reflection off of the SPOF (solid line) and the reflection off of a homogeneous medium with the current driven constitutive parameters (dotted line) of the SPOF. There is less agreement near the magnetic resonance around $\lambda_0 \approx 680nm$ and also near the electric resonance around $\lambda_0 \approx 500nm$. There is also quite good agreement near the electric resonance near $\lambda_0 \approx 900nm$. Despite a small amount of error, the calculate constitutive parameters successfully predict reflection from an interface between vacuum and a SPOF crystal.

The constitutive parameters calculated using the method described in Secs. 4.2 and 4.3 pass both the test of predicting the correct dispersion rela-

tion and predicting the reflection amplitude of a plane wave from an interface with a metamaterial. Still, there are serious problems with the constitutive parameters returned by this method. The most obvious is the curious fact that ζ_{zy} was nonzero while ξ_{yz} was uniformly zero. This clearly violates Lorentz reciprocity. Also, the fact that all magnetic activity appeared in the quantity ζ_{zy} while μ_{zz} was uniformly equal to 1. It should be noted that if Pendry's method of fields averaging (Refs [50, 60] and Sec. 1.2) is used with the prescription of driving the metamaterial crystal with external electric and magnetic current described in Sec. 4.2 one obtains constitutive parameters very similar to those found above. Most notably, the curious result that ξ is always zero and μ always unity with all magnetic activity appearing in ζ. In addition to the lack of Lorentz reciprocity, the fact mentioned in Sec. 4.3 that the averaging procedure can only be performed with a finite valued $\mathbf{k}$ has important consequences. If one calculates the constitutive parameters for a crystal with rotational symmetry (the SPOF does not have rotational symmetry and would not be a good example in this case) in the limit $\mathbf{k} \to \mathbf{0}$ one finds that this limit is not well defined and that the constitutive parameters converge to slightly different values depending on the direction of $\mathbf{k}$.

One might strongly suspect that the claim that bianisotropy can be caused by spatial dispersion is itself unnecessary and wrong. For the case of the SPOF the ambiguity in the constitutive parameters outlined in Sec. 4.4 allow us to hide ζ_{zy} inside μ_{zz}. However, the theoretical justification for spatial dispersion causing bianisotropy presented in Sec. 2.2 in still valid and we will

see in the next two chapters that this is a very real and important effect.

The shortcomings of the homogenization procedure described in this chapter and the constitutive parameters that result from it are too great to be ignored. Ultimately, this must be considered a ambitious but failed attempt at metamaterial homogenization. Still, this effort is not a total loss. First, the idea of driving a crystal with magnetic current in addition to electric current is essential to solving for a significant number of constitutive parameters. Second, though the constitutive parameters produced by this procedure are flawed, they did lead the author to the theoretical argument outlined in Sec. 2.2 for the presence of bianisotropy in highly symmetric crystals due to spatial dispersion. This idea had been previously suggested by Li [40] and later by Alu [6] and is a characteristic feature of metamaterials with spatial dispersion.

Chapter 5

A 1D Model of a Metamaterial

5.1 Introduction

In the last chapter we presented an ambitious homogenization procedure that could calculate 36 constitutive parameters of a metamaterial. However, the returned parameters had some serious shortcomings, not the least of which was the lack of Lorentz reciprocity. In this chapter we will look at a more modest plan for metamaterial homogenization. This method requires some of the same assumptions of symmetry that we have criticized in the averaging methods outlined in Secs. 1.2 and 1.3. The advantage of this procedure is that even though it can only be used on crystals with a certain amount of symmetry, like the method in Chapter 4 it does calculate constitutive parameters as a function of both ω and $\mathbf{k}$. In addition, unlike the method of the last chapter this new method obeys Lorentz reciprocity. Finally, now that we have physically acceptable constitutive parameters, we will see in Chapter 6 that the ability to calculate partial derivatives of the constitutive parameters with respect to ω and $\mathbf{k}$ allow us to calculate important physical quantities related to energy flux and dissipative loss. This new homogenization procedure was originally published in Ref. [22].

As explained in Sec. 5.2 the homogenization method described in this chapter combines the idea of exciting a metamaterial with external electric and magnetic currents [41, 21] (Secs. 1.5 and 4.2) with the idea of modeling a metamaterial with thin surfaces of polarizable media [59] known as metasurfaces. This 1D array is excited with both electric and magnetic external current densities that are harmonic in time and space. This external current produces a response in the metamaterial that we quantify by calculating the polarization of the metasurfaces, which is then used to define the polarization density of the 1D array. The ratio of the polarization density of the array to the external current is related to a linear susceptibility matrix $\hat{\chi}$, which is then used to calculate the constitutive matrix $\hat{C}$ defined by Eq. (5.1). We also derive a few simple properties of the calculated constitutive parameters. In Sec. 5.2.3, we show how a real metamaterial with the appropriate symmetry can be described with the 1D model by calculating the surface polarizability of a thin layer of the metamaterial one unit cell thick. This is done by relating the surface polarizability to the S-matrix of a metasurface for plane waves of normal incidence. By inserting the surface polarizability of an actual metamaterial layer into our simple 1D model we can calculate the constitutive parameters of the metamaterial as a function of arbitrary frequency ω and wavevector $\mathbf{k}$.

In Sec. 5.3 we use the 1D model to calculate the constitutive parameters for an almost lossless 2D metamaterial. We test the calculated constitutive parameters for their ability to reproduce the correct dispersion relation, pro-

vide correct boundary conditions, and predict the correct emission from a metamaterial antenna.

5.2 Homogenization of 1D array of metasurfaces

5.2.1 Definition of the 1D model

Several authors have analyzed 3D models of interacting dipoles in a cubic lattice [9, 58, 57]. As pointed out by Smith [59], for a wave whose wavevector is along a principal axis of the crystal, the interaction between adjacent planes of dipoles is largely mediated by a simple electromagnetic plane wave. Near field evanescent waves do contribute to the coupling and perhaps should be considered in more sophisticated models, but in this dissertation we ignore all evanescent interactions. As in Ref. [59], we approximately model a metamaterial crystal as a lattice of thin metasurfaces interacting through plane waves.

As mentioned earlier, a certain degree of symmetry must be present in the metamaterial crystal of interest in order to model it as a 1D array. We will only consider 2D square arrays or 3D cubic array which are periodic in all dimensions. Also, we only consider propagation along an lattice direction of the crystal and we assume that the crystal has reflection symmetry in the two lattice directions perpendicular to the wavevector $\mathbf{k}$. This ensures that the wavevector lies along a principle axis of the crystal (which we choose to be the $\hat{\mathbf{x}}$ direction: $\mathbf{k} = k_x\hat{\mathbf{x}}$). We do not require that our crystal have reflection symmetry in the $\hat{\mathbf{x}}$ direction since due to spatial dispersion the wavevector $\mathbf{k} =$

$k_x\hat{\mathbf{x}}$ will break this symmetry regardless [40, 21]. Because of the symmetries we have already assumed, the two possible polarizations are both linear and independent and can be analyzed separately. Therefore, we only consider fields with the polarization the polarization $\mathbf{E} = \mathrm{E}_y\hat{\mathbf{y}}$ and $\mathbf{H} = \mathrm{H}_z\hat{\mathbf{z}}$. The analysis for the orthogonal polarization is analogous. Due to these symmetries and the fact that we only consider waves with a single polarization propagating in the $\hat{\mathbf{x}}$ direction we can describe these waves with only four constitutive parameters by defining the constitutive matrix

$$\hat{C}(\omega, k_x) \equiv \begin{pmatrix} \epsilon_{yy}(\omega, k_x) & \xi_{yz}(\omega, k_x) \\ \zeta_{zy}(\omega, k_x) & \mu_{zz}(\omega, k_x) \end{pmatrix}, \tag{5.1}$$

yielding the following constitutive relationship for a wave with a single frequency and wavevector

$$\begin{pmatrix} \mathrm{D}_y \\ \mathrm{B}_z \end{pmatrix} = \hat{C} \begin{pmatrix} \mathrm{E}_y \\ \mathrm{H}_z \end{pmatrix}. \tag{5.2}$$

Eq. (5.2) relates the macroscopic electric displacement D_y and magnetic flux density B_z fields to the macroscopic electric E_y and magnetic H_z fields. For the purpose of homogenization, all macroscopic fields are plane waves that are harmonic in time and space and obey the 1D Maxwell Equations

$$\begin{aligned} -k_x\mathrm{E}_y + \frac{\omega}{c}\mathrm{B}_z &= \mathrm{i}\frac{\mathrm{I}_z}{c}, \\ -k_x\mathrm{H}_z + \frac{\omega}{c}\mathrm{D}_y &= \mathrm{i}\frac{\mathrm{J}_y}{c}. \end{aligned} \tag{5.3}$$

Here $\mathrm{J}_y = \mathrm{J}_2 e^{\mathrm{i}(\omega t - k_x x)}$ and $\mathrm{I}_z = \mathrm{I}_3 e^{\mathrm{i}(\omega t - k_x x)}$ are electric and magnetic current densities that are harmonic in time and space.

Our 1D metamaterial model consists of an infinite array of metasurfaces that lie in the $\hat{\mathbf{y}}$-$\hat{\mathbf{z}}$ plane. The metasurfaces are separated in the $\hat{\mathbf{x}}$ direction by the lattice constant a. In between the metasurfaces the microscopic field equations (Maxwell equations) for this 1D system are

$$\begin{aligned} -\frac{\partial \mathrm{e}_y}{\partial x} - \mathrm{i}\frac{\omega}{c}\mu_b \mathrm{h}_z &= \frac{\mathrm{I}_z}{c}, \\ -\frac{\partial \mathrm{h}_z}{\partial x} - \mathrm{i}\frac{\omega}{c}\epsilon_b \mathrm{e}_y &= \frac{\mathrm{J}_y}{c}. \end{aligned} \tag{5.4}$$

Once again, e_y and h_z are the microscopic electric and magnetic fields and ω is the frequency. ϵ_b and μ_b are the background permittivity and permeability of the material filling the space between the metasurfaces.

The coupling of the microscopic fields to the metasurfaces is described by the boundary conditions of the fields across the metasurfaces. The metasurfaces have a polarization given by

$$\begin{pmatrix} \mathrm{p}_y \\ \mathrm{m}_z \end{pmatrix} = \hat{\alpha}(\omega) \begin{pmatrix} \mathrm{E}_y^{loc} \\ \mathrm{H}_z^{loc} \end{pmatrix} = \begin{pmatrix} \alpha_{yy}^{ee}(\omega) & \alpha_{yz}^{em}(\omega) \\ \alpha_{zy}^{me}(\omega) & \alpha_{zz}^{mm}(\omega) \end{pmatrix} \begin{pmatrix} \mathrm{E}_y^{loc} \\ \mathrm{H}_z^{loc} \end{pmatrix}. \tag{5.5}$$

Here p_y and m_z are the electric and magnetic polarization of a metasurface and can be thought of a electric and magnetic dipole moment densities per unit area of the metasurface. $\hat{\alpha}(\omega)$, which has units of length, is the surface polarizability matrix and the quantities E_y^{loc} and H_z^{loc} are the local electric and magnetic

fields at the location of the metasurface at $x = 0$. As mentioned below, the microscopic electric and magnetic fields (e_y and h_z) are discontinuous across the metasurface, so in Eq. (5.5) the local fields are defined as the average value of the field on both sides of the metasurface,

$$\begin{pmatrix} \mathrm{E}_y^{loc} \\ \mathrm{H}_z^{loc} \end{pmatrix} = \frac{1}{2} \begin{pmatrix} \mathrm{e}_y(0^+) + \mathrm{e}_y(0^-) \\ \mathrm{h}_z(0^+) + \mathrm{h}_z(0^-) \end{pmatrix}. \tag{5.6}$$

This is the same definition used in Ref. [35]. The boundary conditions of the fields across the metasurface are given by

$$\begin{aligned} \Delta \mathrm{h}_z &= \mathrm{h}_z(0^+) - \mathrm{h}_z(0^-) = -\mathrm{i}\frac{\omega}{c}\mathrm{p}_y, \\ \Delta \mathrm{e}_y &= \mathrm{e}_y(0^+) - \mathrm{e}_y(0^-) = -\mathrm{i}\frac{\omega}{c}\mathrm{m}_z. \end{aligned} \tag{5.7}$$

Thus the quantities $\mathrm{i}\omega \mathrm{p}_y/c$ and $\mathrm{i}\omega \mathrm{m}_z/c$ should be interpreted as electric and magnetic surface currents respectively.

Once the model has been defined it can be easily solved. To review, the field equations given by Eq. (5.4) must be solved with the boundary conditions across the metasurface given by Eqs. (5.5-5.7). Because the 1D array is periodic, the field equations only need to be solved in a single cell of the crystal with Bloch periodic boundary conditions on the outer boundaries of the domain. In Sec. 5.2.4, we derive an analytic solution to the model which can be evaluated numerically. We have also solved the 1D model using the commercial finite element software COMSOL Multiphysics and confirmed that the results agree with the analytic solution. Once the model is solved and the

resulting polarization density of the metamaterial crystal is calculated, it is possible to calculate the constitutive parameters.

5.2.2 Calculation of the constitutive matrix

After solving the 1D model, the solution can be used to calculate the macroscopic constitutive parameters. We define the macroscopic polarization density as

$$\begin{pmatrix} \mathrm{P}_y \\ \mathrm{M}_z \end{pmatrix} = \begin{pmatrix} \mathrm{p}_y/a \\ \mathrm{m}_z/a \end{pmatrix}, \tag{5.8}$$

where p_y and m_z are the polarizations of the metasurface in the unit cell of the 1D model calculated according to Eqs. (5.5,5.6). We can relate the macroscopic polarization density to the macroscopic E_y and H_z fields by the relation

$$\begin{pmatrix} \mathrm{P}_y \\ \mathrm{M}_z \end{pmatrix} = \hat{\chi} \begin{pmatrix} \mathrm{E}_y \\ \mathrm{H}_z \end{pmatrix} = \begin{pmatrix} \epsilon_{yy} - \epsilon_b & \xi_{yz} \\ \zeta_{zy} & \mu_{zz} - \mu_b \end{pmatrix} \begin{pmatrix} \mathrm{E}_y \\ \mathrm{H}_z \end{pmatrix} \tag{5.9}$$

Here we have defined the susceptibility $\hat{\chi}$ to be the constitutive matrix $\hat{C}$ with the background permittivity ϵ_b and permeability μ_b subtracted off.

The macroscopic Maxwell equations in Eq. (5.3) can be rearranged to yield

$$\frac{1}{c} \begin{pmatrix} \mathrm{J}_y \\ \mathrm{I}_z \end{pmatrix} = -\mathrm{i} \left[\frac{\omega}{c} \hat{\chi} + \underbrace{\begin{pmatrix} \epsilon_b \omega/c & -k_x \\ -k_x & \mu_b \omega/c \end{pmatrix}}_{\hat{K}} \right] \begin{pmatrix} \mathrm{E}_y \\ \mathrm{H}_z \end{pmatrix}. \tag{5.10}$$

We now define the matrices

$$\hat{\mathcal{J}} = \frac{1}{c}\begin{pmatrix} \mathrm{J}_y^1 & \mathrm{J}_y^2 \\ \mathrm{I}_z^1 & \mathrm{I}_z^2 \end{pmatrix}, \qquad \hat{\mathcal{P}} = \begin{pmatrix} \mathrm{P}_y^1 & \mathrm{P}_y^2 \\ \mathrm{M}_z^1 & \mathrm{M}_z^2 \end{pmatrix}. \tag{5.11}$$

Similarly to Sec. 4.2, in order to solve for all four components of the constitutive matrix it's necessary to solve the 1D model twice, each time with different amounts of electric and magnetic current. The electric currents J_y^1 and J_y^2 are the external electric currents for the first and second solutions of the model respectively. Likewise I_z^1 and I_z^2 are the external magnetic currents for the first and second solutions of the model. The electric and magnetic external currents must be chosen so that the vectors in $\hat{\mathcal{J}}$ are linearly independent. Aside from this condition, the external currents are completely arbitrary. Similarly, the matrix $\hat{\mathcal{P}}$ contains the macroscopic polarizations densities calculated from the two solutions. Using Eqs. (5.9,5.10) we can relate the susceptibility matrix $\hat{\chi}$ to the matrices $\hat{\mathcal{J}}$ and $\hat{\mathcal{P}}$ with the equation

$$\hat{\mathcal{P}} = \mathrm{i}\underbrace{\hat{\chi}\left(1 + \omega/c\hat{K}^{-1}\hat{\chi}\right)^{-1}}_{\hat{Q}}\hat{K}^{-1}\hat{\mathcal{J}} = \mathrm{i}\hat{Q}\hat{K}^{-1}\hat{\mathcal{J}}. \tag{5.12}$$

Here we have defined $\hat{Q}$ as the matrix relating the polarization to the external current. Eq. (5.12) can be solved for $\hat{\chi}$ resulting in

$$\hat{\chi} = \left(1 - \omega/c\hat{Q}\hat{K}^{-1}\right)^{-1}\hat{Q}. \tag{5.13}$$

$\hat{\chi}$ is related to the constitutive matrix by Eq. (5.9) providing the relation

$$\hat{C}(\omega, \mathbf{k}) = \begin{pmatrix} \epsilon_b & 0 \\ 0 & \mu_b \end{pmatrix} + \hat{\chi}(\omega, \mathbf{k}) \tag{5.14}$$

Since the 1D model is excited with external currents that are harmonic in time and space ($\mathrm{J}_y = \mathrm{J}_2 e^{\mathrm{i}(\omega t - k_x x)}$ and $\mathrm{I}_z = \mathrm{I}_3 e^{\mathrm{i}(\omega t - k_x x)}$), the excited macroscopic fields are also harmonic with frequency ω and wavenumber k_x. As a result, the constitutive parameters calculated for this 1D metamaterial crystal are functions of frequency ω and wavenumber k_x. These potentially complex ω and k_x are arbitrary and in general not related to each other by the dispersion relation of eigenmodes of the metamaterial crystal. The constitutive parameters are also functions of the background permittivity ϵ_b and permeability μ_b and the surface polarizability $\hat{\alpha}$. In order to use this model to describe realistic metamaterials we need to connect an specific metamaterial crystal to the parameters ϵ_b, μ_b and $\hat{\alpha}$.

5.2.3 Calculation of a surface polarizability from the S-matrix

In to homogenize specific metamaterial crystals with our 1D model it is necessary to replace a plane of metamaterial inclusions with a metasurface. We propose to calculate the surface polarizability of a single metasurface by numerically measuring the S-matrix of scattering amplitudes for plane waves incident from both sides of the metasurface at an incident angle normal to the metasurface. We define our S-matrix as

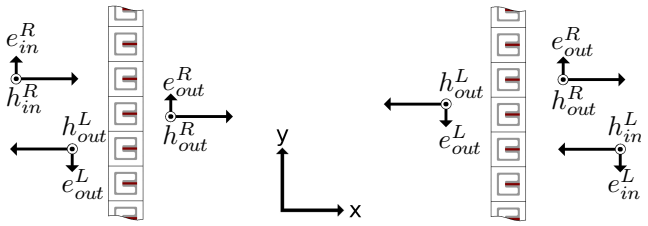

Figure 5.1: Calculation of the S-matrix S^{H} of a single layer of metamaterial for p-polarized waves. The S-matrix is defined as the ratio of the h_z fields of outgoing planes wave to the h_z fields of incoming plane waves. The amplitudes of the waves are evaluated at the center of the metamaterial layer as if the scattering object had zero width.

$$\begin{pmatrix} \mathrm{h}^L_{out} \\ \mathrm{h}^R_{out} \end{pmatrix} = \underbrace{\begin{pmatrix} S^{\mathrm{H}}_{11} & S^{\mathrm{H}}_{12} \\ S^{\mathrm{H}}_{21} & S^{\mathrm{H}}_{22} \end{pmatrix}}_{S^{\mathrm{H}}} \begin{pmatrix} \mathrm{h}^R_{in} \\ \mathrm{h}^L_{in} \end{pmatrix}. \tag{5.15}$$

Here, h^L_{in} and h^R_{in} are the amplitudes of the magnetic fields of waves incident onto the metasurface moving to the left (in the negative $\hat{\mathbf{x}}$ direction) and moving to the right (in the positive $\hat{\mathbf{x}}$ direction) respectively. h^L_{out} and h^R_{out} are the magnetic field amplitudes of waves moving outward from the metasurface moving to the left and right respectively. By combining Eqs. (5.5,5.7) we find an equation relating the discontinuity in the fields from the positive x side to the negative x side of the metasurface to the local field defined in Eq. (5.6).

$$\begin{pmatrix} \Delta \mathrm{h}_z \\ \Delta \mathrm{e}_y \end{pmatrix} = -\mathrm{i}\frac{\omega}{c}\hat{\alpha} \begin{pmatrix} \mathrm{E}^{loc}_y \\ \mathrm{H}^{loc}_z \end{pmatrix} \tag{5.16}$$

The h_z and e_y fields on both sides of the metasurface can be constructed from

the incoming and outgoing h_z field amplitudes in Eq. (5.15). On the left side of the metasurface we have $\mathrm{h}_z = \mathrm{h}^R_{in} + \mathrm{h}^L_{out}$ and $\mathrm{e}_y = z_b(\mathrm{h}^R_{in} - \mathrm{h}^L_{out})$ where $z_b = \sqrt{\mu_b/\epsilon_b}$ is the impedance of the background material. Similarly, on the right side of the metasurface we have $\mathrm{h}_z = \mathrm{h}^R_{out} + \mathrm{h}^L_{in}$ and $\mathrm{e}_y = z_b(\mathrm{h}^R_{out} - \mathrm{h}^L_{in})$. By using the S-matrix S^{H} to relate the outgoing fields to the incoming fields (Eq. (5.15)) and by using the fact that this relation is true for all possible incoming fields we find the relation

$$\begin{pmatrix} -S^{\mathrm{H}}_{11} + S^{\mathrm{H}}_{21} - 1 & -S^{\mathrm{H}}_{12} + S^{\mathrm{H}}_{22} + 1 \\ z_b(S^{\mathrm{H}}_{11} + S^{\mathrm{H}}_{21} - 1) & z_b(S^{\mathrm{H}}_{12} + S^{\mathrm{H}}_{22} - 1) \end{pmatrix} = -\frac{\mathrm{i}\omega\hat{\alpha}}{2c} \begin{pmatrix} z_b(-S^{\mathrm{H}}_{11} + S^{\mathrm{H}}_{21} + 1) & z_b(-S^{\mathrm{H}}_{12} + S^{\mathrm{H}}_{22} - 1) \\ S^{\mathrm{H}}_{11} + S^{\mathrm{H}}_{21} + 1 & S^{\mathrm{H}}_{12} + S^{\mathrm{H}}_{22} + 1 \end{pmatrix}, \tag{5.17}$$

which can be solved for $\hat{\alpha}$ to give

$$\hat{\alpha} = -\frac{2\mathrm{i}}{\omega/c(1 + S^{\mathrm{H}}_{12} + S^{\mathrm{H}}_{21} - \det(S^{\mathrm{H}}))} \times \begin{pmatrix} \left[1 + \det(S^{\mathrm{H}}) + (S^{\mathrm{H}}_{11} + S^{\mathrm{H}}_{22})\right]/z_b & (S^{\mathrm{H}}_{12} - S^{\mathrm{H}}_{21}) + (S^{\mathrm{H}}_{11} - S^{\mathrm{H}}_{22}) \\ (S^{\mathrm{H}}_{12} - S^{\mathrm{H}}_{21}) - (S^{\mathrm{H}}_{11} - S^{\mathrm{H}}_{22}) & \left[1 + \det(S^{\mathrm{H}}) - (S^{\mathrm{H}}_{11} + S^{\mathrm{H}}_{22})\right] z_b \end{pmatrix}. \tag{5.18}$$

It can immediately be seen that for a reciprocal metamaterial layer with transmission amplitudes that are equal regardless of which side the incoming beam is incident upon ($S^{\mathrm{H}}_{12} = S^{\mathrm{H}}_{21}$), the surface polarizability has the property

$$\alpha^{em}_{yz} = -\alpha^{me}_{zy}, \tag{5.19}$$

indicating that the metasurface is reciprocal.

Though we derived Eq. (5.18) for an infinitesimally thin surface, we can use it to assign effective surface polarizabilities to thin layers of metamaterials (Fig. 5.1). For a particular metamaterial inclusion, it is straightforward to perform a numerical simulation that calculates the S-matrix by calculating the reflection and transmission amplitudes of plane waves scattering off of a single layer of metamaterial one unit cell thick. By using Eq. (5.18), we can then use the S-matrix to assign an effective surface polarizability to the metamaterial layer. Using this effective surface polarizability and the analytic solution to the 1D model provided in Sec. 5.2.4, one can then calculate the constitutive parameters of the metamaterial crystal using Eqs. (5.13,5.14).

5.2.4 Analytic solution to the 1D model

In this section we derive an analytic solution to the 1D model described in Sec 5.2.1. To review, the model is a one dimensional system with all fields harmonic in time with frequency ω. The spatial domain is separated into unit cells of length a. In the center of each cell is a metasurface with surface polarizability $\hat{\alpha}$ defined in Eq. (5.5). The space between each metasurface is filled with a homogeneous material with a background permittivity ϵ_b, permeability μ_b and impedance $z_b = \sqrt{\mu_b/\epsilon_b}$. Since we limit ourselves to the polarization $\mathbf{E} = \mathrm{E}_y\hat{\mathbf{y}}$ and $\mathbf{H} = \mathrm{H}_z\hat{\mathbf{z}}$, in between the metasurfaces the equations of motion that we solve are given in Eq. (5.4). The metasurfaces interact with each other through free plane waves with frequency ω and wavenumber

$k_0 = \sqrt{\epsilon_b \mu_b}\omega$. Across each metasurface, the e_y and h_z fields are discontinuous according to Eq. (5.16). The polarization of the metasurfaces which defines the discontinuity is equal to the surface polarizability times the local field strength. Since the fields are discontinuous across each metasurface the local field strength at the each metasurface is defined in Eq. (5.6) as the average value of the field from both sides of the metasurface. Finally, the entire system is driven with external electric and magnetic current

$$\mathrm{J}_y = \mathrm{J}_2 e^{\mathrm{i}(\omega t - k_x x)}, \qquad \mathrm{I}_z = \mathrm{I}_3 e^{\mathrm{i}(\omega t - k_x x)}, \tag{5.20}$$

where the current strengths J_2 and I_3 are chosen arbitrarily. The solution to Eq. (5.4) with the external current in Eq. (5.20) is

$$\begin{pmatrix} \mathrm{e}_y \\ \mathrm{h}_z \end{pmatrix} = \frac{\mathrm{i}e^{-\mathrm{i}k_x x}}{\epsilon_b \mu_b \omega^2/c^2 - k_x^2} \begin{pmatrix} \mu_b \omega/c & k_x \\ k_x & \epsilon_b \omega/c \end{pmatrix} \frac{1}{c} \begin{pmatrix} \mathrm{J}_2 \\ \mathrm{I}_3 \end{pmatrix} + \begin{pmatrix} z_b a_n e^{-\mathrm{i}k_0 x} - z_b b_n e^{\mathrm{i}k_0 x} \\ a_n e^{-\mathrm{i}k_0 x} + b_n e^{\mathrm{i}k_0 x} \end{pmatrix}. \tag{5.21}$$

The coefficients a_b and b_n are the amplitudes of the right and left moving free plane waves that mediate interactions between adjacent metasurfaces. The subscript n specifies the particular metasurface that the plane waves interact with. For example the n and $n+1$ metasurfaces interact with the right and left moving plane waves with amplitudes a_n and b_n respectively. These coefficients are related to each other by the Bloch phase condition

$$\begin{pmatrix} a_{n+1} \\ b_{n+1} \end{pmatrix} = \begin{pmatrix} e^{-\mathrm{i}(k_x - k_0)a} & 0 \\ 0 & e^{-\mathrm{i}(k_x + k_0)a} \end{pmatrix} \begin{pmatrix} a_n \\ b_n \end{pmatrix}. \tag{5.22}$$

The coefficients are also determined by the boundary conditions across each metasurface given by Eq. (5.16). The left hand side of Eq. (5.16) is related to the coefficients by

$$\begin{pmatrix} \Delta \mathrm{h}_z \\ \Delta \mathrm{e}_y \end{pmatrix} = \underbrace{\begin{pmatrix} 1 & 1 \\ z_b & -z_b \end{pmatrix} \begin{pmatrix} e^{-\mathrm{i}(k_x - k_0)a} - 1 & 0 \\ 0 & e^{-\mathrm{i}(k_x + k_0)a} - 1 \end{pmatrix}}_{\hat{A}} \begin{pmatrix} a_b \\ b_n \end{pmatrix}. \tag{5.23}$$

The field strength on the right hand side of Eq. (5.5) is the sum of two solutions, the inhomogeneous solution to Eq. (5.4) that does not obey the correct boundary conditions and the homogeneous solutions to Eq. (5.4) which corresponds to the free waves mediating interactions between adjacent metasurfaces. We choose our coordinates so that $x = 0$ at the location of the nth metasurface. The value of the inhomogeneous solution at the location of the nth metasurface is

$$\begin{pmatrix} \mathrm{E}_y^{loc} \\ \mathrm{H}_z^{loc} \end{pmatrix}_{driven} = \mathrm{i} \underbrace{\frac{1}{\epsilon_b \mu_b \omega^2/c^2 - k_x^2} \begin{pmatrix} \mu_b \omega/c & k_x \\ k_x & \epsilon_b \omega/c \end{pmatrix}}_{\hat{K}^{-1}} \frac{1}{c} \begin{pmatrix} \mathrm{J}_2 \\ \mathrm{I}_3 \end{pmatrix}, \tag{5.24}$$

where the matrix $\hat{K}$ was defined in Eq. (5.10). The value of the homogeneous solution at the location of the nth metasurface is defined in Eq. (5.6) as the average value from both sides of the metasurface and is given by

$$\begin{pmatrix} \mathrm{E}_y^{loc} \\ \mathrm{H}_z^{loc} \end{pmatrix}_{free} = \underbrace{\begin{pmatrix} z_b & -z_b \\ 1 & 1 \end{pmatrix} \frac{1}{2} \begin{pmatrix} e^{-\mathrm{i}(k_x - k_0)a} + 1 & 0 \\ 0 & e^{-\mathrm{i}(k_x + k_0)a} + 1 \end{pmatrix}}_{\hat{B}} \begin{pmatrix} a_n \\ b_n \end{pmatrix}. \tag{5.25}$$

Combining Eq. (5.16) with Eqs. (5.23-5.25), we find an equation relating the coefficients a_n and b_n to the external current.

$$\hat{A}\begin{pmatrix} a_n \\ b_n \end{pmatrix} = \frac{\omega}{c}\hat{\alpha}\hat{K}^{-1}\frac{1}{c}\begin{pmatrix} J_2 \\ I_3 \end{pmatrix} - \mathrm{i}\frac{\omega}{c}\hat{\alpha}\hat{B}\begin{pmatrix} a_n \\ b_n \end{pmatrix}, \tag{5.26}$$

which can be solved for the coefficients to give

$$\begin{pmatrix} a_n \\ b_n \end{pmatrix} = \left(\hat{A} + \mathrm{i}\frac{\omega}{c}\hat{\alpha}\hat{B}\right)^{-1}\frac{\omega}{c}\hat{\alpha}\hat{K}^{-1}\frac{1}{c}\begin{pmatrix} J_2 \\ I_3 \end{pmatrix}. \tag{5.27}$$

We can relate the coefficients to the polarization density with Eq. (5.5) yielding

$$\begin{aligned} \begin{pmatrix} \mathrm{P}_y \\ \mathrm{M}_z \end{pmatrix} &= \frac{1}{a}\begin{pmatrix} \mathrm{p}_y \\ \mathrm{m}_z \end{pmatrix} \\ &= \mathrm{i}\frac{\hat{\alpha}}{a}\hat{K}^{-1}\frac{1}{c}\begin{pmatrix} J_2 \\ I_3 \end{pmatrix} + \frac{\hat{\alpha}}{a}\hat{B}\begin{pmatrix} a_n \\ b_n \end{pmatrix} \\ &= \underbrace{\mathrm{i}\frac{\hat{\alpha}}{a}\left[1 - \left(\frac{\omega}{c}\hat{\alpha} - \mathrm{i}\hat{A}\hat{B}^{-1}\right)^{-1}\frac{\omega}{c}\hat{\alpha}\right]}_{\hat{Q}}\hat{K}^{-1}\frac{1}{c}\begin{pmatrix} J_2 \\ I_3 \end{pmatrix} \end{aligned} \tag{5.28}$$

Here we have identified the matrix $\hat{Q}$, defined in Eq. (5.12) as the matrix relating the polarization and the external current. The matrix $\hat{A}\hat{B}^{-1}$ is evaluated to be

$$\hat{A}\hat{B}^{-1} = \frac{2\mathrm{i}}{\cos(k_x a) + \cos(k_0 a)}\begin{pmatrix} \sin(k_0 a)/z_b & -\sin(k_x a) \\ -\sin(k_x a) & z_b \sin(k_0 a) \end{pmatrix}. \tag{5.29}$$

Putting this into Eq. (5.28) allows us to evaluate $\hat{Q}$ which we can then use to evaluate $\hat{C}$ using Eqs. (5.13,5.14).

Finally, from Eq. (5.27) we see that we can derive a dispersion relation for free eigenmodes traveling through the one dimensional crystal by setting the determinant of $\hat{A}\hat{B}^{-1} + \mathrm{i}\omega\hat{\alpha}/c$ equal to zero, producing

$$\underbrace{\left(1 + \frac{\omega^2}{c^2}\frac{\alpha_{yy}^{ee}\alpha_{zz}^{mm} - \alpha_{yz}^{em}\alpha_{zy}^{me}}{4}\right)}_{\mathrm{M}_1}\cos(k_x a) + \underbrace{\frac{\omega}{c}\frac{\alpha_{zy}^{me} + \alpha_{yz}^{em}}{2}}_{\mathrm{M}_2}\sin(k_x a) =$$

$$\underbrace{\left(1 - \frac{\omega^2}{c^2}\frac{\alpha_{yy}^{ee}\alpha_{zz}^{mm} - \alpha_{yz}^{em}\alpha_{zy}^{me}}{4}\right)\cos(k_0 a) - \frac{\omega}{c}\frac{\alpha_{yy}^{ee}z_b + \alpha_{zz}^{mm}/z_b}{2}\sin(k_0 a)}_{\mathrm{M}_3}, \tag{5.30}$$

which in terms of M_1, M_2 and M_3 can be solved for k_x:

$$k_x = \pm\frac{1}{a}\arccos\left[\frac{\mathrm{M}_3}{\sqrt{\mathrm{M}_1^2 + \mathrm{M}_2^2}}\right] + \frac{1}{\mathrm{i}a}\log\left[\frac{\mathrm{M}_1 + \mathrm{i}\mathrm{M}_2}{\sqrt{\mathrm{M}_1^2 + \mathrm{M}_2^2}}\right]. \tag{5.31}$$

Notice that for a reciprocal metasurface ($\alpha_{yz}^{em} = -\alpha_{zy}^{me}$) the quantity M_2 vanishes and the solutions to Eq. (5.30) are even in k_x, which is to be expected for a reciprocal crystal. For a nonreciprocal metasurface the solutions to Eq. (5.30) are not even in k_x.

5.2.5 Properties of the constitutive parameters

Here we briefly outline several properties of the constitutive parameters calculated according to the method just described. These properties are proven directly from the analytic model derived in Sec. 5.2.4. First, as we have already

seen in Sec. 5.2.3 the surface polarizability describing a reciprocal metasurface has the property $\alpha_{yz}^{em} = -\alpha_{zy}^{me}$. If ω and k_x are nonzero then from Eq. (5.28) it can easily be shown that $\hat{Q}$ has the properties

$$\begin{aligned} Q_{11}(\omega, -k_x) &= Q_{11}(\omega, k_x), \\ Q_{22}(\omega, -k_x) &= Q_{22}(\omega, k_x), \\ Q_{12}(\omega, -k_x) &= -Q_{21}(\omega, k_x). \end{aligned} \tag{5.32}$$

In general, $\hat{Q}$ is not always invertable. For example, if $\hat{\alpha}$ contains only an electric response in α_{yy}^{ee} and all other components of the surface polarizability are zero, then it can be seen from Eq. (5.28) that Q_{11} is nonzero and all other components of $\hat{Q}$ are zero, therefore making $\hat{Q}$ singular and not invertable. In practice, real metamaterials have both an electric (α_{yy}^{ee}) and magnetic (α_{zz}^{mm}) response so $\hat{Q}$ usually will be invertable. When this is the case, Eq. (5.13) can be rewritten as

$$\hat{\chi} = \left(\hat{Q}^{-1} - \omega/c\hat{K}^{-1}\right)^{-1}. \tag{5.33}$$

In this form it is easy to see that $\hat{\chi}$ has the same symmetry properties as $\hat{Q}$ in Eq. (5.32). As a result, the constitutive parameters have the properties

$$\begin{aligned} \epsilon_{yy}(\omega, -k_x) &= \epsilon_{yy}(\omega, k_x), \\ \mu_{zz}(\omega, -k_x) &= \mu_{zz}(\omega, k_x), \\ \xi_{yz}(\omega, -k_x) &= -\zeta_{zy}(\omega, k_x), \end{aligned} \tag{5.34}$$

which is to say that the constitutive parameters obey Lorentz reciprocity. Though this is easy to prove only when $\hat{Q}$ is invertable, numerical tests indicate that this is true even when $\hat{\alpha}$ and $\hat{Q}$ are not invertable.

Another property of the constitutive parameters exists relating to loss. If ω, k_x, ϵ_b and μ_b are real valued numbers then it is easy to see from Eqs. (5.10,5.29) that the matrices $\hat{K}$ and $\mathrm{i}\hat{A}\hat{B}^{-1}$ are both hermitian. If $\hat{\alpha}$ is also hermitian, indicating a lossless metasurface, then from the expression for $\hat{Q}$ in Eq. (5.28) it is easy to see that $\hat{Q}$ will be hermitian. Combining this with Eqs. (5.13,5.14) shows that $\hat{C}$ is hermitian as well

$$\hat{C} = \hat{C}^{\dagger}. \tag{5.35}$$

We emphasize that this is no longer strictly true if ω or k_x are complex.

Combining Eqs. (5.5,5.8,5.9) we see a relationship between the macroscopic field at the location of the thin metasurface and the local field

$$\hat{\chi}\begin{pmatrix}\mathrm{E}_y\\ \mathrm{H}_z\end{pmatrix} = \frac{\hat{\alpha}}{a}\begin{pmatrix}\mathrm{E}_y^{loc}\\ \mathrm{H}_z^{loc}\end{pmatrix} \tag{5.36}$$

Since in general $\hat{\chi} \neq \hat{\alpha}/a$ the immediate implication of this equation is that in general the macroscopic electric and magnetic fields are nonlocal. However, it can be seen from Eq. (5.29) that $\hat{A}\hat{B}^{-1}$ has the property

$$\lim_{\substack{\omega a/c\to 0\\ k_x a\to 0}} \hat{A}\hat{B}^{-1} = \mathrm{i}\hat{K}a. \tag{5.37}$$

Inserting this into the expression for $\hat{Q}$ in Eq. (5.28) yields

$$\lim_{\substack{\omega a/c\to 0\\ k_x a\to 0}} \hat{Q} = \frac{\hat{\alpha}}{a} - \frac{\hat{\alpha}}{a}\left(\frac{\omega}{c}\hat{\alpha} + \hat{K}a\right)^{-1}\frac{\omega}{c}\hat{\alpha}. \tag{5.38}$$

Putting this result into the expression for $\hat{\chi}$ in Eq. (5.13) produces

$$\lim_{\substack{\omega a/c\to 0\\ k_x a\to 0}} \hat{\chi} = \frac{\hat{\alpha}}{a}. \tag{5.39}$$

Thus, we see that in the long wavelength limit, the constitutive matrix is simply the background constitutive matrix plus $\hat{\alpha}/a$ and the macroscopic field is equal to the local field.

5.3 1D Example: Split Ring Resonator

5.3.1 Description of crystal unit cell and calculation of constitutive parameters

We now describe a metamaterial crystal that we will use to test this 1D homogenization procedure. The metamaterial is an lowloss 2D split ring resonator (SRR) embedded in vacuum [65]. A diagram of the SRR is shown in Fig. 5.2. The lattice constant of the square unit cell is a while the length of the square SRR is $0.7a$. The metal is a perfect electric conductor with thickness $0.07a$. The length of the capacitor is $0.45a$ and the capacitor gap is $0.07a$ and is filled with a dielectric with permittivity $\epsilon_{cap} = 4 - \mathrm{i}0.0001$. All rounded corners are circular with a radius of $0.04a$. This 2D SRR has been shown to support subwavelength ($\lambda_0 \gg a$) magnetic resonances [65].

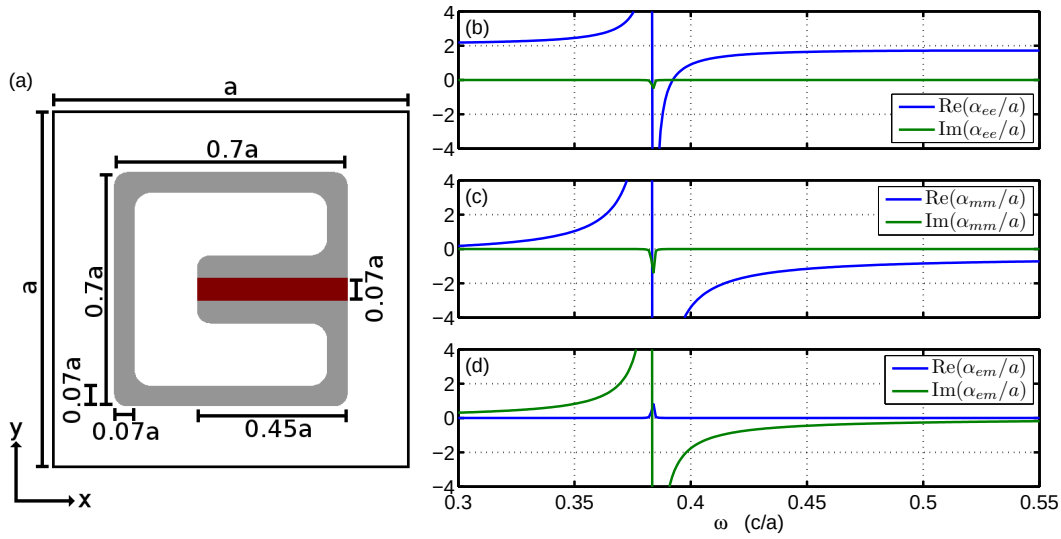

Figure 5.2: (a) The unit cell of the SRR. (b) α_{yy}^{ee}. (c) α_{zz}^{mm}. (d) α_{yz}^{em}. $\hat{\alpha}$ is calculated from the S-matrix of a single layer of SRR's infinite in the $\hat{\mathbf{y}}$ direction calculated using Eq. (5.18). Note that the real part of α_{yz}^{em} and the imaginary parts of α_{yy}^{ee} and α_{zz}^{mm} are zero except near the resonance.

The surface polarizability of a single layer of SRR's is also plotted in Fig. 5.2. Since the SRR is reciprocal the transmission coefficients for waves incident on either side of the SRR layer are equal ($S_{12}^{\mathrm{H}} = S_{21}^{\mathrm{H}}$). According to Eq. (5.18) this implies that $\alpha_{yz}^{em} = -\alpha_{zy}^{me}$, therefore only α_{yz}^{em} is plotted in Fig. 5.2. All components of the surface polarizability resonate at the same frequency of $\omega \simeq 0.383$. Since this SRR is mostly lossless ($\epsilon_{cap} = 4 - \mathrm{i}0.0001$), $\hat{\alpha}$ is approximately hermitian. We emphasize that $\hat{\alpha}(\omega)$ is only a function of frequency as opposed to $\hat{C}(\omega, k_x)$ which is a function of frequency and wavenumber.

Once we have calculated the surface polarizability $\hat{\alpha}$, we can use the

procedure described in Sec. 5.2.2 to calculate $\hat{C}(\omega, k_x)$ for any frequency and wavenumber. Since we are often interested in the constitutive parameters of crystal eigenmodes, we will first calculate the parameters on the dispersion curve or $\hat{C} = \hat{C}(\omega, k_x(\omega))$. This will allow us to test $\hat{C}(\omega, k_x(\omega))$ by using it to independently calculate $k_x(\omega)$ of a homogeneous medium that corresponds to the SRR crystal. In Fig. 5.3 we see the dispersion curve calculated from an finite element eigenvalue simulation [14] (solid lines). Taking Eq. (5.10), we can remove the source terms to obtain the generalized eigenvalue problem

$$\frac{\omega}{c}\hat{C}\begin{pmatrix}\mathrm{E}_y\\ \mathrm{H}_z\end{pmatrix} = k_x\begin{pmatrix}0 & 1\\ 1 & 0\end{pmatrix}\begin{pmatrix}\mathrm{E}_y\\ \mathrm{H}_z\end{pmatrix}. \tag{5.40}$$

Superimposed on top of the numerically calculated dispersion curve in Fig. 5.3 is the solution to Eq. (5.40) (dotted lines) solved using the constitutive parameters calculated by exciting the crystal with a frequency and wavenumber along the numerically calculated dispersion curve $k_x = k_x(\omega)$.

Fig. 5.3 shows that the dispersion curve calculated from the extracted constitutive parameters agrees with the numerically exact dispersion curve calculated from a finite element eigenvalue simulation [14] with only a small disagreement near the resonance.

Because the SRR is reciprocal (see Sec. 5.2.5), the constitutive parameters obey the Lorentz reciprocity relations in Eq. (5.34). This is true despite the fact that there is no reflection symmetry of the SRR crystal in the $\hat{\mathbf{x}}$ direction. Because of reciprocity we can write the constitutive parameters as

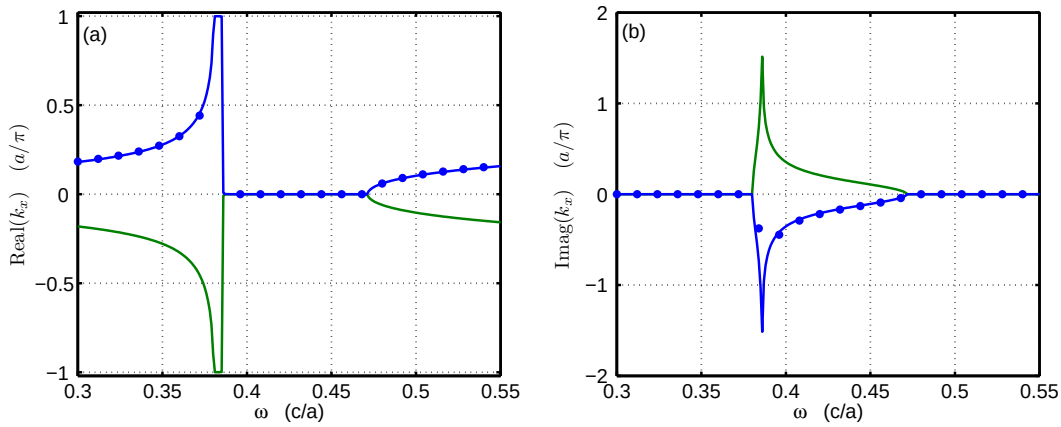

Figure 5.3: Dispersion curve of a p-polarized ($\mathbf{H} = \mathrm{H}_z(x,y)\hat{\mathbf{z}}$) wave propagating through a 2D array of the SRR unit cell shown in Fig. 5.2. Real (a) and imaginary (b) parts of $k_x(\omega)$ vs. ω where $\mathbf{k} = k_x\hat{\mathbf{x}}$. Solid lines: dispersion curves for a p-polarized wave obtained from an eigenvalue simulation [14]. Dotted lines: dispersion curves calculated from the constitutive parameters in Eq. (5.14) by solving the generalized eigenvalue problem in Eq. (5.40).

$$\hat{C} = \begin{pmatrix} \epsilon_{yy} & \kappa_o + \kappa_e \\ \kappa_o - \kappa_e & \mu_{zz} \end{pmatrix}. \tag{5.41}$$

Here ϵ_{yy}, μ_{zz} and κ_e are even functions of k_x but κ_o is an odd function of k_x. κ_e (κ even) describes intrinsic bianisotropy due to the asymmetry of the SRR [44]. κ_o (κ odd) describes extrinsic bianisotropy due to spatial dispersion in the SRR crystal [40, 20, 21]. This extrinsic bianisotropy would be present even in a crystal with reflection symmetry in the $\hat{\mathbf{x}}$ direction. The calculated constitutive parameters are shown in Fig. 5.4. Combining these constitutive parameters with Eq. (5.40) produces the dispersion relation

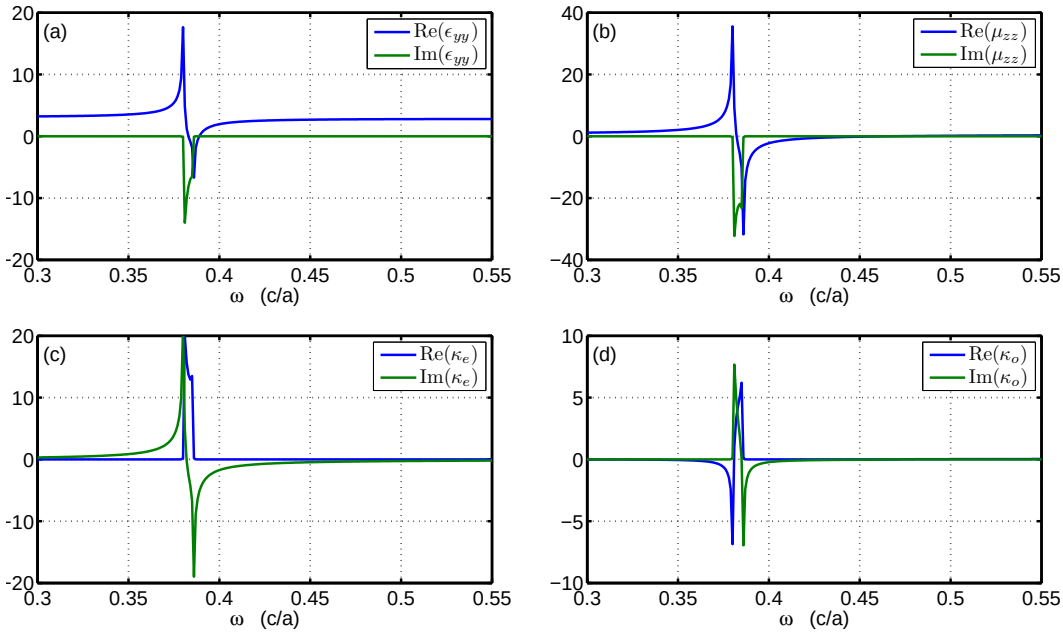

Figure 5.4: The constitutive parameters of the SRR crystal calculated on the dispersion curve $k_x = k_x(\omega)$ plotted in Fig. 5.3. The SRR unit cell parameters are the same as in Fig. 5.2.

$$(k_x - \omega\kappa_o/c)^2 = \left(\epsilon_{yy}\mu_{zz} + \kappa_e^2\right)\omega^2/c^2. \tag{5.42}$$

5.3.2 Test of Maxwell boundary conditions

Since the constitutive parameters reproduce the correct dispersion curve the next test is whether the constitutive parameters provide the correct boundary conditions. To test this, the reflection of a plane wave at normal incidence from the interface between semi-infinite vacuum and a semi-infinite SRR crystal is calculated in two different ways. First, the reflection is calculated with

a finite element simulation. We can compare this reflection coefficient to the expected reflection of a plane wave from the interface between semi-infinite vacuum and a semi-infinite homogeneous medium with the constitutive parameters of a SRR crystal. By taking the eigenvector of Eq. (5.40) that corresponds to a right moving wave ($\mathrm{Im}(k_x) < 0$), we can define the impedance as the ratio of the transmitted electric field and the transmitted magnetic field $z^+ = \mathrm{E}_y^{\mathrm{trans}}/\mathrm{H}_z^{\mathrm{trans}}$. The + superscript indicates that this impedance is for a rightward moving wave. Due to the asymmetry of the SRR in the $\hat{\mathbf{x}}$ direction there are two impedances [41]. One for a right moving wave z^+ and one for a left moving wave z^-. Using the Maxwell equations we see that in terns of ω, k_x and the constitutive parameters the right and left moving impedances are

$$z^{\pm} = \frac{k_x(\omega) - \omega\kappa_o/c \mp \omega\kappa_e/c}{\omega\epsilon/c} = \frac{\omega\mu/c}{k_x(\omega) - \omega\kappa_o/c \pm \omega\kappa_e/c}. \tag{5.43}$$

Here all constitutive parameters are calculated for a right moving wavenumber k_x that satisfies the dispersion relation in Eq. (5.42). Using the impedances in Eq. (5.43) we can calculate the reflection from a semi-infinite homogeneous medium defined as the amplitude of the magnetic field of the reflected wave divided by the amplitude of the magnetic field of the incident wave. By ignoring spatial dispersion and assuming Maxwell boundary conditions (continuity of E_y and H_z) we find that the reflection amplitude of a plane wave incident upon an interface between semi-infinite vacuum and a semi-infinite homogeneous medium with the constitutive parameters of a SRR array is

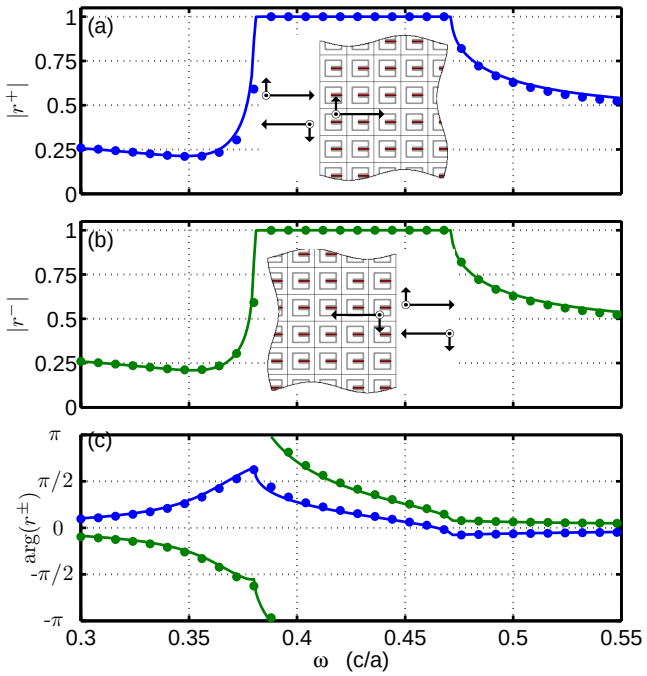

Figure 5.5: (a) Absolute value of the reflection coefficient r^+ for a rightward moving normally incident wave as shown in the diagram. (b) Absolute value of the reflection coefficient r^- for a leftward moving normally incident wave as shown in the diagram. (c) Phase of the reflection coefficients r^+ (blue) and r^- (green). Solid lines are reflection coefficients from the interface of vacuum and a semi-infinite SRR crystal. Dotted lines are reflection coefficients from the interface of vacuum and a semi-infinite homogeneous medium with the constitutive parameters calculated for a SRR crystal (dotted lines).

$$r^{\pm} = \frac{\mathrm{H}_z^{\mathrm{refl}}}{\mathrm{H}_z^{\mathrm{inc}}} = \frac{1 - z^{\pm}}{1 + z^{\pm}}, \tag{5.44}$$

where r^+ is the reflection coefficient from the vacuum-metamaterial interface for a rightward moving incident beam in vacuum and r^- is the reflection coefficient from the interface for a leftward moving incident beam in vacuum.

The two reflection coefficients are related due to the fact that the SRR crystal is almost lossless. For the case of a completely lossless crystal and a real valued frequency outside the bandgap of the SRR, k_x for a freely propagating wave will be real valued and the constitutive matrix will be hermitian. This implies that ϵ_{yy} and μ_{zz} are real valued and $\xi_{yz} = \zeta_{zy}^*$. This in turn implies that $z^+ = (z^-)^*$ and $r^+ = (r^-)^*$. Thus we see that for a lossless crystal at a real valued frequency in a propagating band the two reflection coefficients will always have an absolute value that is equal $|r^+| = |r^-|$ and a phase that is equal and opposite $\arg(r^+) = -\arg(r^-)$. These relations will not be valid inside the bandgap due to k_x being complex valued. However, the absolute values of the two reflection coefficients will still be equal since they must both be equal to unity for a real valued frequency inside the bandgap of a lossless crystal.

Fig 5.5 shows both reflection coefficients. Both agree with each other very well with a small error near the SRR resonance. The absolute values of the two reflection coefficients are approximately equal both inside and outside the bandgap and the phases of the reflection coefficients are approximately equal and opposite outside the bandgap. One interesting feature in Fig. 5.5 is the complex value of the reflection coefficients at frequencies outside the bandgap. For light reflecting off of a lossless crystal without intrinsic bianisotropy at a frequency outside the bandgap, the phase of the reflection coefficients will always be either 0 or $\pm\pi$. The complex values of the reflection coefficient are entirely due to the asymmetry of the SRR crystal which results in the intrinsic

bianisotropy characterized by κ_e.

5.3.3 Effective constitutive parameters and comparison to S-parameter retrieval

In the last chapter, we compared the constitutive parameters calculated using that chapter's homogenization procedure to the parameters return by the S-parameter retrieval method. The original S-parameter retrieval method [61] assumes symmetry of the crystal in the direction of propagation, which is not true for the SRR crystal. But as we mentioned in Sec. 1.3, a generalization of the S-parameter retrieval method [41] allows it be be applied to crystals that lack symmetry in the propagation direction. Since these S-parameter retrieval methods calculate the effective permittivity and permeability of the metamaterial from the index of refraction and impedance, which are associated with the dispersion curve and boundary conditions respectively, we should expect that these S-matrix constitutive parameters should reproduce the correct dispersion curve and boundary conditions. In fact, in the case of our SRR crystal they do. However, these S-matrix constitutive parameters disagree with the constitutive parameters we have calculated for the SRR crystal. Similar to the situation in Sec. 4.5, there is a relationship between the constitutive parameters calculated form the 1D model and those calculated using the asymmetric S-parameter retrieval method. We can transform between the two sets of constitutive parameters using the relations in Eqs. (4.13,4.14). For our highly symmetric p-polarized system, these equations simplify to

$$\frac{k_x - \omega\xi_{yz}/c}{\epsilon_{yy}} = \frac{k_x - \omega\xi_{yz}^{eff}/c}{\epsilon_{yy}^{eff}}, \tag{5.45}$$

$$\frac{k_x - \omega\zeta_{yz}/c}{\mu_{yy}} = \frac{k_x - \omega\zeta_{yz}^{eff}/c}{\mu_{yy}^{eff}}. \tag{5.46}$$

The asymmetric S-parameter retrieval method assumes the presence of intrinsic bianisotropy (κ_e), but no extrinsic bianisotropy (κ_o) due to spatial dispersion. This means that the constitutive parameters take the form

$$\hat{C}^S(\omega) = \begin{pmatrix} \epsilon_{yy}^S(\omega) & \kappa^S(\omega) \\ -\kappa^S(\omega) & \mu_{zz}^S(\omega) \end{pmatrix} \tag{5.47}$$

By taking Eqs. (5.45,5.46) and assuming that $\xi_{yz}^{eff} = -\zeta_{zy}^{eff}$ we can derive a set of effective constitutive parameters

$$\hat{C}^{eff}(\omega, k_x) = \begin{pmatrix} \epsilon_{yy}^{eff}(\omega, k_x) & \kappa^{eff}(\omega, k_x) \\ -\kappa^{eff}(\omega, k_x) & \mu_{zz}^{eff}(\omega, k_x) \end{pmatrix}, \tag{5.48}$$

where

$$\epsilon_{yy}^{eff} = \frac{\epsilon_{yy}}{1 - \omega\kappa_o/(k_x c)}, \qquad \mu_{zz}^{eff} = \frac{\mu_{zz}}{1 - \omega\kappa_o/(k_x c)}, \qquad \kappa^{eff} = \frac{\kappa_e}{1 - \omega\kappa_o/(k_x c)}. \tag{5.49}$$

It should be noted that these effective constitutive parameters leave the dispersion curve and impedances unchanged. By substituting the effective parameters into the dispersion relation in Eq. (5.42) it becomes

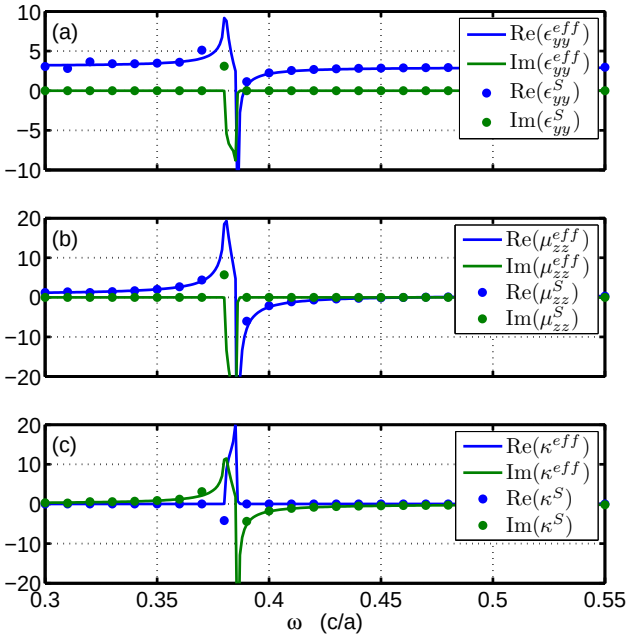

Figure 5.6: (a) ϵ^{eff}_{yy} and ϵ^{S}_{yy}. (b) μ^{eff}_{zz} and μ^{S}_{zz}. (c) κ^{eff} and κ^{S}. The effective parameters are plotted with solind lines and the parameters returned by the asymmetric S-parameter retrieval method are plotted with dotted lines.

$$k_x^2 = \left[\epsilon^{eff}_{yy}\mu^{eff}_{zz} + (\kappa^{eff})^2\right]\omega^2/c^2, \tag{5.50}$$

and the right and left moving impedances in Eq. (5.43) become

$$z^{\pm} = \frac{k_x(\omega) \mp \omega\kappa^{eff}/c}{\omega\epsilon^{eff}_{yy}/c} = \frac{\omega\mu^{eff}_{zz}/c}{k_x(\omega) \pm \omega\kappa^{eff}/c}. \tag{5.51}$$

Since the impedances are unchanged, the reflection amplitudes calculated with Eq. (5.44) are also unchanged.

While the constitutive parameters obtained by the S-parameter retrieval method in Eq. (5.47) are functions of only ω the effective constitutive parameters in Eq. (5.48) are functions of frequency and wavenumber. When the effective parameters are calculated on the dispersion curve then the effective parameters correspond to the constitutive parameters obtained by S parameter retrieval or $\hat{C}^S(\omega) \approx \hat{C}^{eff}(\omega, k_x(\omega))$.

Fig. 5.6 shows the effective constitutive parameters superimposed with parameters calculated from the asymmetric S-parameter retrieval method [41]. The S-matrix used was numerically measured from a SRR slab five unit cells thick. The effective constitutive parameters agree very well with the parameters calculated from S parameter retrieval.

5.3.4 Emission from a SRR metamaterial antenna

So far all of the constitutive parameters presented and tested have been calculated on the dispersion curve, meaning $\hat{C} = \hat{C}(\omega, k_x(\omega))$. One significant advantage of calculating the constitutive parameters of a metamaterial by exciting it with external current is that one can excite fields that have a frequency and wavenumber that do not lie on the dispersion curve and therefore calculate constitutive parameters off of the dispersion curve. This is useful for a number of reasons including the need to calculate partial derivatives of the constitutive parameters with respect to frequency or wavenumber and evaluating a Green's function to calculate the electromagnetic field generated by an external current. This latter ability is essential for analyzing a metamaterial

antenna.

An important subfield of metamaterial research is the topic of metamaterial antennas [18, 69, 5, 67, 19]. It is hoped that by using the novel electromagnetic properties of metamaterials it will be possible to improve the performance of antennas. Most studies on metamaterial antennas hypothesize the existence ideal metamaterials that are isotropic, local and broadband. To analyze more realistic metamaterials it is necessary to be able to fully characterize a metamaterial in a way that includes anisotropy, bianisotropy and temporal and spatial dispersion.

Calculating the emission of a metamaterial antenna involves solving a Green's function problem for a current source inside the metamaterial. In a 3D bulk metamaterial the monochromatic electric field generated by the time harmonic electric current source $\mathbf{J}(\mathbf{x})e^{i\omega t}$ is

$$\mathbf{E}(t,\mathbf{x}) = e^{i\omega t}\int d^3x'\hat{\mathrm{G}}(\omega,\mathbf{x}-\mathbf{x}')\mathbf{J}(\mathbf{x}')/c + \ \mathbf{E}^{free}(t,\mathbf{x}), \tag{5.52}$$

where $\hat{\mathrm{G}}(\omega,\mathbf{x}-\mathbf{x}')$ is a Green's function given by

$$\hat{\mathrm{G}}(\omega,\mathbf{x}-\mathbf{x}') = \int d^3k\ e^{-i\mathbf{k}\cdot(\mathbf{x}-\mathbf{x}')}\mathrm{i}\hat{\mathrm{D}}_3(\omega,\mathbf{k})^{-1}, \tag{5.53}$$

calculated with the differential wave operator in ω and $\mathbf{k}$ space given by the 3x3 matrix

$$\hat{\mathrm{D}}_3(\omega,\mathbf{k}) = \left(\mathbf{k}\times+\frac{\omega}{c}\hat{\xi}\right)\hat{\mu}^{-1}\left(\mathbf{k}\times-\frac{\omega}{c}\hat{\zeta}\right)+\frac{\omega^2}{c^2}\hat{\epsilon}. \tag{5.54}$$

The free waves $\mathbf{E}^{free}$ in Eq. (5.52) are solutions to the homogeneous differential equation (source free Maxwell equations) and satisfy the dispersion relation $\hat{\mathrm{D}}_3(\omega,\mathbf{k})\cdot\mathbf{E}^{free}(\omega,\mathbf{k}) = 0$. The amplitudes of the free waves are chosen to satisfy the boundary conditions of the problem. The constitutive parameters $\hat{\epsilon}$, $\hat{\xi}$, $\hat{\zeta}$ and $\hat{\mu}$ in the differential operator are functions of ω and $\mathbf{k}$ because they include both temporal and spatial dispersion. In order to calculate the electric field generated by the electric current source it is necessary to know how the constitutive parameters vary as functions of ω and $\mathbf{k}$.

We now demonstrate a simplified metamaterial antenna. This metamaterial antenna is a slab of 2D SRR crystal that is infinite in the $\hat{\mathbf{y}}$ and $\hat{\mathbf{z}}$ directions but only five layers thick in the $\hat{\mathbf{x}}$ direction (see diagram in Fig. 5.7). To make this slab a metamaterial antenna we add the electric current source $\mathrm{J}_y(\mathbf{x})e^{\mathrm{i}\omega t} = \mathrm{J}_2 e^{\mathrm{i}(\omega t - k_x x)}$ inside the metamaterial slab. Outside the metamaterial slab the electric current is zero.

Fig. 5.7 shows emission from two types of antenna slabs. The solid lines plot emission from an actual slab made of SRR's for three different frequencies as a function of k_x. The three frequencies were chosen so that one is below the band gap ($\omega = 0.35\ (c/a)$), one is inside the band gap ($\omega = 0.45\ (c/a)$), and one is above the band gap ($\omega = 0.55\ (c/a)$) as can be seen in Fig. 5.3. The emission was calculated from an electromagnetic finite element simulation performed with the software package COMSOL Multiphysics. The dotted lines

plot emission from a slab of a homogeneous medium with the constitutive parameters of the SRR crystal and the same thickness as the metamaterial slab. The fields inside the homogeneous slab are a combination of the solution to the inhomogeneous differential equation (Maxwell equations with source terms) which we refer to as the driven wave and the solution to the homogeneous differential equation (source free Maxwell equations) which we refer to as free waves. While the constitutive parameters for the free waves are calculated on the dispersion curve, the constitutive parameters of the driven wave are calculated with a ω and k_x that in general do not lie on the dispersion curve providing us with a test of these off dispersion curve parameters. The electric current generates electric and magnetic fields inside the homogeneous slab according to Eqs. (5.52-5.54) which for p-polarized waves excited by current with a single wavenumber reduces to

$$\mathrm{E}_y(t,x) = e^{i(\omega t - k_x x)} \mathrm{i} \mathrm{D}_1(\omega, k_x)^{-1} \mathrm{J}_2 + \ \mathrm{E}_y^{free}(t,x), \tag{5.55}$$

where the operator $\mathrm{D}_1(\omega, k_x)$ is given by

$$\mathrm{D}_1(\omega, k_x) = \left(\epsilon_{yy} + \frac{\kappa_e^2}{\mu_{zz}}\right) \frac{\omega^2}{c^2} - \frac{1}{\mu_{zz}} \left(k_x - \frac{\omega}{c}\kappa_0\right)^2. \tag{5.56}$$

The free waves E_y^{free} in Eq. (5.55) satisfy the dispersion relation $\mathrm{D}_1(\omega, k_x) = 0$ which is equivalent to Eq. (5.42). The boundary conditions for our system are that the tangential electric and magnetic fields E_y and H_z are continuous across the boundary between the homogeneous slab and vacuum and that the free

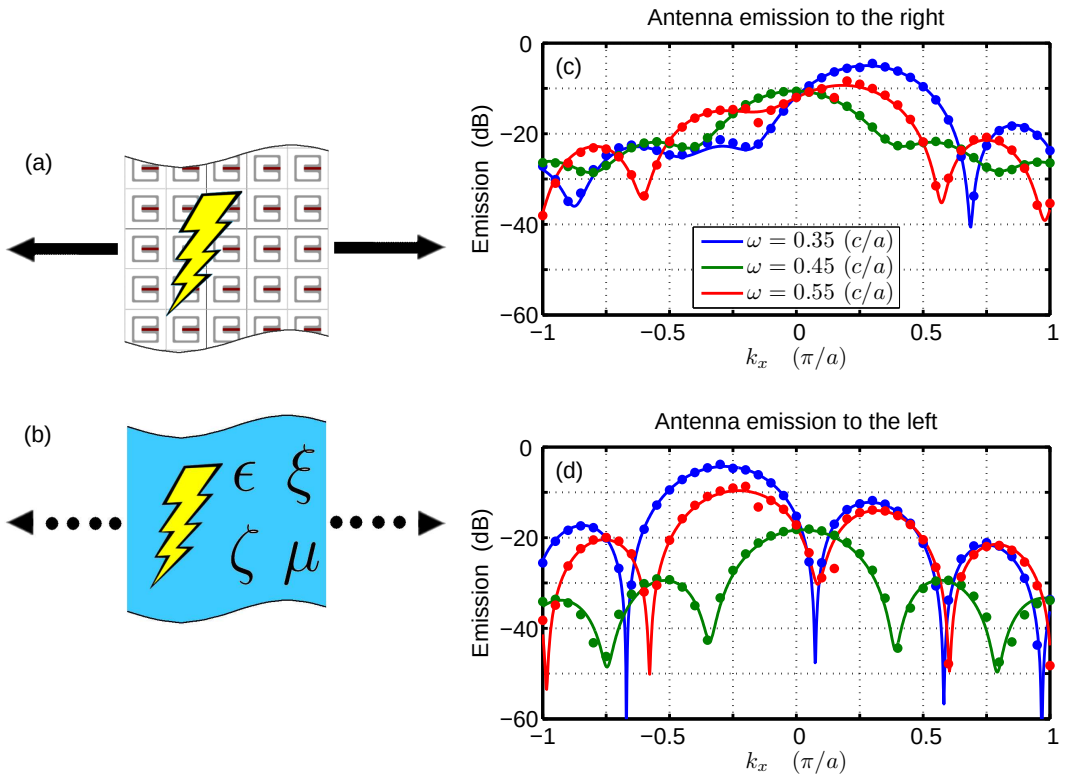

Figure 5.7: (a) Diagram a emission from a SRR antenna. (b) Diagram of emission from an antenna slab made from a homogeneous medium with the constitutive parameters of the SRR array. In both cases the antennas emit both to the left (negative $\hat{\mathbf{x}}$ direction) and the right (positive $\hat{\mathbf{x}}$ direction). (c) Emission to the right (positive $\hat{\mathbf{x}}$ direction) from a SRR antenna (solid lines) and a slab of a homogeneous medium (dotted lines). (d) Emission to the left (negative $\hat{\mathbf{x}}$ direction) from a SRR antenna (solid lines) and a slab of a homogeneous medium (dotted lines). Emission is plotted for three different excitation frequencies as a function of k_x. Both slabs have a thickness of $5a$ in the $\hat{\mathbf{x}}$ direction and are infinite in extent in the $\hat{\mathbf{y}}$ and $\hat{\mathbf{z}}$ directions.

fields outside the slab are moving outwards from the slab. Because the driven fields in Eq. (5.55) do not satisfy these boundary conditions it is necessary to choose the amplitudes of the free waves so that the total fields do satisfy

the boundary conditions. The free waves outside the homogeneous slab carry energy away from the slab and this energy emission is plotted as the dotted lines in Fig. 5.7.

Fig. 5.7 shows good agreement between the emission calculated for a homogeneous medium with the constitutive parameters of a SRR crystal and the actual emission from a slab of SRRs. The location of the emission peaks for $\omega = 0.35\ (c/a)$ and $\omega = 0.55\ (c/a)$ approximately correspond to the dispersion relation $k_x = k_x(\omega)$ as can be seen in Fig. 5.3. That the emission profile is asymmetric with respect to leftward and rightward emission is due to the asymmetry of the SRR. This asymmetry causes the intrinsic bianistropy characterized by the constitutive parameter κ_e. Finally, for $\omega = 0.45\ (c/a)$ the emission seems to be suppressed due to the bandgap. The comparison of emission from a SRR metamaterial antenna slab and a homogeneous antenna slab provides a good test of the constitutive parameters for ω and k_x off of the dispersion curve.

5.4 1D Example: Split Pair One Film (SPOF)

In Chapter 4 we tested that chapter's homogenization procedure only on the Split Pair One Film (SPOF) metamaterial. In this chapter it was useful to look at an asymmetric crystal which is why we tested this chapter's homogenization procedure on the SRR metamaterial. Still, it will be instructive to quickly check and see how this 1D model we use for homogenization applies to the SPOF. In particular, when we use the constitutive parameters to calculate

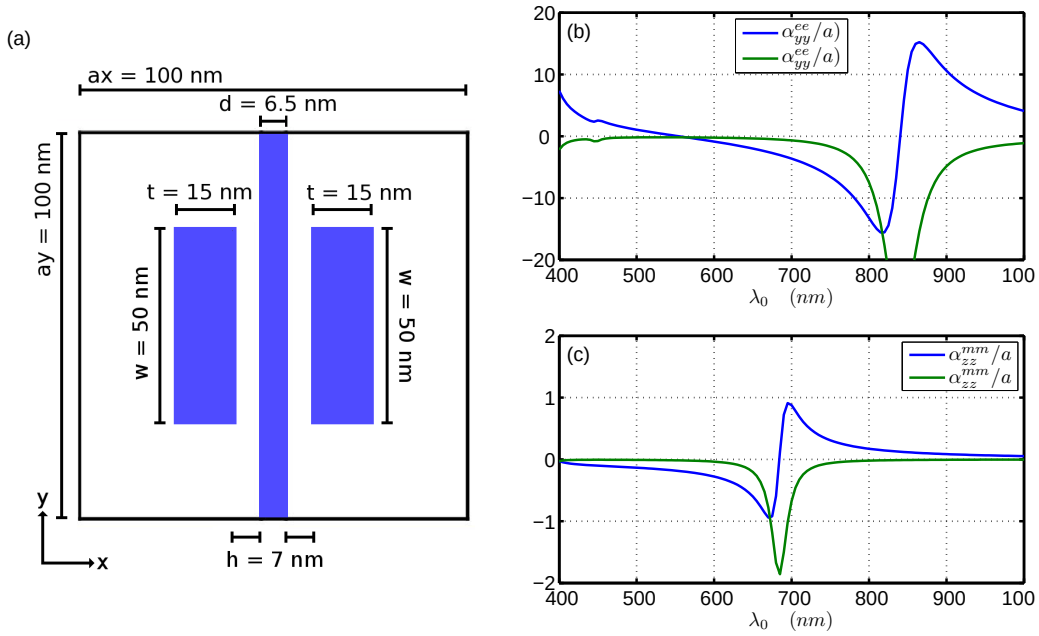

Figure 5.8: (a) Diagram of the SPOF unit cell. (b) Electric surface polarizability. (c) Magnetic surface polarizability.

reflection from a vacuum-SPOF interface we will see some ambiguous results that will lead us to the next chapter.

The surface polarizability for a single layer of the SPOF is plotted in Fig. 5.8, along with a diagram of the SPOF unit cell. This is the same SPOF unit cell and matrial parameters used in Chapter 4. We see in Fig. 5.8 an electric resonance near $\lambda_0 \approx 830nm$ and a magnetic resonance at around $\lambda_0 \approx 690nm$.

When we use put these surface polarizabilities into the 1D model of an array of metasurfaces, for a λ_0 and a k_x determined by the dispersion curve of

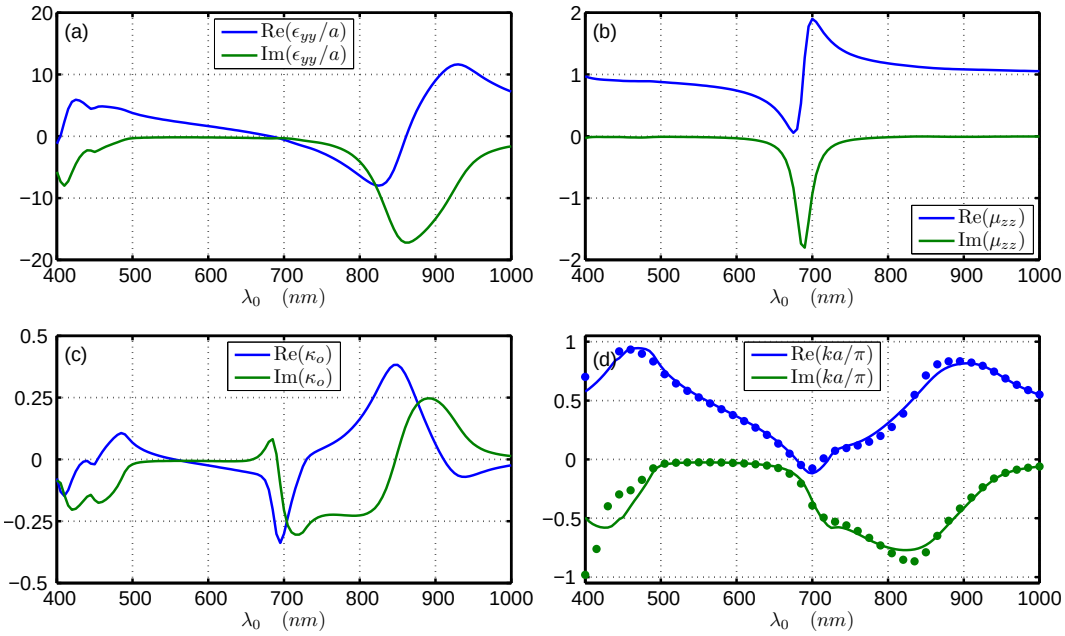

Figure 5.9: The constitutive parameters of the SPOF metamaterial calculated on the dispersion curve $\hat{C} = \hat{C}(\omega, k_x(\omega))$. (a) Permittivity ϵ_{yy}. (b) Permeability μ_{zz}. (c) Extrinsic bianisotropic parameter κ_o. (d) Dispersion curve of the SPOF crystal calculated from an eigenvalue simulation [14]) (solid lines) and from the constitutive parameters according to Eq. (5.57).

the SPOF crystal (calculated from a finite element eigenvalue simulation [14]), we get the constitutive parameters plotted in Fig. 5.9. Fig. 5.9 also plots the dispersion curve of the SPOF metamaterial calculated from the eigenvalue simulation (solid lines) and from the constitutive parameters of the SPOF according to

$$(k_x - \omega\kappa_o/c)^2 = \epsilon_{yy}\mu_{zz}\omega^2/c^2. \tag{5.57}$$

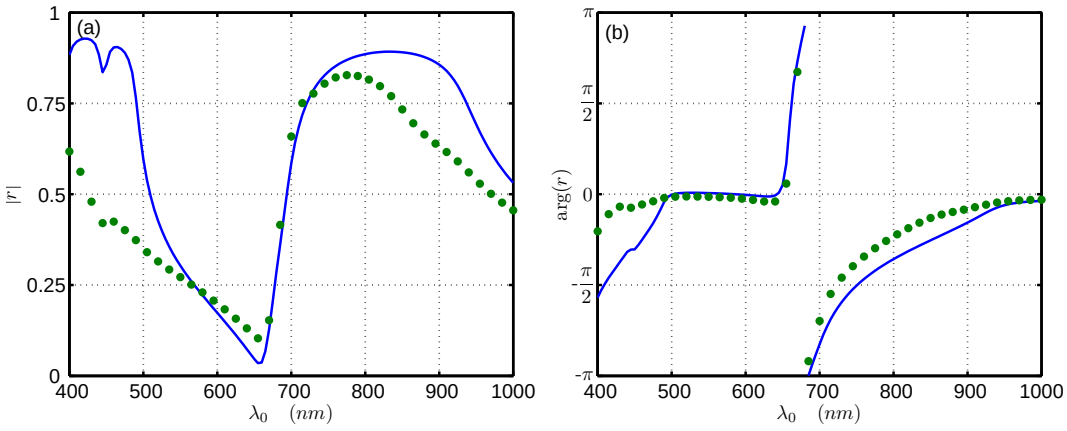

Figure 5.10: (a) Absolute value of reflection coefficients. (b) Argument of reflection amplitudes. Solid lines plot reflection amplitudes calculated from a finite element simulation. Dotted lines plot reflection amplitudes calculated according to Eq. (5.58) from the constitutive parameters of the SPOF calculated on the dispersion curve.

Using these constitutive parameters we can calculate the reflection of a plane wave from the interface between vacuum and a homogeneous medium with the constitutive parameters of the SPOF with the equation

$$r = \frac{1-z}{1+z} \qquad\qquad z = \sqrt{\frac{\mu_{zz}}{\epsilon_{yy}}} \tag{5.58}$$

where r is the reflection amplitude and z is the impedance of the homogeneousmedium. Note that extrinsic bianisotropic parameter κ_o does not appear in the impedance. This reflection amplitude can then be compared to the reflection of a plane wave from the interface between semi-infinite vacuum and a semi-infinite SPOF crystal calculated from a finite element simulation. These reflection amplitudes are plotted in Fig. 5.10.

There is considerable error between the two reflection amplitudes plotted in Fig. 5.10. Much more error than we saw when comparing reflection amplitudes for the SRR. It turns out that the cause seems to be very strong spatial dispersion. We will see this in the next chapter when we explore some consequences of spatial dispersion.

Chapter 6

Evidence of Spatial Dispersion

6.1 Anomalous boundary effects due to spatial dispersion

We saw in the last chapter that Maxwell boundary conditions combined with the constitutive parameters calculated using our 1D metamaterial model, correctly predict the reflection of a plane wave from the interface between vacuum and a SRR array (Fig. 5.5). We then saw that in the case of reflection from the interface between vacuum and a SPOF array, the Maxwell boundary conditions predicted slightly incorrect reflection amplitudes (Fig. 5.10). The SPOF crystal is less subwavelength than the SRR crystal so we should expect spatial dispersion to be stronger. From Chapter 2 we know that spatial dispersion can effect the Poynting flux in a medium and it seems reasonable that this could modify the required boundary conditions at an interface. While modified boundary conditions are beyond the scope of this dissertation, a study of the effect of spatial dispersion on energy flux, particularly at an interface, will inform us about the importance of this effect. This study will also demonstrate the importance of being able to calculate partial derivatives of the constitutive parameters with respect to $\mathbf{k}$.

To study the effect of spatial dispersion on energy flux we propose a

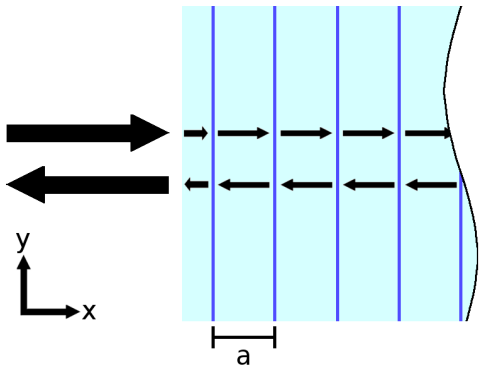

Figure 6.1: Diagram of reflection model. Metamaterial is a semi-infinite 1D array of metasurfaces. Each metasurface is separated by a medium with background permittivity ϵ_b and permeability μ_b and lattice constant a. Incident waves excite a crystal eigenmode at the interface between vacuum and the crystal. Reflected wave and crystal eigenmode carry energy away from the interface.

simple model. In Chapter 5 we modeled a metamaterial as a one dimensional array of metasurfaces. In this section we focus on the interface between vacuum and this one dimensional metamaterial. A diagram of the model is shown in Fig. 6.2. There is an interface between semi-infinite vacuum and a semi-infinite crystal. The crystal is made up of an infinite number of metasurfaces characterized by the surface polarizability $\hat{\alpha}$. The metasurfaces are separated by length a by a medium with background permittivity ϵ_b and μ_b. The interface between vacuum and the crystal is a distance $a/2$ from the first metasurface.

This model is similar to the one dimensional model in Sec. 5.2.4 except their is no driving current and there is now an interface between the semi-infinite crystal and vacuum. The one dimensional domain of the model is divided in 3 subdomains: the semi-infinite vacuum, the domain between the

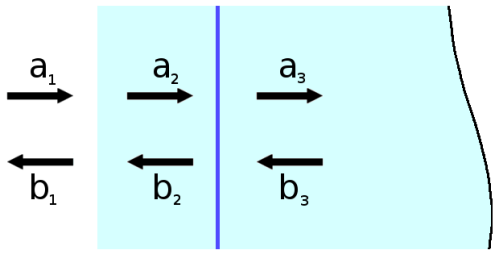

Figure 6.2: Three subdomains of the reflection model. The first is vacuum with $\epsilon = 1$ and $\mu = 1$. The second and third subdomains are filled with a background medium with $\epsilon = \epsilon_b$ and $\mu = \mu_b$. At each of the two internal boundaries there are two boundary conditions. On the external boundaries a_3 and b_3 are related to represent a rightward moving crystal eigenmode and $a_1 = 1$.

vacuum-crystal interface and the first metasurface, and the domain between the first and second metasurfaces. The field inside each domain is described by two coefficients, the amplitudes for rightward and leftward moving waves in that domain. The magnetic and electric fields in any domain are

$$\mathrm{H}_z = a_i e^{-\mathrm{i}k_x x} + b_i e^{\mathrm{i}k_x x} \qquad \mathrm{E}_z = z a_i e^{-\mathrm{i}k_x x} - z b_i e^{\mathrm{i}k_x x} \tag{6.1}$$

where a_i is the amplitude of the rightward moving wave and b_i is the amplitude for the leftward moving wave in the ith subdomain, $k_x \equiv \sqrt{\epsilon_b \mu_b}\omega/c$ is the wavenumber of a wave propagating in the background medium and $z \equiv \sqrt{\mu_b/\epsilon_b}$ is the impedance of the background medium. We have omitted the harmonic time dependence $e^{\mathrm{i}\omega t}$ where ω is the frequency. The coefficients (a_1, b_1) are related to (a_2, b_2) by Maxwell boundary conditions at the interface between the semi-infinite vacuum and the background medium, continuity of H_z and E_y.

The coefficients (a_2, b_2) are related to (a_3, b_3) by Eqs. (5.5-5.7) which describe the discontinuity of the electric and magnetic field across a metasurface. So far we have imposed four boundary conditions on six degrees of freedom. In the third domain the coefficients a_3 and b_3 should represent an eigenmode of the crystal that is carrying energy away from the vacuum-crystal interface. As mentioned in Sec. 5.2.4, a set of coefficients describing an eigenmode obey the equation

$$\left(\hat{A}\hat{B}^{-1} + \mathrm{i}\omega\hat{\alpha}/c\right)\begin{pmatrix} a_3 \\ b_3 \end{pmatrix} = e^{-\mathrm{i}ka}\begin{pmatrix} a_3 \\ b_3 \end{pmatrix} \tag{6.2}$$

where $\hat{A}\hat{B}^{-1}$ is given by Eq. (5.29) and k is the Bloch wavenumber of the eigenmode. The fifth boundary condition is that the ratio a_3/b_3 be equal to the ratio between two coefficients representing a crystal eigenmode propagating away from the interface ($\mathrm{Im}(k) < 0$). The final boundary condition is set by the amplitude of the incident wave which we normalize to unity ($a_1 = 1$). We now have six equations of constraint allowing us to solve for the six unknown amplitudes.

Our original concern was that spatial dispersion modifies the energy flux into the crystal at the vacuum crystal interface according to Eq. (2.22), and that this causes the electromagnetic field to obey non-Maxwellian boundary conditions at the interface. Let's rewrite Eq. (2.22) for this simple 1D system to remind ourselves of the role played by spatial dispersion. The simple 1D medium interacts with p-polarized light according to four simple constitutive parameters

$$\begin{pmatrix} \mathrm{D}_y \\ \mathrm{B}_z \end{pmatrix} = \hat{C} \cdot \begin{pmatrix} \mathrm{E}_y \\ \mathrm{H}_z \end{pmatrix} \qquad \hat{C} = \begin{pmatrix} \epsilon_{yy} & \xi_{yz} \\ \zeta_{zy} & \mu_{zz} \end{pmatrix} \tag{6.3}$$

Here D_y, B_z, E_y and H_z are the complex valued macroscopic fields in the homogenized metamaterial crystal. The energy flux due to these macroscopic fields is given by

$$\mathrm{S} = \mathrm{S}_0 + \mathrm{S}_1 \qquad \mathrm{S}_0 = c\frac{\mathrm{Re}(\mathrm{E}_y \mathrm{H}_z^*)}{2} \qquad \mathrm{S}_1 = -\frac{1}{4}\mathrm{Re}\left[\begin{pmatrix} \mathrm{E}_y \\ \mathrm{H}_z \end{pmatrix}^\dagger \cdot \omega \frac{\partial \hat{C}}{\partial k_x} \cdot \begin{pmatrix} \mathrm{E}_y \\ \mathrm{H}_z \end{pmatrix} \right]. \tag{6.4}$$

S_0 is the standard expression for time averaged Poynting flux and S_1 is the first order correction to Poynting flux due to spatial dispersion.

After solving the 1D reflection model, we calculate the macroscopic fields from our reflection model by measuring the polarization of the metasurface adjacent to the vacuum-crystal interface according to Eqs. (5.5,5.6). We relate this polarization to the macroscopic fields according to Eqs. (5.8,5.9). Since these fields are located at the position of the metasurface, we recover the values of the fields at the vacuum-crystal interface by dividing by the factor $e^{-\mathrm{i}k_x a/2}$ where k_x is the wavenumber of the crystal eigenmode. The macroscopic fields at the interface can then by used to calculate both S_0 and S_1 on the crystal side of the vacuum-crystal interface.

As an example of this reflection model, we first examine a crystal made of magnetic resonating metasurfaces. The polarizability tensor of this metasurface is

$$\hat{\alpha} = \begin{pmatrix} 3.5a & 0 \\ 0 & \alpha_{zz}^{mm} \end{pmatrix},$$

$$\frac{\alpha_{zz}^{mm}}{a} = -\frac{0.5(c/a)^2}{\omega^2 - (0.5c/a)^2 - \mathrm{i}(0.1c/a)\omega} - \frac{2.5(c/a)^2}{\omega^2 - (2.5c/a)^2 - \mathrm{i}(0.05c/a)\omega}. \tag{6.5}$$

The magnetic surface polarizability α_{zz}^{mm} models a metasurface with two magnetic resonances $\omega = 0.5c/a$ and $\omega = 2.5c/a$. Magnetic resonators are typically made of metal, and at low frequencies metsurfaces tend to have positive nonzero electric polarizabilities represented by our choice of $\alpha_{ee} = 3.5a$. This model approximates a magnetic resonator imperfectly. The electric polarizability will naturally have resonances even if the fundamental resonance is magnetic. Also, metal inclusions tend to contribute to a negative magnetic polarizability between $-a$ and 0 at low frequencies. Still, this simple model of a metasurface sufficiently captures the resonant behavior that we are interested in.

The power flux at the vacuum-crystal interface for this model is plotted in Fig. 6.3. Of particular interest is Fig. 6.3d which plots the macroscopic Poynting flux terms S_0 and $\mathrm{S}_0 + \mathrm{S}_1$ as well as the microscopic Poynting flux averaged over the interface $\langle s \rangle$.

From Fig. 6.3 we see that the $0th$ order Poynting flux S_0 often disagrees with the true Poynting flux calculated from microscopic fields $\langle s \rangle$. We see better agreement between $\langle s \rangle$ the sum of the $0th$ and $1st$ order Poynting terms $\mathrm{S}_0 + \mathrm{S}_1$, but there are still frequencies where there is little agreement. By

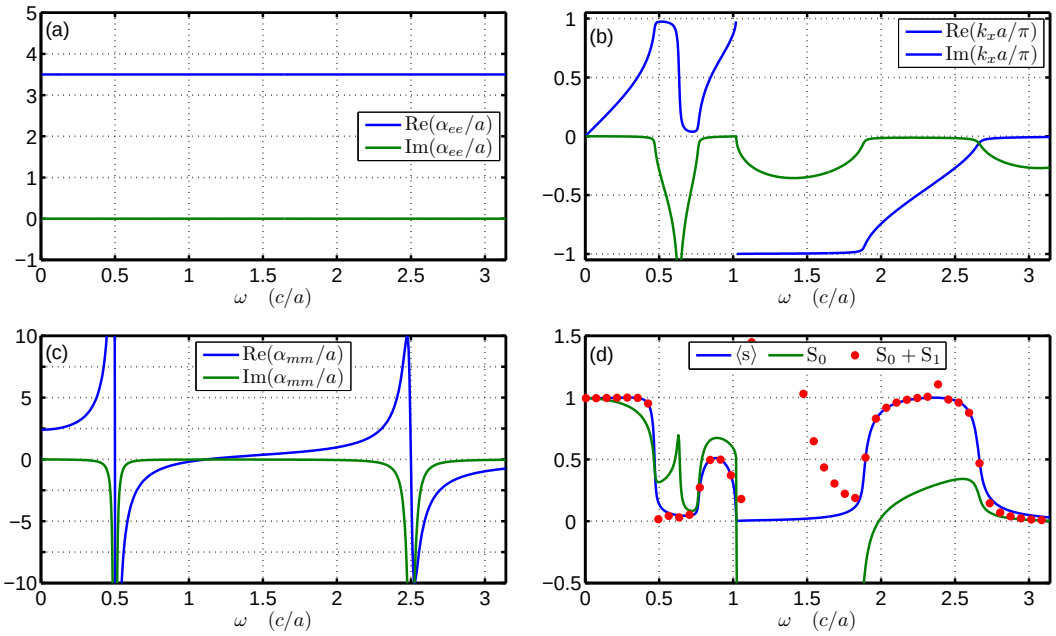

Figure 6.3: Poynting flux at the vacuum-crystal interface for a crystal array of metasurfaces with surface polarizability given by Eq. (6.5). (a) Electric surface polarizability α_{ee}. (b) k_x vs. ω dispersion curve of the crystal eigenmode. (c) Magnetic surface polarizability α_{mm}. (d) Microscopic Poynting flux $\langle s \rangle$, $0th$ order macroscopic Poynting flux S_0 and $0th$ plus $1st$ order macroscopic Poynting flux $S_0 + S_1$. The $S_0 + S_1$ calculation of Poynting flux agrees with the true Poynting flux $\langle s \rangle$ when $\mathrm{Im}(k_x)$ is small.

comparing the Poynting fluxes (Fig. 6.3d) with the dispersion curve(Fig. 6.3b) it is clear that the disagreement between $S_0 + S_1$ and $\langle s \rangle$ seems to occur when $\mathrm{Im}(k_x a)$ is large. Recalling the derivation of the modified Poynting flux in Chapter 2 there are two possible reasons for this disagreement. The first would be the anomalous terms in Eq. (2.3), however, for a wave that is simply decaying in space according to the decay factor $e^{-\mathrm{Im}(k_x)x}$ the anomalous terms should vanish. The second possibility is that higher order terms are necessary

for correctly calculating the true energy flux into the crystal. This seems to be the true cause of the disagreement between $|s|$ and $S_0 + S_1$. This makes sense if we recall that in the derivation in Chapter 2 the decay of the wave is contained in the field envelope $\mathbf{F}_0(t, \mathbf{x})$. For a monochromatic wave with a small $\mathrm{Im}(k_x a)$ the field envelope in ω and $\mathbf{k}$ space is approximately a delta function or $\mathbf{F}_0(\alpha, \mathbf{q}) \approx \delta^4(\alpha, \mathbf{q})$. When this is true the Taylor expansion of $\omega\hat{\mathrm{C}}$ to first order is sufficient, because the spread of the field envelope $\mathbf{F}_0(\alpha, \mathbf{q})$ is very narrow. For a wave with a large $\mathrm{Im}(k_x a)$ the field envelope becomes broader as a function of k_x with a width of $2\mathrm{Im}(k_x)$. Now the Taylor expansion of $\omega\hat{\mathrm{C}}$ to first order is insufficient. Unfortunately, to the best knowledge of the author, there is no known way to calculate the relevant higher order corrections.

Our motivation for this investigation of the modified Poynting flux was the error encountered in Sec. 5.4 between the reflection at the interface between vacuum and a SPOF crystal and the reflection at the interface between vacuum and a homogeneous medium with the constitutive parameters of the SPOF. Unfortunately, the modified Poynting flux provides only a partial answer to this error. As we saw in Fig. 6.3, the modified expression for the Poynting flux is only accurate when $\mathrm{Im}(k_x a)$ is small. In Fig. 6.4 we have plotted the reflection coefficient for reflection of a plane wave from the interface between semi-infinite vacuum and a semi-infinite SPOF crystal (r), a semi-infinite array of metasurfaces with the polarizability of a single layer of a SPOF crystal (r_A) and a semi-infinite homogeneous medium with the constitutive parameters of

the SPOF crystal (r_C). We have also replotted the dispersion curve of the SPOF eigenmode along with the surface polarizability of the SPOF and the various values for Poynting flux at the vacuum-SPOF interface. As we see from the dispersion curve, for wavelengths of $500nm$ to $680nm$ $\mathrm{Im}(k_x a)$ is small and true energy flux $\langle s \rangle$ agrees very well with the modified Poynting flux $\mathrm{S}_0 + \mathrm{S}_1$. However, for wavelengths above $680nm$ the SPOF crystal has a broad electric bandgap causing the eigenmode to be evanescent and $\mathrm{Im}(k_x a)$ to be large. In this region there is considerable error between the true energy flux and the modified Poynting flux.

There have been other attempts to quantify the contribution to the Poynting flux in a metamaterial due to spatial dispersion [55, 13]. In particular, in Ref. [13] Costa et al. plot curves similar to Fig. 6.4 comparing the averaged microscopic Poynting Flux $\langle s \rangle$ to the nonlocal Poynting flux $\mathrm{S}_0 + \mathrm{S}_1$ where S_1 is calculated using Silveirinha's homogenization procedure [54] described in Sec. 1.4. Ref. [13] also shows good agreement between $\langle s \rangle$ and $\mathrm{S}_0 + \mathrm{S}_1$ for crystal eigenmodes when $\mathrm{Im}(k)$ is small. However, they avoid comparing $\langle s \rangle$ and $\mathrm{S}_0 + \mathrm{S}_1$ when $\mathrm{Im}(k)$ is large. In Ref. [55] it is claimed that macroscopic Poynting flux can only be calculated when $\mathrm{Im}(k)$ is small.

We conclude that though the $1st$ order correction to the Poynting flux does play an important role in modifying the boundary conditions for metamaterials with strong spatial dispersion, there are likely extra terms in the expression for Poynting flux that also contribute significantly. Still, the partial agreement between the true energy flux $\langle s \rangle$ and the modified Poynting flux

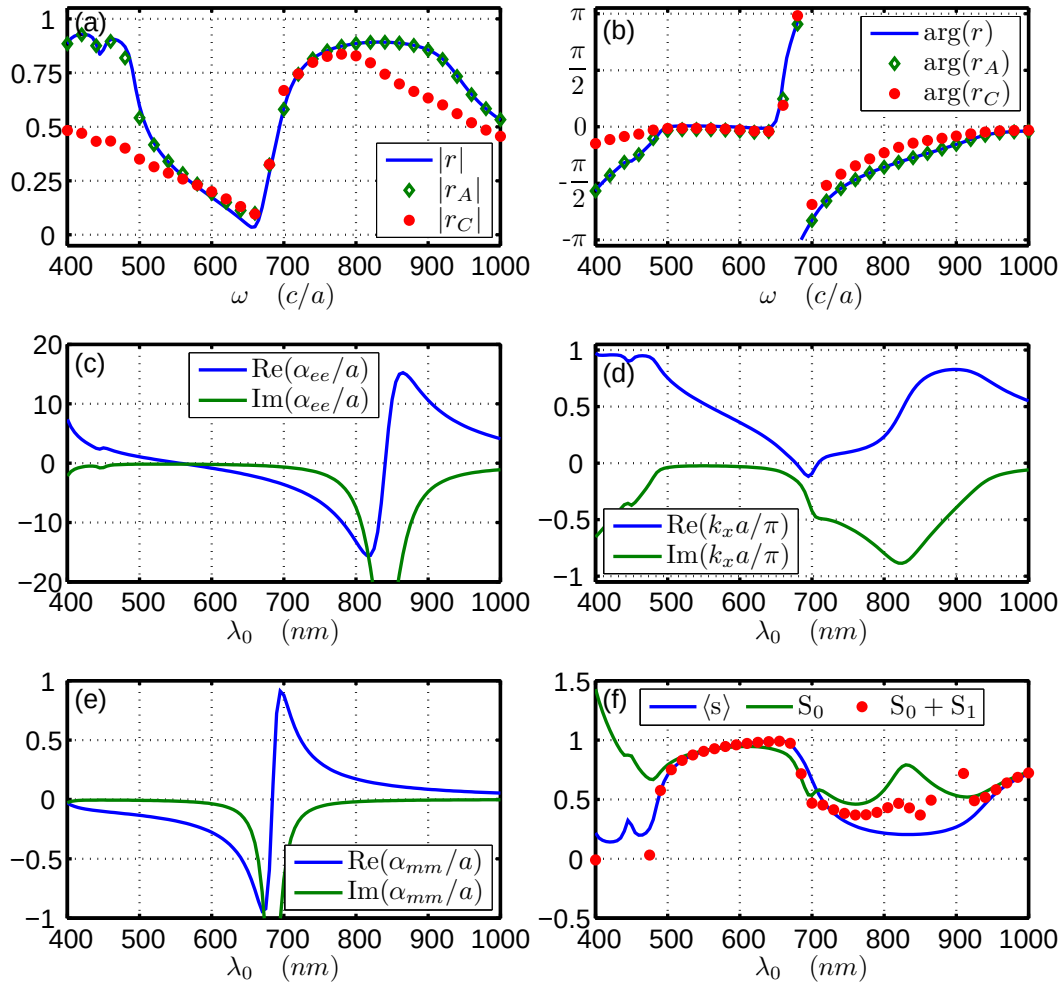

Figure 6.4: (a) absolute value and (b) argument of the reflection coefficient for a plane wave reflecting from the interface between vacuum and a semi-infinite SPOF crystal (solid lines), array of metasurfaces (diamonds) and a homogeneous medium (dotted lines). (c) Electric surface polarizability α_{ee}. (d) k_x vs. ω dispersion curve of the crystal eigenmode. (e) Magnetic surface polarizability α_{mm}. (f) Microscopic Poynting flux $\langle s \rangle$, $0th$ order macroscopic Poynting flux S_0 and $0th$ plus $1st$ order macroscopic Poynting flux $\mathrm{S}_0 + \mathrm{S}_1$.

$S_0 + S_1$ when $\mathrm{Im}(k_x a)$ is small does provide evidence that the partial derivatives of the constitutive parameters used to calculate the $1st$ order Poynting flux correction are physically significant and are correctly calculated using the homogenization procedure from Chapter 5. This validates the simple one dimensional homogenization theory and also highlights the importance of spatial dispersion in metamaterials.

6.2 Anti-resonances in metamaterials

Shortly after it was suggested by Smith et. al. that the constitutive parameters of a metamaterial be inferred from the scattering matrix of a thin metamaterial slab [61] it was discovered that this procedure also produces effective constitutive parameters with apparently unphysical lineshapes. This phenomenon, dubbed antiresonance, typically involves constitutive parameters with the wrong sign of the partial derivatives with respect to frequency ($\partial(\omega\epsilon)/\partial\omega$ and $\partial(\omega\mu)/\partial\omega$) and the wrong sign of the imaginary part of the parameters ϵ and μ. There is also usually a pairing between a resonance and an unphysical appearing antiresonance so that when the permittivity of a metamaterial is resonant the permeability is anti-resonant and vice versa. There are many examples of this behavior when constitutive parameters are calculated from scattering matrices [49, 34, 73, 31, 66, 41], but there are also examples of anti-resonances for other retrieval methods [49, 48, 60, 20]. An example of effective constitutive parameters exhibiting a typical antiresonance is plotted in Fig. 6.5

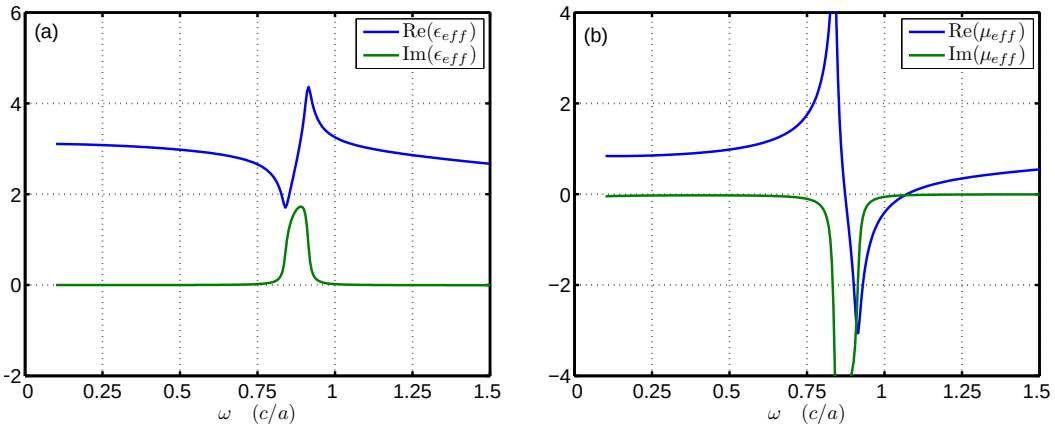

Figure 6.5: Effective permittivity (a) and permeability (b) for a 2D crystal array of magnetic resonators shown in Fig. 6.6. The effective parameters are calculated according to Eq. (5.49) from the constitutive parameters resulting from the 1D model presented in Sec. 5.2. Note that for a passive medium, the imaginary parts of ϵ and μ should both be less than or equal to zero but here the imaginary part of ϵ_{eff} is positive. Also, the derivative $\mathrm{Re}(d\epsilon_{eff}/d\omega)$ is negative for frequencies far from the resonance. This mistakenly implies negative energy density.

It has long been argued that antiresonances are caused by spatial dispersion [34]. However, since homogenization procedures such as S-parameter retrieval cannot separate the dependence of constitutive parameters on ω and $\mathbf{k}$, there have been no quantitative arguments of the importance of spatial dispersion to the antiresonance phenomenon. Serious questions remain about the interpretation of the imaginary part of the constitutive parameters near an anti-resonance. The imaginary parts of ϵ and μ are associated with loss (or gain) in the medium. While the imaginary part of μ_{eff} in Fig. 6.5 implies the medium is lossy the imaginary part of ϵ_{eff} implies that medium also has gain.

For a discussion of this problem, please refer to the comments [15, 16] on the original antiresonance paper by Koschny et. al. [34] as well as the reply to these comments [33]. We will now briefly summarize the problem outlined in the previous references.

The standard expression for heat generated by a monochromatic wave in a passive isotropic medium is given by [26, 4, 38]

$$L(\mathbf{x}) = \int_{\Omega} d^3x \left[\mathrm{Im}[-\epsilon(\omega_0)] \frac{|\mathbf{E}_0|^2}{2} + \mathrm{Im}[-\mu(\omega_0)] \frac{|\mathbf{H}_0|^2}{2} \right], \tag{6.6}$$

where $\mathbf{E}_0(t, \mathbf{x})$ and $\mathbf{H}_0(t, \mathbf{x})$ are complex valued fields. In Ref. [34], Koschny et. al. argue that it is okay for either $\mathrm{Im}(\epsilon)$ or $\mathrm{Im}(\mu)$ to have the incorrect sign as long as $L(t, \mathbf{x})$ is positive. However, Depine et al. [15] and Efros [16] both provide simple examples involving interfering plane waves where they claim $L(t, \mathbf{x})$ is negative antiresonance. All parties seem to agree that spatial dispersion plays an important role in the constitutive parameters though it is not clear how to quantify this since S-parameter retrieval doesn't separate the dependence of the constitutive parameters between ω and $\mathbf{k}$. The ability to calculate constitutive parameters as a function of both ω and $\mathbf{k}$ is essential to resolving this issue.

There are two reasons why $\mathrm{Im}(\epsilon_{yy}^{eff})$ is perceived to have the wrong sign due to spatial dispersion. The first is that the effective parameters are not the correct constitutive parameters but are related to the correct constitutive parameters by Eq. (5.49). Specifically, the bianisotropy caused by spatial

dispersion is ignored in S-parameter retrieval and many other homogenization methods. When we allow for bianisotropy in a symmetric crystal, the question of the sign of the imaginary parts of ϵ and μ becomes a question of the signs of the eigenvalues of the antihermitian part of the constitutive matrix. Alu has demonstrated that taking bianisotropy into account also helps resolve the issue of the signs of $\partial(\omega\epsilon)/\partial\omega$ and $\partial(\omega\mu)/\partial\omega$ [7], though we will not concern ourselves with that here.

The second reason for the wrong sign is that the constitutive parameters are evaluated on the dispersion curve. As mentioned in Chapter 2 the derivation for Eq. (6.6) assumes that any change in the strength of the fields is slow and contained in the field envelopes $\mathbf{E}_0$ and $\mathbf{H}_0$. As a result, in Eq. (6.6) the imaginary parts of the constitutive parameters are evaluated for real frequencies and wavevectors. In other words, for a fields with a complex frequency $\omega_0 = \omega_0' + \mathrm{i}\omega_0''$ and/or wavevector $\mathbf{k}_0 = \mathbf{k}_0' + \mathrm{i}\mathbf{k}_0''$, the quantities $\mathrm{Im}[\epsilon(\omega', \mathbf{k}_0')]$ and $\mathrm{Im}[\mu(\omega_0', \mathbf{k}_0')]$ must be used in Eq. (6.6) when calculating loss. However, the parameters returned by the S-parameter retrieval method, in addition to ignoring bianisotropy due to spatial dispersion, are calculated from waves that are propagating through a metamaterial slab. These free eigenmodes have a real valued frequency, but they have a complex valued wavevector due to the waves decaying as they propagate through the lossy metamaterial slab. Therefore, the constitutive parameters returned by S-parameter retrieval for a complex wavevector are $\epsilon_{yy}^{eff}(\omega_0', \mathbf{k}_0' + \mathrm{i}\mathbf{k}_0'')$ and $\mu_{yy}^{eff}(\omega_0', \mathbf{k}_0' + \mathrm{i}\mathbf{k}_0'')$. Because the effective constitutive parameters are evaluated for a complex valued wavevec-

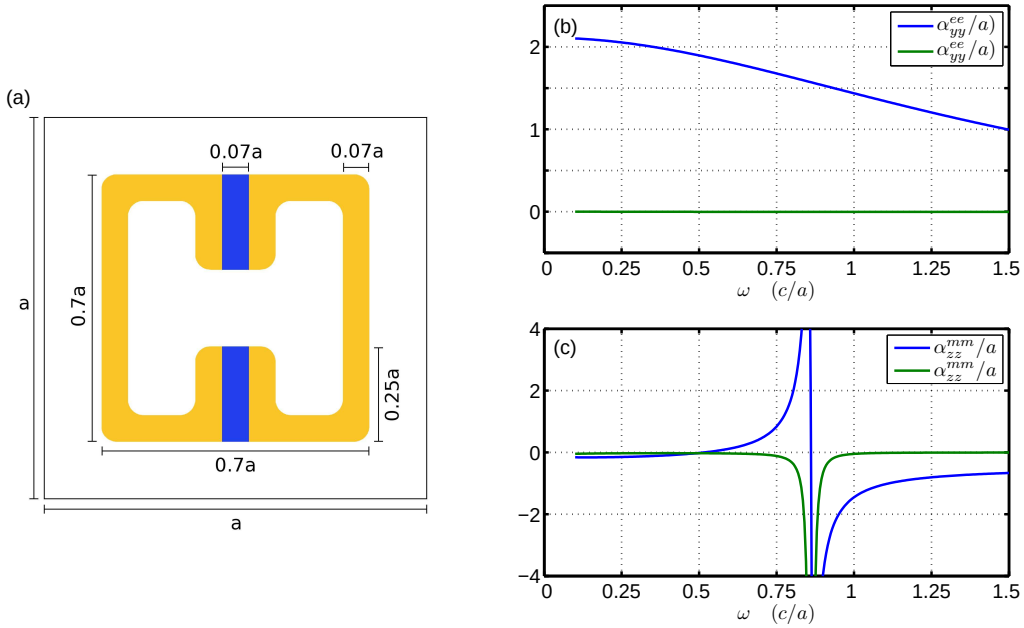

Figure 6.6: (a) Diagram of a magnetic resonator. The metal (gold colored) is Au with permittivity $\epsilon_{Au} = 1 - \omega_p^2/(\omega(\omega - \mathrm{i}\gamma))$ where $\omega_p = 1.367 \cdot 10^{16}/s$ and $\gamma = 4 \cdot 10^{13}/s$. The dielectric (blue colored) has the permittivity $\epsilon_d = 2.25$. The lattice constant of the crystal is $a = 5\mu m$. (b) Electric surface polarizability of the magnetic resonator. (c) Magnetic surface polarizability of the magnetic resonator.

tor they should not be used for calculating loss in a medium. It should be noted that constitutive parameters calculated by field averaging eigenmodes of a crystal [49, 60] have this same shortcoming.

We now demonstrate this on a simple 2D metamaterial. This is a 2D array of magnetic resonators pictured in Fig. 6.6. The resonator is a symmetric split ring made of Au with permittivity $\epsilon_{Au} = 1 - \omega_p^2/(\omega(\omega - \mathrm{i}\gamma))$ where the plasma frequency is $\omega_p = 1.367 \cdot 10^{16}/s$ and the damping frequency

is $\gamma = 4 \cdot 10^{13}/s$. The capacitor gap is filled with a dielectric with permittivity $\epsilon_d = 2.25$. The lattice constant of the crystal is $a = 5\mu m$. We see from the electric and magnetic surface polarizabilities plotted in Fig. 6.6 that there is a magnetic resonance near $\omega = 0.85c/a$. The constitutive parameters for this crystal where calculated using the 1D model described in Chapter 5,

$$\hat{C} = \begin{pmatrix} \epsilon_{yy} & \kappa_o \\ -\kappa_o & \mu_{zz} \end{pmatrix}, \tag{6.7}$$

and are plotted in Fig. 6.7 along with the dispersion curve for the eigenmode of the crystal. The constitutive parameters were calculated on the dispersion curve or $\hat{C} = \hat{C}(\omega, \mathbf{k}(\omega))$.

We will now calculate dissipative loss for an eigenmode of the crystal. There are three possible ways to calculate loss inside a unit cell of the crystal. First loss can be calculated from microscopic fields and integrated over a unit cell. Since $\mu = 1$ inside the unit cell, microscopically all loss is electrical.

$$\langle \mathrm{L}_m \rangle = \frac{1}{a^2} \int_\Omega d^2x \left[\mathrm{Im}(-\epsilon) \frac{|\mathbf{e}|^2}{2} \right]. \tag{6.8}$$

Here ϵ is the microscopic permittivity and $\mathbf{e}$ is the microscopic electric field. This gives us the true loss which we can compare to other measures of loss.

The second option for calculating loss is the incorrect method of calculating loss from the imaginary parts of the effective constitutive parameters, which of course appear to imply gain in the electric antiresonance.

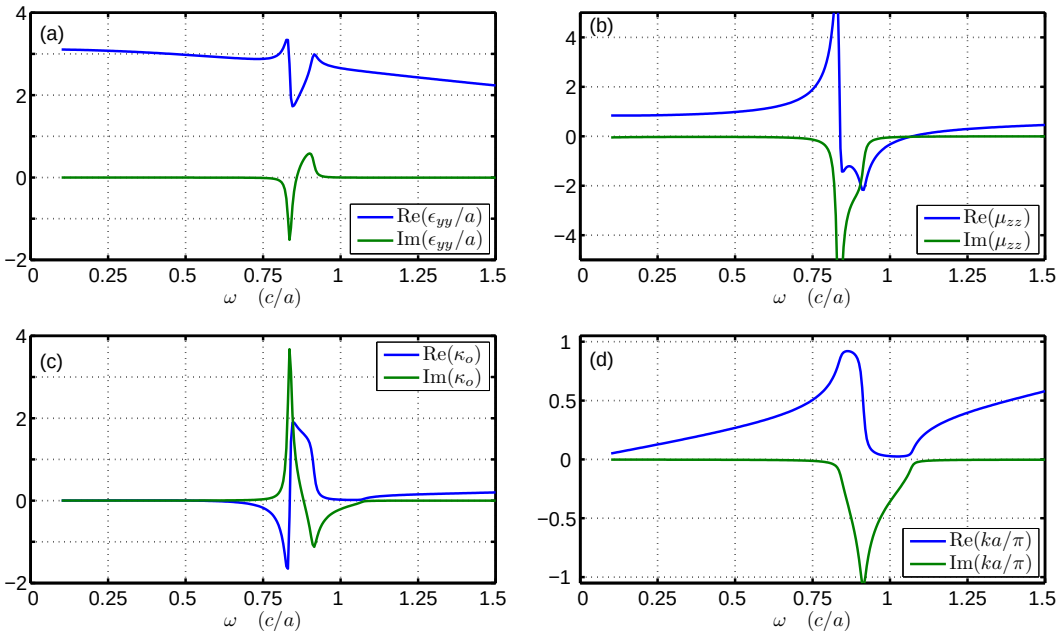

Figure 6.7: The constitutive parameters for an array of magnetic resonators pictured in Fig. 6.6. All constitutive parameters are calculated on the dispersion curve $\hat{C} = \hat{C}(\omega, \mathbf{k}(\omega))$. (a) ϵ_{yy}. (b) μ_{zz}. (c) κ_o. (d) Dispersion curve for freely propagating eigenmodes of the 2D array of magnetic resonators.

$$\langle \mathrm{L}_{anti} \rangle = \frac{1}{a} \int_{\Omega} dx \left[\mathrm{Im}(-\epsilon_{eff}) \frac{|\mathrm{E}_{y0}|^2 e^{-2k_x'' x}}{2} + \mathrm{Im}(-\mu_{eff}) \frac{|\mathrm{H}_{z0}|^2 e^{-2k_x'' x}}{2} \right] \quad (6.9)$$

Here $\mathrm{E}_y = \mathrm{E}_{y0} e^{-\mathrm{i}k_x x}$ and $\mathrm{H}_z = \mathrm{H}_{z0} e^{-\mathrm{i}k_x x}$ are macroscopic planes waves whose amplitude is determined from the polarization of the magnetic resonator metasurface according to Eqs. (5.5,5.6) and Eqs. (5.8,5.9). The local field is measured at the boundary of the unit cell.

The third way to calculate loss is to use the constitutive parameters calculated from the 1D model described in Chapter 5. These parameters include

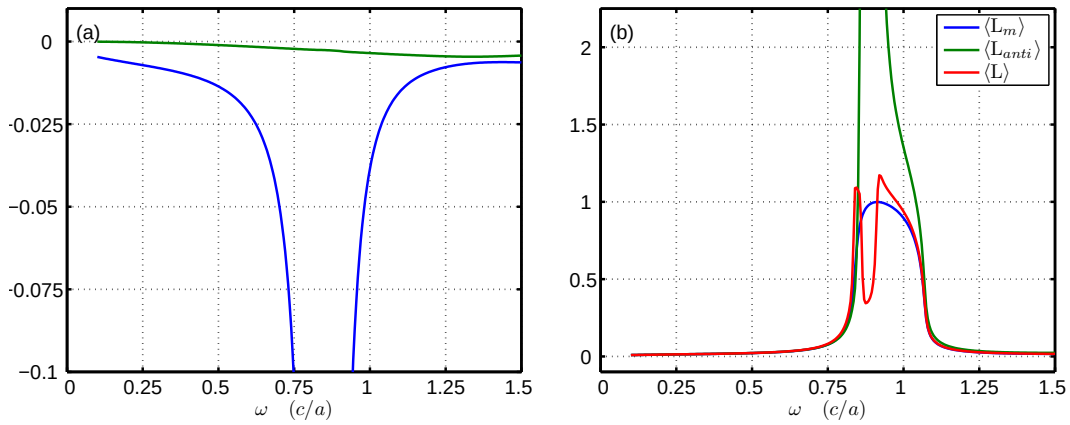

Figure 6.8: (a) Eigenvalues of the matrix $[(\omega\hat{C}) - (\omega\hat{C})^\dagger]/2$. Both eigenvalues are negative implying a lossy medium. (b) Loss calculated using three different methods. All values for loss are normalized to the incoming microscopic Poynting flux divided by the lattic constant, therefore loss should always be between 0 and 1.

the bianisotropic parameter κ_o which is due to spatial dispersion. In order to calculate the loss correctly we must calculate these constitutive parameters for a real valued wavevector or $\hat{C} = \hat{C}(\omega, \mathbf{k}'(\omega))$. The correctly calculated dissipative loss is

$$\begin{aligned} \langle \mathrm{L} \rangle &= -\frac{1}{a}\int_\Omega dx \left[\begin{pmatrix} \mathrm{E}_{y0} \\ \mathrm{H}_{z0} \end{pmatrix}^\dagger \cdot \frac{(\omega\hat{C}) - (\omega\hat{C})^\dagger}{2\mathrm{i}} \cdot \begin{pmatrix} \mathrm{E}_{y0} \\ \mathrm{H}_{z0} \end{pmatrix} e^{-2k_x'' x} \right] \\ &= -\left[\begin{pmatrix} \mathrm{E}_{y0} \\ \mathrm{H}_{z0} \end{pmatrix}^\dagger \cdot \frac{(\omega\hat{C}) - (\omega\hat{C})^\dagger}{2\mathrm{i}} \cdot \begin{pmatrix} \mathrm{E}_{y0} \\ \mathrm{H}_{z0} \end{pmatrix} \right] \frac{\sinh(k_x'' a)}{k_x''} \end{aligned} \tag{6.10}$$

The results of these three methods for calculating loss are plotted in Fig 6.8, along with the eigenvalues of the matrix $[(\omega\hat{C}) - (\omega\hat{C})^\dagger]/2$. The values

for loss are all normalized to the microscopic Poynting Flux entering the unit cell, therefore loss should always be between 0 and 1. Since loss is calculated from a matrix in Eq (6.10) we cannot simply look at the imaginary parts of the constitutive parameters, but must instead look at the eigenvalues of the hermitian matrix $[(\omega\hat{C})-(\omega\hat{C})^{\dagger}]/2$. Both eigenvalue are negative for the entire frequency range guaranteeing that we will only observe loss and no gain. We also see in Fig. 6.8 that all three measures of loss agree with each other except near the resonance. Near the resonance $\langle \mathrm{L}_{anti} \rangle$ becomes larger than 1 implying that there is more energy lost in the unit cell than there is energy entering the unit cell. The correctly calculated loss $\langle \mathrm{L} \rangle$ is less than 1 for almost the entire frequency band, but it also disagrees with the true loss $\langle \mathrm{L}_m \rangle$ near the resonance. The inclusion of spatial dispersion is clearly necessary for correctly calculating dissipative loss near a resonance.

We see that spatial dispersion is an important effect and must be accounted for when calculating loss in a metamaterial. However, the correct expression for calculating loss (Eq (6.10)) is only a modest improvement over the incorrect method using effective constitutive parameters with complex valued wavenumbers.

Chapter 7

Conclusion

7.1 Characterizing metamaterials with spatial dispersion

Throughout our discussion of metamaterial homogenization, we have emphasized the importance of understanding the effects of spatial dispersion in metamaterials. This has been accomplished by providing examples of the failures encountered when spatial dispersion is neglected as well as by studying the advantages of including spatial dispersion in the characterization of metamaterials. We briefly summarize the results of this dissertation and then we will touch upon some general conclusions.

In Chapter 1 we introduced the concept of metamaterial homogenization. We then described four important previous attempts by others at metamaterial homogenization. The first by John Pendry [50] marked the origin of the field of metamaterial research. This method involves averaging microscopic electromagnetic fields over the edges and faces of a crystal unit cell. The second method, S-parameter retrieval, by David Smith et al. [61], has become the workhorse of theoreticians working to characterize new potential metamaterial designs. S-parameter retrieval is essentially an inverse scattering problem where one infers the constitutive parameters of a thin sample of meta-

material from that sample's scattering matrix. The third and fourth methods we reviewed are less well known, but they are both important because unlike the first two methods they attempt to characterize spatial dispersion in metamaterials. The first of the two methods by Mário G. Silveirinha [54] attempts to describe a complex metamaterial with only a permittivity tensor. The second of the two methods by Jenson Li et al. [40] attempts to calculate all 36 linear constitutive parameters. Both methods have similar field averaging procedures with the similar limitations. However, these attempts to characterize spatial dispersion mark an important new direction for the field of metamaterial homogenization. In addition, Jensen Li's prediction of bianisotropy in centrosymmetric crystals due to spatial dispersion seems to be correct and essential for understanding most metamaterials.

In Chapter 2 we introduced the topic of spatial dispersion and justified its importance in the field of metamaterials. We studied how the symmetry of a crystal affects the symmetry of its constitutive tensors/pseudotensors and we examined how this dependence changes in the presence of spatial dispersion. We were able to justify and explain the result of Li that spatial dispersion allows for bianisotropy in centrosymmetric crystals, a prediction which is new and potentially controversial. We then looked at the effects of spatial dispersion on the calculation of Poynting flux and dissipative loss. In the case of Poynting flux, we examined an extra term in the Poynting flux caused by spatial dispersion and proportional to $[\partial(\omega\hat{\mathrm{C}})/\partial\mathbf{k} + (\partial(\omega\hat{\mathrm{C}})/\partial\mathbf{k})^{\dagger}]/2$. In the case of dissipative loss, we have shown that it is necessary to calculate loss

using constitutive parameters evaluated for real valued ω and $\mathbf{k}$. This is important because spatial dispersion causes the constitutive parameters to vary as a function of $\mathbf{k}$.

Next, in Chapter 3, we described a new method of calculating complex $\mathbf{k}$ dispersion curves for 3D crystals using a finite element method simulation. This method is a generalization of a 2D eigenvalue finite element simulation [14, 17]. Knowledge of the complex $\mathbf{k}$ dispersion curves of metamaterial/photonic crystals is important for evaluating metamaterial experiments. Because the frequency ω is real valued and the wavevector $\mathbf{k}$ is generally complex valued in experiments is is important to evaluate the constitutive parameters on the correct $\mathbf{k} = \mathbf{k}(\omega)$ dispersion curve when using a current driven homogenization procedure like those described in Secs. 1.4 and 1.5 and Chapters 4 and 5.

In Chapter 4 we present an early attempt by the author at metamaterial homogenization. This method attempts to calculate all 36 linear constitutive parameters of a metamaterial crystal. It uses the concept of driving a crystal with external electric and magnetic current (similar to Li [40] and Silveirinha [54] though Silveirinha only uses electric current) and averages the resulting microscopic fields with edge and volume integrals over the crystal unit cell. The field averaging procedure is somewhat similar to Pendry's averaging prescription described in Sec. 1.2 and produces similar results when Pendry's method is combined with external driving currents. This method is very ambitious, attempting to calculate all 36 constitutive parameters, and

is somewhat successful. It reproduces correct dispersion curves and correctly predicts reflection from a vacuum-SPOF crystal interface. Still, this method has some serious shortcomings, not the least of which is the lack of Lorentz reciprocity in the calculated constitutive parameters.

In Chapter 5 we presented a simpler homogenization procedure. This method is based on modeling a metamaterial crystal as an 1D array of metasurfaces. The metasurfaces serve as proxies for individual layers of a metamaterial crystal by responding to electromagnetic fields according to $\hat{\alpha}$, the surface polarizability. This model assumes a certain degree of symmetry, similar to the methods described in Secs. 1.2 and 1.3, making this method less general than the method described in Chapter 4. Still, this simple homogenization procedure has several advantages, the main one being that it obeys Lorentz reciprocity. This method also exhibits bianisotropy in metamaterials due solely to spatial dispersion and because of Lorentz reciprocity we saw how this extrinsic bianisotropy can be separated from the intrinsic bianisotropy caused by the asymmetry of a metamaterial crystal. This 1D model for homogenization passes some basic tests of a homogenization procedure, including reproducing the correct dispersion relation and the reflection from a vacuum-SRR crystal interface. However, reflection from a vacuum-SPOF crystal interface was less accurate. This implies a necessary modification of the Maxwell boundary conditions due to spatial dispersion and leads us to the next chapter.

In Chapter 6 we examined the effects of spatial dispersion on the Poynting flux at the interface between vacuum and two different metamaterials.

First we looked at a toy model of a metamaterial and saw that the additional term for the Poynting flux predicts the correct energy flux as long as $\mathrm{Im}(k_x a)$ is small where k_x is the wavenumber of the eigenmode propagating into the metamaterial and a is the lattice constant. We then examined the Poynting flux at a vacuum-SPOF crystal interface and saw a similar result. Whenever $\mathrm{Im}(k_x a)$ is small the agreement between the Poynting flux and the true energy flux is very good. When $\mathrm{Im}(k_x a)$ is large the agreement breaks down. This necessarily complicates the issue of modified boundary conditions due to spatial dispersion. In Chapter 6 we also looked at the calculation of dissipative loss in a metamaterial, taking into account the role of spatial dispersion. We saw that when we evaluate the matrix proportional to dissipative loss, $[(\omega\hat{C}) - (\omega\hat{C})^{\dagger}]/2$, this matrix is negative definite, guaranteeing that loss will always be positive and that we should observe no gain near an antiresonance of a metamaterial.

The main theme of this dissertation is that it is essential to consider spatial dispersion when characterizing a typical metamaterial due to the fact that most realistic metamaterials are not very subwavelength. We have provided several examples of the manifestation of spatial dispersion including extrinsic bianisotropy, modified Poynting flux and a resolution of the antiresonance controversy. While we have made significant progress in justifying the importance of spatial dispersion, our ability to characterize general metamaterials is not complete.

7.2 Future Work

The 1D homogenization model presented in Chapter 5 is a significant advance in metamaterial homogenization theory, but it is limited in its application. It assumes a great deal of symmetry in the crystal to be homogenized which prevents it from being applied to a wide class of asymmetric metamaterials crystals. In addition, it requires that the wavevector $\mathbf{k}$ be perpendicular to the metasurfaces that make up the model, preventing any study of constitutive parameters for oblique angle wavevectors.

An obvious generalization of this method requires that the model incorporate longitudinal polarization (field polarization perpendicular to the metasurface) in addition to the current transverse polarization. This polarizability should depend on the wavevector parallel to the metasurface in addition to ω. Such a characterization of a metasurface has proven to be very difficult. At the moment there is no general method for characterizing a metasurface with longitudinal polarization though there is at least one published attempt [24] that as an approximation assumes spatial dispersion in the direction parallel to the metasurface is negligible.

While the 1D model is quite successful in characterizing simple highly symmetric crystals, it may be that it is a dead end as a path to a more general homogenization procedure. At the moment it is difficult to tell. A more general method of metamaterial homogenization might require a new insight that applies to a more general class of classical fields, possibly including acoustic metamaterials. There are many similarities between the field of

electromagnetic metamaterials and acoustic metamaterials but there are still enough differences that studying both fields might provide an important clue towards a future research direction.

There are a few things we can anticipate about a future homogenization procedure. It should be general enough to calculate all of the necessary constitutive parameters. And it must include the effects of spatial dispersion through a dependence of the constitutive parameters on the wavevector $\mathbf{k}$.

Bibliography

[1] *MUltifrontal Massively Parallel Solver (MUMPS 4.9.2) User's guide*. Lyon, 2009.

[2] V. M. Agranovich. *Spatial Dispersion in Crystal Optics and the Theory of Excitons*, page 11. Interscience Publishers, New York, 1966.

[3] V. M. Agranovich. *Spatial Dispersion in Crystal Optics and the Theory of Excitons*. Interscience Publishers, New York, 1966.

[4] V. M. Agranovich. *Spatial Dispersion in Crystal Optics and the Theory of Excitons*, pages 56–62. Interscience Publishers, New York, 1966.

[5] K. B. Alici and E. Ozbay. Radiation properties of a split ring resonator and monopole composite. *Phys. Stat. Sol. (b)*, 244:1192–1196, 2007.

[6] A. Alú. First-principle homogenization theory for periodic metamaterial arrays. *arXiv:1012.1351v2*, 2011.

[7] A. Alu. Restoring the physical meaning of metamaterial constitutive parameters. *Phys. Rev. B*, 83:081102, 2011.

[8] Satish Balay, Jed Brown, , Kris Buschelman, Victor Eijkhout, William D. Gropp, Dinesh Kaushik, Matthew G. Knepley, Lois Curfman McInnes,

Barry F. Smith, and Hong Zhang. PETSc users manual. Technical Report ANL-95/11 - Revision 3.1, Argonne National Laboratory, 2010.

[9] P. A. Belov and C. R. Simovski. Homogenization of electromagnetic crystals formed by uniaxial resonant scatterers. *Phys. Rev. E*, 72:026615, 2005.

[10] C. F. Bohren and D. R. Huffman. *Absorption and Scattering of Light by Small Particles*. John Wiley & Sons, New York, 1998.

[11] H. Brandsmeier, K. Schmidt, and C. Schwab. A multiscale hp-FEM for 2D photonic crystal bands. *J. Comput. Phys.*, 230:349–374, 2011.

[12] M. Conforti and M. Guasoni. Dispersive properties of linear chains of lossy metal nanoparticles. *J. Opt. Soc. Am. B*, 27:1576–1582, 2010.

[13] J. T. Costa, M. G. Silveirinha, and A. Alu. Poynting vector in negative-index metamaterials. *PRB*, 83:165120, 2011.

[14] M. Davanco, Y. Urzhumov, and G. Shvets. The complex bloch bands of a 2d plasmonic crystal displaying isotropic negative refraction. *Optics Express*, 15:9681–9691, 2007.

[15] R. A. Depine and A. Lakhtakia. Comment I on "resonant and antiresonant frequency dependence of the effective parameters of metamaterials". *Phys. Rev. E*, 70:048601, 2004.

[16] A. L. Efros. Comment II on "resonant and antiresonant frequency dependence of the effective parameters of metamaterials". *Phys. Rev. E*, 70:048602, 2004.

[17] C. Engström, C. Hafner, and K. Schmidt. Computations of lossy blosh waves in two-dimensional photonic crystals. *Journal oTheoretical Nanoscience*, 6:1–9, 2009.

[18] S. Enoch, G. Tayeb, P. Sabouroux, N. Guerin, and P. Vincent. A metamaterial for directive emission. *Phys. Rev. Lett.*, 89:213902, 2002.

[19] A. Erentok and R. W. Ziolkowski. Metamaterial-inspired efficient electrically small antennas. *IEEE Trans. Antennas Propag.*, 56:691–707, 2008.

[20] C. Fietz and G. Shvets. Metamaterial homogenization: extraction of effective constitutive parameters. In M. A. Noginov, N. I. Zheludev, A. D. Boardman, and N. Engheta, editors, *Metamaterials: Fundamentals and Applications II*, page 739219, Bellingham, WA, 2009. SPIE.

[21] C. Fietz and G. Shvets. Current-driven metamaterial homogenization. *Physica B*, 405:2930–2934, 2010.

[22] C. Fietz and G. Shvets. Homogenization theory for simple metamaterials modeled as one-dimensional arrays of thin polarizable sheets. *Phys. Rev. B*, 82:205128, 2010.

[23] C. Fietz and G. Shvets Y. Urzhumov. Complex k band diagrams of 3d metamaterial/photonic crystals. *arXiv:1106.0043v1*, 2011.

[24] C. L. Holloway, A. Dienstfreyb, E. F. Kuesterc, J. F. OHarad, A. K. Azadd, and A. J. Taylor. A discussion on the interpretation and characterization of metafilms/metasurfaces: The two-dimensional equivalent of metamaterials. *Metamaterials*, 3:100–112, 2009.

[25] E. Istrate, A. A. Green, and E. H. Sargent. Behavior of light at photonic crystal interfaces. *Phys. Rev. B*, 71:195122, 2005.

[26] J. D. Jackson. *Classical Electrodynamics*, page 263. John Wiley and Sons, Inc, Hoboken, 3rd edition, 1998.

[27] J. D. Jackson. *Classical Electrodynamics*, pages 273–274. John Wiley and Sons, Inc, Hoboken, 3rd edition, 1998.

[28] J. Jin. *The Finite Element Method in Electromagnetics*. John Wiley & Sons, Inc., New York, 2d edition, 2002.

[29] J. D. Joannopoulos, R. D. Meade, and J. N. Winn. *Photonic Crystals: Molding the Flow of Light*. Princeton University Press, New Jersey, 2nd edition, 2008.

[30] E. O. Kamenetskii. Energy balence equation for electromagnetic waves in bianisotropic media. *PRE*, 54:4359–4367, 1996.

[31] B. Kanté, A. de Lustrac, J. M. Lourtioz, and S. N. Burokur. Infrared cloaking based on the electric response of split ring resonators. *Opt. Express*, 16:9191–9198, 2008.

[32] J. A. Kong. *Electromagnetic Wave Theory.* John Wiley and Sons, Inc, 1986.

[33] T. Koschny, P. Markos, D. R. Smith, and C. M. Soukoulis. Reply to comments on "resonant and antiresonant frequency dependence of the effective parameters of metamaterials". *Phys. Rev. E*, 70:048603, 2004.

[34] T. Koschny, P. Markŏs, D. R. Smith, and C. M. Soukoulis. Resonant and antiresonant frequency dependence of the effective parameters of metamaterials. *Phys. Rev. E*, 68:065602, 2003.

[35] E.F. Kuester, M.A. Mohamed, M. Piket-May, and C.L. Holloway. Averaged transition conditions for electromagnetic fields at a metafilm. *IEEE Trans. Antennas Propag.*, 51:2641–2651, 2003.

[36] L. D. Landau, E. M. Lifshitz, and L. P. Pitaevskii. *Electrodynamics of Continuous Media*, pages 359–360. Elsevier, Oxford, 2nd edition, 1984.

[37] L. D. Landau, E. M. Lifshitz, and L. P. Pitaevskii. *Electrodynamics of Continuous Media*, pages 361–362. Elsevier, Oxford, 2nd edition, 1984.

[38] L. D. Landau, E. M. Lifshitz, and L. P. Pitaevskii. *Electrodynamics of Continuous Media*, pages 272–273. Elsevier, Oxford, 2nd edition, 1984.

[39] R. B. Lehoucq, D. C. Sorensen, and C. Yang. *ARPACK Users' Guide, Solution of Large-Scale Eigenvalue Problems by Implicitly Restarted Arnoldi Methods*. SIAM, Philadelphia.

[40] J. Li and J. B. Pendry. Non-local effective medium of metamaterial. *arXiv:cond-mat/0701332v1*, 2007.

[41] Z. Li, K. Aydin, and E. Ozbay. Determination of the effective constitutive parameters of bianisotropic metamaterials from reflection and transmission coefficients. *Phys. Rev. E*, 79:026610, 2009.

[42] Z. Y. Li and L. L. Lin. Photonic band structure solved by a plane-wave–based transfer-matrix method. *Phys. Rev. E*, 67:046607, 2003.

[43] V. Lomakin, Y. Fainman, Y. Urzhumov, and G. Shvets. Doubly negative metamaterials in the near infrared and visible regimes based on thin film nanocomposites. *Optics Express*, 14:11164–11177, 2006.

[44] R. Marqués, F. Medina, and R. Rafii-El-Idrissi. Role of bianisotropy in negative permeability and left-handed metamaterials. *Phys. Rev. B*, 65:144440, 2002.

[45] K. J. Maschhoff and D. C. Soerensen. PARPACK: An efficient portable large scale eigenvalue package for distributed memory parallel architectures. *Lect. Notes Comp. Sci.*, 1184:478–486, 1996.

[46] F. Moulin. Magnetic monopoles and lorentz force. *Il Nuovo Cimento B*, 116B:869–877, 2001.

[47] M. Notomi. Theory of light propagation in strongly modulated photonic crystals: Refractionlike behavior in the vicinity of the photonic band gap. *Phys. Rev. B*, 62:10696, 2000.

[48] S. O'Brien and J. B. Pendry. Magnetic activity at infrared frequencies in structured metallic photonic crystals. *J. Phys.: Condens. Matter*, 14:6383–6394, 2002.

[49] S. O'Brien and J. B. Pendry. Photonic band-gap effects and magnetic activity in dielectric composites. *J. Phys.: Condens. Matter*, 14:4035–4044, 2002.

[50] J. B. Pendry, A. J. Holden, D. J. Robbins, and W. J. Stewart. Magnetism from conductors and enhanced nonlinear phenomena. *IEEE Trans. Microw. Theory Tech.*, 47:2075–2084, 1999.

[51] J. E. Roman, E. Romero, and A. Tomas. SLEPc users manual. Technical Report DSIC-II/24/02 - Revision 3.1, D. Sistemas Informáticos y Computación, Universidad Politécnica de Valencia, 2010.

[52] K. Sakoda. *Optical properties of photonic crystals*. Springer, New York, 2nd edition, 2004.

[53] G. Shvets and Y. A. Urzhumov. Engineering the electromagnetic properties of periodic nanostructures using electrostatic resonances. *Phys. Rev. Lett.*, 93:243902, 2004.

[54] M. G. Silveirinha. Metamaterial homogenization approach with application to the characterization of microstructured composites with negative parameters. *Phys. Rev. B*, 75:115104, 2007.

[55] M. G. Silveirinha. Poynting vector, heating rate , and stored energy in structured materials: A first-principles derivation. *PRB*, 80:235120, 2009.

[56] P. P. Silvester and R. L. Ferrari. *Finite elements for electrical engineers*. Cambridge University Press, Cambridge, 3rd edition, 1996.

[57] C. R. Simovski. Bloch material parameters of magneto-dielectric metamaterials and the concept of bloch lattices. *Metamaterials*, 1:62–80, 2007.

[58] C. R. Simovski and S. A. Tretyakov. Local constitutive parameters of metamaterials from an effective-medium perspective. *Phys. Rev. B*, 75:195111, 2007.

[59] D. R. Smith. Analytic expressions for the constitutive parameters of magnetoelectric metamaterials. *Phys. Rev. E*, 81:036605, 2010.

[60] D. R. Smith and J. B. Pendry. Homogenization of metamaterials by field averaging. *J. Opt. Soc. Am. B*, 23:391–403, 2006.

[61] D. R. Smith, S. Schultz, P. Markŏs, and C. M. Soukoulis. Determination of effective permittivity and permeability of metamaterials from reflection and transmission coefficients. *Phys. Rev. B*, 65:195104, 2002.

[62] D. R. Smith, D. C. Vier, N. Kroll, and S. Schultz. Direct calculation of permeability and permittivity for a left-handed metamaterial. *Appl. Phys. Lett.*, 77:2246–2248, 2000.

[63] T. Suzuki and P.K. L. Yu. Tunneling in photonic band strucures. *J. Opt. Soc. Am. B*, 12:804, 1995.

[64] F. Tisseur and K. Meerbergen. The quadratic eigenvalue problem. *SIAM Review*, 43:235–286, 2001.

[65] Y. A. Urzhumov and G. Shvets. Optical magnetism and negative refraction inplasmonic metamaterials. *Solid State Communications*, 146:208–220, 2008.

[66] J. F. Wang, S. B. Qu, H. Ma, Y. M. Yand, and X. Wu. Wide-angle polarization-independent planar left-handed metamaterials based on dielectric resonators. *PIER B*, 12:243–258, 2009.

[67] R. Wang, B. Yuan, G. Wang, and F. Yi. Efficient design of directive patch antennas in mobile communications using metamaterials. *Int J Infrared Milli Waves*, 28:639–649, 2007.

[68] A. J. Ward, J. B. Pendry, and W. J. Stewart. Photonic dispersion surfaces. *J. Phys.: Condens. Matter*, 7:2217–2224, 1995.

[69] B. I. Wu, W. Wang, J. Pacheco, X. Chen, T. Grzegorczyk, and J. A. Kong. A study of using metamaterials as antenna substrate to enhance gain. *PIER*, 51:295–328, 2005.

[70] Shuang Zhang, Wenjun Fan, K. J. Malloy, S. R. J. Brueck, N. C. Panoiu, and R. M. Osgood. Near-infrared double negative metamaterials. *Optics Express*, 613:4922, 2005.

[71] X. Zhang, M. Davanco, K. Miller, T. W. Jarvis C. Wu, C. Fietz, D. Korobkin, X. Li, G. Shvets, and S. R. Forrest. Interferometric characterization of a subwavelength near-infrared negative index metamaterial.

[72] X. Zhang, M. Davanco, Y. Urzhumov, and G. Shvets. A subwavelength near-infrared negative index material. *Appl. Phys. Lett.*, 94:131107, 2009.

[73] J. Zhou, T. Koschny, and C. M. Soukoulis. Magnetic and electric excitations in split ring resonators. *Opt. Express*, 15:17881–17890, 2007.

[74] W. B. J. Zimmerman. *Process Modelling and Simulation with Finite Element Methods*. World Scientific, Singapore, 2004.

Vita

Chris Fietz grew up in Council Bluffs, Iowa and attended St. Albert Catholic Schools from kindergarten through high school. He then attended Iowa State University and studied Chemical engineering for two years before switching majors and earning a Bachelor of Science in Physics in Dec 2004. In 2005 he began his graduate studies at the University of Texas at Austin in the Physics department.

Permanent address: fietz.chris@gmail.com

This dissertation was typeset with LaTeX[†] by the author.

[†]LaTeX is a document preparation system developed by Leslie Lamport as a special version of Donald Knuth's TeX Program.